

THE PHOTORECEPTORS AND NEURAL CIRCUITS DRIVING
THE PUPILLARY LIGHT REFLEX

by
Alan C. Rupp

A dissertation submitted to Johns Hopkins University in conformity with the
requirements for the degree of Doctor of Philosophy

Baltimore, Maryland
January 28, 2016

This work is protected by a Creative Commons license:
Attribution-NonCommercial
CC BY-NC

Abstract

The visual system utilizes environmental light information to guide animal behavior. Regulation of the light entering the eye by the pupillary light reflex (PLR) is critical for normal vision, though its precise mechanisms are unclear. The PLR can be driven by two mechanisms: (1) an intrinsic photosensitivity of the iris muscle itself, and (2) a neural circuit originating with light detection in the retina and a multisynaptic neural circuit that activates the iris muscle. Even within the retina, multiple photoreceptive mechanisms—rods, cone, or melanopsin phototransduction—can contribute to the PLR, with uncertain relative importance. In this thesis, I provide evidence that the retina almost exclusively drives the mouse PLR using bilaterally asymmetric brain circuitry, with minimal role for the iris intrinsic photosensitivity. Intrinsically photosensitive retinal ganglion cells (ipRGCs) relay all rod, cone, and melanopsin light detection from the retina to brain for the PLR. I show that ipRGCs predominantly relay synaptic input originating from rod photoreceptors, with minimal input from cones or their endogenous melanopsin phototransduction. Finally, I provide evidence that rod signals reach ipRGCs using a non-conventional retinal circuit, potentially through direct synaptic connections between rod bipolar cells and ipRGCs. The results presented in this thesis identify the initial steps of the PLR and provide insight into the precise mechanisms of visual function.

Thesis advisor: Samer Hattar, Ph.D.

Secondary reader: Nicholas Marsh-Armstrong, Ph.D.

Thesis committee: Marnie Halpern, Ph.D.

Alapakkam Sampath, Ph.D.

Preface

Graduate school has been a great time of growth and change for me. This thesis represents not just 6 years of work, but 6 years of changing hypotheses, learning new techniques, discussing ideas with colleagues, growing awareness of the diversity of biological problems, and personal and professional maturation. Writing this thesis has given me the opportunity to reflect on this time and to recognize many helpful people in a way that I may not have if I did not have a devoted time of reflection. I don't have the space to name everyone who has helped over the years, but I want to use this preface to recognize a few.

First, I'd like to thank my advisor, Samer Hattar, for his scientific direction. Samer is a truly inspiring scientist, always willing to tackle hard problems and to push until he has gotten to the core of the question. His tenacity and perseverance in the face of science's constant rejection have been a great lesson for me that most of science is failure and those rare moments of success only come after intense resolve. I am certain I would not be at this point if it weren't for him.

Of course, the Hattar lab does not work alone, and the entirety of the Mouse Tri-Lab has been a scientific advisor to me in some way. Both Rejji Kuruvilla and Haiqing Zhao have been thoughtful and incredibly giving of their time to guide me in experiments, publishing, and general career and life advice. Just the opportunity to share space and lab meetings with their labs has opened up my interest in a wide variety of questions and ways to do science.

I can't think of a better environment to do a Ph.D. than the Mouse Tri-Lab. It operates like a small family, sharing Thanksgivings, holidays, and other celebrations.

And day-to-day, being able to interact with helpful people who are interested in a wide variety of questions and techniques has been beneficial for me growing as a scientist. Many members of the Zhao and Kuruvilla labs have been inspirations to me for how to do science well and enjoy doing it, including (but definitely not limited to) Kate Cygnar, Aaron Stephan, Maria Ascano, Dan Bodmer, Phil Borden, Chih-Ming Chen, Ami Patel, and Jessica Houtz.

Within the Hattar lab, I need to thank the people who have been critical to my development. Cara Altimus was my first mentor in the lab and was the guiding force for the questions and techniques I would address and she set the bar incredibly high for what it means to be a successful grad student. I feel lucky to have been able to sit next to an extremely knowledgeable post-doc, Tiffany Schmidt, who over the course of three-plus years allowed me to bounce scientific ideas off her, design experiments, and really pushed me to think hard about my projects. Many other Hattar lab members over the years have been great in helping with experiments, discussing ideas, or just in general making the lab a great place to come every day, including Tara LeGates, Shih-Kuo Chen, Kylie Chew, Diego Fernandez, and Bill Keenan, among many others I don't have the space to name.

My thesis committee—Marnie Halpern, Nick Marsh-Armstrong, Alapakkam Sampath, and for a few years Michael Deans—has been supportive of me since my first meeting. They have been especially helpful while I've navigated the complicated world of scientific disagreements and publishing. And lastly, I appreciate their general experimental and career advice, and Nick Marsh-Armstrong in particular for his helpful and insightful comments on this thesis.

I would never have been in graduate school if it weren't for specific advisors I had earlier in my life. Despite me being a relatively inexperienced engineering student, Akira Takashima gave me the opportunity to work in academic biomedical research, and more importantly pushed me to do great science and not settle. Rhonda Moore went out of her way to find co-op experiences for me that were more in line with my interests in biology research than the standard engineering student. And S.P. Srinivas and Larry Thibos were extremely understanding and giving of their time in training me as a college student while I was learning how to do research and learn new questions and techniques.

It goes without saying that I would not have been able to accomplish what I have in life without my family. My parents, Chuck and Panna Rupp, have always encouraged me to pursue the things I'm interested in and do them well. They instilled in me a basic wonder in the world and taught me how to rigorously critique ideas long before I wanted that to be my job. And throughout graduate school they've been a constant source of encouragement and interest in my work. I've been fortunate to have my brother, Brad Rupp, in Baltimore throughout most of my time in grad school to commiserate about the pains of being a graduate student, the ups and downs of my projects, and to have family nearby for the little things.

And lastly, I need to thank my wife, Jessica Ameling, who has been always supportive of my desire to go to graduate school even though it meant moving away from both of our families and has never flinched in her support, even during the most stressful times. There is no certainty or predictability in science, and through countless late nights, early mornings, weekends, traveling, and other times when science took preference over everything else, she always understood and was a constant source of grounding and

reminder of the truly important things in life. With her and our daughters, Evelyn and Emma, I have been able to come home every day and know that I have people who are backing me through everything and want to share in my joys and frustrations. This thesis is dedicated to them.

Table of Contents

Chapter 1: Introduction	1
The retina and visual system	2
Information flow in the retina	4
Segregation of rod and cone circuits.....	7
Intrinsically photosensitive retinal ganglion cells.....	8
Diversity of ipRGCs.....	12
Retinal connectivity of ipRGCs	15
Melanopsin phototransduction.....	18
The roles of rods, cones, and melanopsin phototransduction in the PLR.....	22
Intrinsic pupillary light reflex in mammals	27
Contents of this thesis.....	29
Figures	32
Chapter 2: Differentiating the contributions of retina and iris phototransduction to controlling pupil size.....	44
Abstract	45
Introduction	46
Results.....	48
The intrinsic PLR operates exclusively at very bright light intensities	48
Limiting amounts of melanopsin in the iris muscle.....	50
Modulation of the strength of the intrinsic PLR	51
Melanopsin phototransduction in the retina, but not iris, is required for the PLR.....	52
Brn3b-positive ipRGCs are required for PLR bilateral asymmetry	55
Discussion	59
Methods	61
Animal husbandry	61
Pupillometry.....	61
Data analysis	62
Optic nerve transection and crush	63
Atropine application.....	63
Statistical analysis	64
Viral infection	64

Confocal microscopy	65
Figures	66
Chapter 3: Rods mediate the rapid pupillary light reflex.....	88
Abstract	89
Introduction	90
Results.....	91
Experimental PLR setup to mimic the natural environment	91
PLR action spectrum matches rhodopsin/melanopsin spectrum.....	92
Rod phototransduction is required for the rapid PLR	92
Rods are sufficient for the full rapid PLR.....	96
The photoreceptor contributions to the pupillary light reflex over time and intensity.....	98
Discussion	99
Methods	102
Animal husbandry	102
Pupillometry.....	102
Data analysis	104
Statistical analysis	105
Heat map generation	105
Figures	107
Chapter 4: Rods use a non-conventional retinal circuit to drive the pupillary light reflex	
.....	120
Abstract	121
Introduction	122
Results.....	123
Anatomical identification of cell types upstream of ipRGCs.....	123
A Cx36-indepdent rod ON circuit mediates the PLR.....	126
Discussion	127
Acknowledgments.....	129
Methods	130
Animal husbandry	130
Molecular cloning and virus production	130
Viral circuit tracing	130

Immunofluorescence	131
Confocal microscopy and image processing	132
Pupillometry	132
Data analysis	133
Statistical analysis	134
Figures	135
Chapter 5: Distinct ipRGC subtypes mediate acute and circadian regulation of body	
temperature	140
Abstract	141
Introduction	142
Results.....	144
Discussion	147
Animal husbandry	150
Telemetry	150
Statistical analysis	150
Viral infection	150
Confocal microscopy	151
Figures	152
Chapter 6: Concluding remarks	
The questions remaining in the PLR	162
The pupillary light reflex as a model visual behavior	164
References.....	167
<i>Curriculum Vitae</i>	192

List of Figures

Figure 1.1: Basic structure of the visual system.	33
Figure 1.2: Evolutionary and genomic relationships of melanopsin.	34
Figure 1.3: Diversity and central projections of ipRGCs.	35
Figure 1.4: Distinct inputs and outputs to different ipRGC subtypes.....	37
Figure 1.5: Phototransduction in ipRGCs closely resembles <i>Drosophila</i> rhabdomeres.....	38
Figure 1.6: Characteristics and evolutionary conservation of PLR.	41
Figure 1.7: Light activation of one eye travels bilaterally through PLR brain circuitry.	42
Figure 2.1: The intrinsic PLR operates exclusively at bright light intensities.	66
Figure 2.2: M3 mAChR are required for a normal PLR.	68
Figure 2.3: Melanopsin immunofluorescence in albino iris.....	69
Figure 2.4: Melanopsin pervasiveness contributes to PLR insensitivity.	70
Figure 2.5: Modulation of intrinsic PLR strength over time.	72
Figure 2.6: Optic nerve crush leads to a reduction in intrinsic PLR over time.	73
Figure 2.7: Enhancement of PLR by atropine requires melanopsin.	74
Figure 2.8: Melanopsin knockout in the retina, not iris, causes PLR deficits.	76
Figure 2.9: Differentiating melanopsin's role in iris and retina.	77
Figure 2.10: <i>Brn3b</i> -positive ipRGCs are both necessary and sufficient for bilateral asymmetry in the PLR.	79
Figure 2.11: Infection of multiple ipRGC subtypes with AAV-DIO-hM3D(G _q).	81
Figure 2.12: Evidence for ipRGC involvement in the intrinsic PLR.	83
Figure 2.13: ipRGCs require brain circuitry to drive the PLR.	84
Figure 2.14: Mice lacking M1 ipRGCs lack PLR bilateral asymmetry.	85
Figure 2.15: Enhanced direct over consensual PLR occurs in <i>Brn3b</i> -DTA mice at bright light intensities.	87
Figure 3.1: Experimental setup to mimic environmental light.	107
Figure 3.2: Action spectrum of the pupillary light reflex in wild-type mice matches rods and/or melanopsin.	108
Figure 3.3: Mutant mouse lines used in this study.	110
Figure 3.4: Rods are required for the rapid PLR.....	112
Figure 3.5: Both cones and rods are required for the PLR to UV light.	114
Figure 3.6: Melanopsin is not required for rapid PLR in response to environmentally relevant overhead light.	116
Figure 3.7: Rods are the only photoreceptors that are sufficient for the full rapid PLR.	117
Figure 3.8: The photoreceptor contribution landscape of the pupillary light reflex.	119
Figure 4.1: Transsynaptic circuit tracing reveals rod bipolar cells upstream of ipRGCs.	135
Figure 4.2: Using genetically labeled pre- and postsynapses to identify ipRGC synaptic input locations.	137
Figure 4.3: A non-conventional rod circuit drives the PLR.	139

<i>Figure 5.1: Mice use light information to both photoentrain and acutely regulate body temperature.</i>	<i>152</i>
<i>Figure 5.2: Light intensity-dependence of acute body temperature decrease.</i>	<i>154</i>
<i>Figure 5.3: Melanopsin is both necessary and sufficient for acute thermoregulation by light.</i>	<i>155</i>
<i>Figure 5.4: Acute activity regulation is intact in melanopsin knockout mice.</i>	<i>156</i>
<i>Figure 5.5: Brn3b-positive ipRGCs are required for acute body temperature decrease by light.</i>	<i>157</i>
<i>Figure 5.6: Acute activity suppression in Brn3b-DTA mice.</i>	<i>158</i>
<i>Figure 5.7: Chemogenetic activation of Brn3b(+) RGCs is sufficient for sustained body temperature decrease.</i>	<i>159</i>
<i>Figure 5.8: CNO has no measureable effect on wildtype body temperature.</i>	<i>160</i>

Chapter 1

Introduction

Portions of this introduction including some figures were previously published in:

Rupp AC, Hattar S. “The functional properties of the G protein-coupled receptor

melanopsin in intrinsically photosensitive retinal ganglion cells.” In:

Martemyanov KA, Sampath AP, editors. *G Protein Signaling Mechanisms in the*

Retina, Springer (2014).

The retina and visual system

Light is a ubiquitous energy source and daily timing cue that organisms use to coordinate behavior and physiology. From night to day, light intensities vary by over 9 orders of magnitude. Organisms have evolved on this predictable change in light intensity and have used it to guide a stunning diversity of behaviors. Virtually all known species with access to light have visual functions, including single-celled species like green algae¹ and even species that live in near complete darkness like cavefish or naked mole rats^{2,3}.

As humans, the most widely appreciated use of light is our conscious visual perception: the ability to see features of the world based on their reflectance of light. Conscious visual perception relies on detecting relative differences in brightness or color of neighboring objects. This requires identifying precisely where the photon came from and comparing its brightness to its neighbors', a difficult problem⁴. To achieve high visual acuity, the retina must be able to detect relatively small differences in brightness or wavelength in regions of the environment that are separated by microns.

However, light is most often used in nature for non-spatial (i.e. non-image forming) functions. For instance, the most famous example is the use of light for energy generation in photosynthetic species such as plants. While it is beneficial for plants to be able to orient toward a source of light, the specific spatial orientation of the world does not matter. If the light is reflected off a tree or a rock makes no difference as long as the total number of effective photons reaching the chloroplasts is the same.

For decades, humans were thought to be devoid of non-spatial forms of vision, which were reserved for 'lower' animal forms lacking the high visual acuity, intelligence,

and complex social structure of humans^{5,6}. However, it has become apparent that light has a variety of non-spatial effects in virtually all mammals, humans included. The most widely appreciated are the alignment of sleep/wake cycles and activity to the environmental light/dark cycle (referred to as circadian photoentrainment)⁷, light's effects on arousal and alertness⁸⁻¹⁰, the exacerbation of migraine headaches¹¹, the effect of light on mood (e.g. season affective disorder and light-responsive forms of depression)¹², and physiological functions such as the control of pupil size by light (pupillary light reflex). Despite widespread uses of non-spatial vision and their critical importance, these forms of vision have been understudied in animals compared to spatial vision and conscious visual perception.

The goal of this thesis is to identify the precise mechanisms that govern how animals accomplish non-spatial visual function. In my time in graduate school, I have worked to understand a variety of non-spatial visual functions, including circadian alignment and acute regulation of sleep and body temperature by light (Chapter 5 of this thesis). However, I have spent the majority of my time on the pupillary light reflex (PLR) because of its ease of study, its widespread conservation in animals, and its importance for vision (Chapters 2-4 of this thesis). Therefore, I will focus this introduction predominantly on the PLR.

As a visual behavior, the PLR is incredibly useful. It occurs within seconds of the presence of light and can be followed in real time, unlike many other non-spatial behaviors that occur over hours or days. In particular, I have focused on the critical first steps in the PLR: how light is detected and how that signal is processed by the neural circuits that drive pupil constriction. Ultimately, I believe that the pupillary light reflex is

an ideal model behavior for precisely dissecting neural circuitry underlying an important physiological function and the findings presented here will inform future studies of how complex visual behaviors are mediated by similar circuits.

Information flow in the retina

The retina, a thin, layered structure that lines the back of the eye, detects light information for both spatial and non-spatial forms of vision. It contains six major neuronal cell types and two glial types that are arranged in stereotypical layers¹³. The six neuronal types include the rod and cone photoreceptors in the outer retina, the horizontal cells, bipolar cells, and amacrine cells in the inner nuclear layer, and the retinal ganglion cells and some amacrine cells in the ganglion cell layer (Fig. 1.1). Spanning all three layers are Müller glia cells that act as supporting cells and below the ganglion cell layer are astrocytes. The flow of light information follows this anatomical arrangement in simple succession: light is detected by the rods and cones, which signal to bipolar cells, which signal to retinal ganglion cells, which then form the optic nerve to relay that light information to the brain. (Horizontal cells and amacrine cells are interneurons that modify the activity of the photoreceptors, bipolar cells, and retinal ganglion cells.)

Light information is encoded in the electrical activity of the retinal neurons. While most neurons maintain a hyperpolarized membrane potential at rest and are ‘activated’ by depolarization, in darkness, the membrane potential of rod and cone photoreceptors is in a relatively depolarized state. This basal depolarization results in their continuous release of synaptic vesicles containing glutamate. Rods and cones detect the presence of light through the expression of a specialized form of G protein-coupled receptors (GPCRs) called opsins, referred to as rhodopsin in rods and cone opsins in

cones¹⁴⁻¹⁶. Opsin proteins are covalently linked to a photosensitive vitamin A derivative called retinal that isomerizes following light detection from 11-*cis* retinal to all-*trans* retinal¹⁷⁻²¹. The isomerization of retinal results in a conformational change in the opsin protein that results in activation of the G protein transducin (GNAT1 in rods and GNAT2 in cones)²²⁻²⁸. Transducin activates a phosphodiesterase signaling cascade that results in the closure of cyclic nucleotide gated (CNG) cation channels (heteromeric CNGA1/B1 in rods and CNGA3/B3 in cones). This closure of the CNG channels results in a decrease in cation influx, hyperpolarizing the rods and cones and leading to a reduction in glutamate release. This change in the release of glutamate is what is detected by the next neurons in the visual circuit: the bipolar cells.

Bipolar cells come in two broad classes: ON and OFF. ON cells depolarize in response to increases in light intensity (i.e. decreases in glutamate from rods and cones) and OFF cells depolarize in response to decreases in light intensity (i.e. increases in glutamate). The ON and OFF bipolar cells generate opposite responses to glutamate through the expression of different classes of glutamate receptors on their dendrites. ON cells utilize a metabotropic glutamate receptor (mGluR6) and a GPCR signaling cascade to keep a cation channel (transient receptor potential melastatin 1, TRPM1) closed in the presence of glutamate²⁹⁻³¹. When glutamate decreases with light increases, the inhibition on the channel is relaxed and the cell depolarizes. In contrast, OFF cells express ionotropic glutamate receptors such as AMPA and kainate receptors^{32,33}. Therefore, in OFF cells the presence of glutamate in darkness or with decreases in light intensity will result in cation influx and the depolarization of the cell. For both ON and OFF bipolar

cells, depolarization leads to their release of glutamate-containing synaptic vesicles, in either a graded fashion or through action potential generation³⁴⁻³⁶.

ON and OFF responses are maintained in the retinal ganglion cells (RGCs). RGCs come in one of three broad classes: ON, OFF, or ON-OFF. As with bipolar cells, ON cells depolarize with increase in light, OFF cells with decreases in light, and ON-OFF cells with both increases and decreases. In general, ON RGCs are synaptically coupled to ON bipolar cells, OFF RGCs to OFF bipolar cells, and ON-OFF RGCs to both (although exceptions to this rule do exist). RGCs maintain the response polarity of the presynaptic bipolar cell by the expression of ionotropic glutamate receptors such as AMPA and NMDA receptors. Ultimately, the depolarization of an RGC will be propagated along its axon as an action potential and lead to the release of glutamate from its synaptic terminal(s)³⁷, activating neurons in the brain regions that mediate visual perception and behavior.

This simple diagram of light information propagation from photoreceptors to bipolar cells to retinal ganglion cells to the brain ignores the extreme complexity of the information. Along the way, distinct types of horizontal cells and amacrine cells modify the signal to detect specific aspects of the visual scene or filter out unwanted aspects³⁸⁻⁴⁴. Additionally, there are multiple subclasses of neurons with distinct physiological properties. In mouse there are two cone classes, one rod, one horizontal cell, about twelve bipolar cell, over forty amacrine cell, and around thirty retinal ganglion cell classes^{13,45,46}. Each neuronal subtype tiles the retina in repeated arrays and forms dedicated 'microcircuits' for the detection of specific visual features at each point in space (See Fig.

1.1). To understand how vision occurs, it is critical to identify these microcircuits and the visual information they encode.

Segregation of rod and cone circuits

Rod and cone photoreceptors are specialized for different kinds of light detection. Rods are exquisitely sensitive, capable of relaying the absorption of a single photon, making them the exclusive photoreceptor for night vision. However, their temporal resolution is relatively poor, which is why hand-eye coordination is worse at night. Cones on the other hand are orders of magnitude less sensitive than rods but capable of rapid light adaptation that allows them to signal robustly across the huge range in light intensities encountered in the day.

Because their signaling specializations differ, it likely comes as no surprise that rods and cones utilize distinct downstream relay cells. While bipolar cells come in two large classes (ON and OFF), there are at least thirteen total subtypes with distinct light response properties, morphology, and synaptic connections^{34,47-50}. Of the thirteen bipolar subtypes, one type forms synapses exclusively with rods: the rod bipolar cell. Rod bipolar cells are ON bipolar cells and the most abundant bipolar cells in the mammalian retina. The other twelve bipolar cell types (seven ON and five OFF) receive synaptic input from cones and are referred to as cone bipolar cells. (Note: this strict separation into rod and cone bipolar cells is not absolute; there is evidence for some cone bipolar cells that receive rod input and some rod bipolar cells that receive cone input⁵¹. However, this does not appear to be widespread and this is the only mention I will make of mixed rod and cone input to different bipolar cell types.)

One major difference among the bipolar cell classes is their ability to sustain depolarization in response to the continued presence or absence of light. Based on this criterion, some bipolar cell classes are referred to as ‘transient’ and others as ‘sustained’³⁶. These two categories (ON/OFF and sustained/transient) encompass the major distinctions of bipolar cell classes. As a result, in the mouse there are four kinds of visual information that bipolar cells relay: ON sustained, OFF sustained, ON transient, and OFF transient, although in species with robust color vision there is an additional chromatic component that is overlaid on top of these^{52,53}.

As light information travels further from the photoreceptors, it acquires more and more specialized information. What began as simple detection of the presence and intensity of light in the rods and cones and was converted to any of four response profiles in different bipolar cells becomes full-fledged ‘feature’ detection in different classes of retinal ganglion cells that are the building blocks of vision.

Intrinsically photosensitive retinal ganglion cells

Everything that the brain knows about the visual world comes from the electrical activity of retinal ganglion cells (RGCs). The multiple different subclasses of RGCs are specialized in the extraction of the visual features they relay to the brain. RGC types differ in their light response characteristics, morphology, gene expression profiles, presynaptic circuits, and targets within the brain. Therefore, for the last 50 years, a major goal of visual neuroscientists has been to identify the complete catalog of RGCs and connect them to specific perceptual and behavioral functions.

To date, it is estimated that there are thirty subtypes of RGCs^{54,55}. Among them are RGCs involved in detecting the direction of object motion (direction-selective

RGCs)⁵⁶⁻⁶¹, RGCs with especially large soma that detect image contrast (alpha RGCs)⁶²⁻⁶⁶, and motion-sensitive RGCs with unusual asymmetric dendrites (J-RGCs)⁶⁷. Arguably, the only subpopulation that has been definitively linked to a specific behavioral or perceptual function is a class known as the intrinsically photosensitive retinal ganglion cells (ipRGCs), which mediate a variety of non-spatial visual behaviors including the pupillary light reflex (PLR) and circadian photoentrainment^{68,69}. Therefore, ipRGCs have become a model system for understanding how a specific RGC subclass extracts its specialized visual features (i.e. its specific retinal circuitry) and how it drives its dedicated visual function(s). I will focus the remainder of this introduction on ipRGCs and their role in the PLR.

One complication in using ipRGCs as a model RGC class is the fact that they are both RGCs and photoreceptors, possessing their own phototransduction cascade that functions in the absence of rods and cones⁷⁰. This remarkable fact adds a layer of complexity to the simple wiring diagram that visual neuroscientists had drawn for decades (and I had drawn in the preceding sections) in which light is detected exclusively by the rods and cones and is refined in greater detail in succeeding synapses. This finding was so surprising that it is worth telling the history of the relatively recent discovery of ipRGCs.

For decades, it had been recognized that mice lacking virtually all rods and cones could still align their circadian rhythms to a light/dark cycle⁷¹⁻⁷³ and constrict their pupils in response to light⁷⁴. These observations were dismissed with a trivial explanation that although the vast majority of photoreceptors were absent (all rods and >99% of cones), the remaining few could mediate the residual response⁷⁵. However, this explanation was

laid to rest when it was found that humans with no conscious visual perception could align their sleep/wake cycles to a light/dark cycle⁷⁶. This suggested that in the complete absence of rod and cone function, there is another functional photoreceptive mechanism. Further experiments in mouse definitively showed that mice lacking all rods and cones still retained photoentrainment, acute suppression of activity by light (masking), the PLR, and melatonin suppression by light⁷⁷⁻⁸⁰. These results prompted the search for a third photoreceptor in the mammalian retina.

Many different classes of opsins exist in the animal kingdom and there have been considerable efforts to identify the full catalog of opsin families (Fig. 1.2). One study by Ignacio Provencio and colleagues revealed a novel opsin that they named melanopsin due to its expression in the photosensitive skin melanophores of *Xenopus laevis*⁸¹. Later, the same group identified a melanopsin homolog (officially referred to as opsin 4 or Opn4) in the mouse and human genomes with a sequence that was more similar to invertebrate opsins than to mammalian rhodopsin and cone opsins⁸² (Fig. 1.2). Intriguingly, they also revealed expression of mammalian melanopsin in a subset of RGCs⁸². This result implied that some RGCs might possess their own phototransduction cascade similar to rods and cones and therefore could mediate light detection in their absence.

Therefore, Provencio et al. hypothesized that the RGCs that express melanopsin would be directly photosensitive and possibly capable of contributing to circadian photoentrainment and the PLR⁸². To test this, in 2002, David Berson and colleagues labeled the RGCs that project to the master circadian pacemaker, the suprachiasmatic nucleus (SCN)⁷⁰. They found that SCN-projecting RGCs continued to depolarize to light

in the absence of synaptic input⁷⁰. This indicated that the RGCs that control circadian photoentrainment are intrinsically photosensitive (thereby named ipRGCs).

In parallel experiments, Samer Hattar, King-wai Yau, and colleagues developed a mouse line to label the cell bodies and axons of the melanopsin-expressing cells (*Opn4^{tauLacZ}*)⁸³. They found that there are about 700 melanopsin-expressing RGCs in each mouse retina, and they project to the SCN and olivary pretectal nucleus (OPN), a midbrain relay for the PLR⁸³, among other brain regions⁸⁴. Altogether, these results identified melanopsin-expressing ipRGCs as the long-sought third photoreceptor in the mammalian retina.

It was then predicted that melanopsin knockout mice would be incapable of circadian photoentrainment or the PLR. In contrast, melanopsin knockout mice were virtually normal in both respects, although they had a small deficit in shifting their circadian phase to light and maximal pupil constriction in response to bright light⁸⁵⁻⁸⁷. It required removal of all three phototransduction mechanisms in the retina (rods, cones, and melanopsin) to abolish photoentrainment and the PLR and create truly blind mice^{88,89}. This confirmed that rods, cones, and ipRGCs are the only photoreceptors in the retina, and put to rest a hypothesis that photosensitive flavin-based molecules called cryptochromes could mediate the PLR and circadian photoentrainment in mammals⁹⁰⁻⁹³. (Notably, a recent study found that there is likely a fourth photoreceptor in the retina that is capable of aligning the endogenous circadian rhythm of the retina to the light/dark cycle in the absence of rod, cone, and ipRGC function⁹⁴. However, this fourth photoreceptor is yet unidentified and in any case incapable of contributing to circadian photoentrainment or the PLR, so I will not discuss it.)

This raised two possibilities: (1) ipRGCs are the sole relays of light information for circadian photoentrainment and the PLR (2) other RGCs could relay rod and cone light information for circadian photoentrainment and the PLR in the absence of ipRGC function⁶⁸. To distinguish these possibilities, multiple groups used genetic means to ablate the ipRGCs and observed an almost complete loss of photoentrainment and PLR⁹⁵⁻⁹⁷. Remarkably, PLR and photoentrainment were absent in these mice despite normal spatial vision and normal rod and cone function⁹⁵. This indicated that ipRGCs are the predominant, if not sole, relay of light information for photoentrainment and the PLR. These results highlight the parallel nature of visual processing in which distinct RGC classes are dedicated to specific visual functions.

Diversity of ipRGCs

Later studies using more sensitive labeling methods showed that there are at least 5 distinct subclasses of RGCs that express melanopsin⁹⁸⁻¹⁰⁴ (Fig. 1.3). These cells are normally grouped together as subtypes of ipRGCs (referred to as M1–M5), although I believe it may be more appropriate to think of them as distinct subtypes of RGCs that happen to all express melanopsin. For instance, the alpha RGCs mediate the detection of low contrast stimuli for spatial vision and one alpha cell type expresses melanopsin, so it has been categorized as the M4 ipRGC^{62,104}. However, if RGCs are categorized based on the visual features they extract, I believe it the M4 ipRGCs should be thought of as a member of the spatial, contrast-sensitive RGC group that happens to express melanopsin. This line of thinking has important implications for how we think about the function of individual ipRGC subtypes. Subtypes that are clustered with conventional RGCs of a

certain function (e.g. contrast-sensitive) will give unique insights into the roles that those subtypes play.

Regardless of how they are categorized, all ipRGCs can be linked by their expression of melanopsin and their ability to respond to light in the absence of rod and cone function. Additionally, one pragmatic reason to group all melanopsin-expressing RGCs together is the lack of genetic tools to separate them. Currently, genetic tools that ablate or activate ipRGCs will ablate or activate virtually all of them⁹⁹. For this reason, from here forward I will stick with convention and refer to the different melanopsin-expressing RGCs as ipRGC subtypes.

Like RGC subtypes, the defined ipRGC subtypes differ in their gene expression profiles, morphology, dendritic stratification, electrophysiological responses to light, connectivity within the retina, and central projections^{62,98–103,105–107} (Fig. 1.3). The M1 ipRGCs are the founding member of the group and comprise the cells that project to the SCN and OPN. However, while exclusively M1 cells innervate the SCN, other types of ipRGCs robustly innervate the OPN^{99,102}. The fact that multiple ipRGC subtypes project to the OPN suggests ipRGC input to the PLR is more complex than to circadian photoentrainment.

Because we have limited knowledge of their precise functions, the other ipRGC subtypes tend to be lumped together as ‘non-M1’ ipRGCs. The only function tied to non-M1 ipRGCs to date is their role in spatial vision. They project to brain regions involved in conscious visual perception, such as the dorsal lateral geniculate nucleus (dLGN) and superior colliculus (SC)^{99,104}. Additionally, non-M1 ipRGCs light detection is critical for normal spatial vision^{62,108–110}, and can even support rudimentary spatial vision in the

absence of rod/cone function^{99,111}. These effects have been proposed to be mediated by the M4 ipRGC⁶², but to date no study has specifically isolated a non-M1 ipRGC subtype *in vivo*.

To gain access to the individual subtypes and separate their function, recent efforts have attempted to identify unique genetic markers. However, to date, there are only limited genetic markers (Fig. 1.3). One is T-box transcription factor 2 (*Tbr2*), which is expressed in multiple RGC types, including M1 cells that do not project to the SCN and M2 ipRGCs^{106,107}. Removal of *Tbr2* from ipRGCs (*Opn4^{Cre/+}; Tbr2^{fl/fl}*) results in PLR defects, although circadian photoentrainment is intact^{106,107}.

The other major marker for ipRGCs is the transcription factor *Brn3b* (whose official name is POU domain, class 4, transcription factor 2, or *Pou4f2*). *Brn3b* is expressed in many RGC subtypes, including all identified ipRGC subtypes except a small population of M1 cells, referred to as Brn3b-negative M1 ipRGCs^{105,112}. Just like the *Tbr2*-negative M1 ipRGCs, these Brn3b-negative M1 ipRGCs project robustly to the SCN, but have minimal projections to the OPN¹⁰⁵. A genetic mouse model that ablates the Brn3b-positive ipRGCs (*Opn4^{Cre/+}; Brn3b^{DTA/+}*) has a severe loss in PLR, but normal photoentrainment, consistent with their innervation pattern¹⁰⁵. This indicates that Brn3b-positive ipRGCs (of which there are 5 subtypes), are required for the PLR, but Brn3b-negative ipRGCs are sufficient for photoentrainment.

The finding that the Brn3b-negative M1 ipRGCs are sufficient for photoentrainment was the first indisputable connection of a specific RGC subtype to a visual function. The specific roles of the other ipRGCs are yet unclear. This is predominantly due to the fact that the projection patterns of each non-M1 subtype are not

known and they have no known specific genetic differences that can be utilized for ablation or activation of one subtype. Most relevant for this thesis, because many ipRGC subtypes project to the OPN and there are no clear ways to silence or activate a single subtype, it still remains unclear which ipRGCs are involved in the PLR. One suggestion is that the M1 subtype is most relevant due to the moderate loss in PLR after exclusive ablation of the majority of M1 cells⁶⁸.

Retinal connectivity of ipRGCs

The distinct electrophysiological responses to light in ipRGC subtypes is likely due to differences in input from upstream cells. In the retina, the specific lamina in which a cell's dendrites stratify is a strong predictor of connectivity. The axons of each different bipolar cell type (of which there are about thirteen) and amacrine cell (of which there are over forty) terminate in a distinct region of the inner plexiform layer (IPL). Each RGC subtype's dendrites stratify in very precise regions of the IPL, thereby allowing them to connect with specific bipolar and amacrine cell types^{55,113–117}. This precise wiring is what generates the diversity and specificity of light responses in each retinal ganglion cell type. Therefore, determining the specific retinal connectivity of each RGC subtype is a current major goal of visual neuroscientists.

The specific circuits presynaptic to ipRGCs remain largely unknown (Fig. 1.4). The most studied circuitry is that of the M1 subtype, partly because these cells have been studied the longest. M1 ipRGCs are unusual for RGCs: they are ON RGCs that do not stratify their dendrites with the rest of the ON RGCs¹¹⁸. Instead, M1 ipRGCs have their dendrites in the outermost layer of the IPL, where predominantly transient OFF signals are relayed.

This means that M1 ipRGCs likely do not get synaptic input through the traditional ON circuits, despite receiving input from ON bipolar cells¹¹⁸. One proposed mechanism for input to ipRGCs is through ON bipolar cells that make *en passant* synapses with M1 ipRGCs as they pass through the OFF layer of the IPL before terminating with conventional axonal endings in the ON layer¹¹⁹⁻¹²¹. Some ipRGCs are located in the inner nuclear layer (so called ‘displaced ipRGCs’). Because of this, their dendrites cannot pass through the ON layer of the IPL and they receive exclusively *en passant* synapses. Studies of these cells have shown that *en passant* synapses are functional, although their synaptic input is much more transient than for those that are located in the ganglion cell layer¹²⁰, indicating that *en passant* synapses are not the predominant bipolar cell input to M1 ipRGCs.

So how do M1 ipRGCs get bipolar cell input? Early electron microscopic analysis of melanopsin-expressing cells found that they receive ribbon synaptic inputs from bipolar cells on their soma and proximal dendrites¹²². The specific subtype of bipolar cell is yet to be identified, but due to the fact that the connections are on the soma and proximal dendrites, it must be a subtype that terminates deep in the IPL. One possible candidate is the rod bipolar cell, which has been proposed to contact M1 ipRGC soma in rats¹²³. However, this proposal has been controversial because direct rod bipolar cell to retinal ganglion cell synaptic connections are thought to be non-existent in the mammalian retina and could not be confirmed for primate ipRGCs¹¹⁹.

The functional significance of M1 ipRGCs having their dendrites in the outermost layer of the IPL is unclear. It seems unlikely that it would be to receive the *en passant* synapses because M1 ipRGCs receive more robust conventional synapses on their

dendrites and soma in the ON layer. Instead, it appears most likely to me that it is to enhance interactions with the dopaminergic amacrine cells (DACs).

DAC cell bodies are positioned in the inner nuclear layer and send broad axonal projections that stratify in the outermost layer of the IPL (in addition to sending small projections to the photoreceptor layer)^{124–126}. M1 ipRGC dendrites and DAC axons are both anatomically and functionally connected^{127,128}. Of the known inputs to ipRGCs, the anatomical link between M1 cells and DACs is by far the strongest. In fact, the coupling of M1 ipRGCs and DACs appears to be so tight that disrupting the DAC stratification pattern results in concordant disruption in M1 ipRGC dendritic stratification¹²⁹.

The synaptic connection suggests dopamine would affect ipRGC function, though the effect of dopamine on ipRGCs has remained unclear. Dopamine is widely known as a neuromodulator that mediates light adaptation in the rod and cone circuits, enhancing visual acuity and contrast sensitivity¹³⁰. Dopamine levels oscillate with a diurnal rhythm and are high during the day and low at night¹³¹. Dopamine can acutely attenuate the ipRGC photocurrent through a cAMP/PKA pathway^{132,133}. However, long-term dopamine exposure enhances expression of melanopsin¹³⁴. Therefore, it is controversial whether dopamine and its daily variation have any effect on ipRGC function¹³⁵, especially *in vivo*.

As of now, the precise presynaptic circuits to the other ipRGC subtypes remain essentially unknown. The M3 and M5 cells are rare and therefore difficult to identify for study, so to date no studies have investigated their presynaptic circuits. The M2 and M4 cells are more common and easy to identify. M2 ipRGCs in mouse appear to receive input from type 8 cone bipolar cells¹²⁷ and primate ON stratifying ipRGCs (presumed to be homologous to the mouse M2 cells) have synaptic connections with the DB6 ON

bipolar cells¹¹⁹ (although the homology of mouse and primate bipolar cells is a matter of debate⁴⁸).

The M4 ipRGCs are synonymous with the sustained ON alpha RGCs that have a characteristic large soma (hence ‘alpha’) and a highly branched dendritic tree^{62,136}.

Physiologically, ON alpha cells are noted for their high contrast sensitivity and frequency doubling response (‘Y type’ response), suggesting they could contribute to visual contrast detection^{137,138}. In mouse, the ON alpha cells are most closely synaptically apposed to type 6 and 7 ON cone bipolar cells, although this is yet to be functionally tested¹³⁹. In addition, they make a transient synaptic connection with rod bipolar cells in development that is pruned away by adulthood¹³⁹.

Because the PLR likely utilizes many subtypes of ipRGCs, it remains possible that all the diverse synaptic inputs to ipRGCs are capable of driving the PLR. To date, there are no means to specifically silence or activate only one class of bipolar cell, making functional testing impossible. Most importantly, though it is possible that many retinal circuits can drive the PLR, we are likely many years away from the ability to test the relative importance of each circuit.

Melanopsin phototransduction

While ipRGCs can relay synaptic input to the brain, they also possess their own melanopsin phototransduction, which makes them unique among mammalian retinal ganglion cells. Whereas rod and cone phototransduction results in hyperpolarization and graded release of synaptic vesicles, in ipRGCs phototransduction leads to depolarization and action potential generation⁷⁰. This indicates that melanopsin uses a different phototransduction cascade than rods and cones.

The specific G protein cascade that each G protein-coupled receptor preferentially activates is determined by its protein sequence. Early bioinformatic analysis shortly after the discovery of melanopsin identified that it is more similar to the rhabdomeric opsins found in invertebrates than the mammalian rod and cone opsins⁸². Invertebrates such as the horseshoe crab (*Limulus*) and the fruit fly (*Drosophila melanogaster*) also have depolarizing phototransduction cascades¹⁴⁰. Therefore, it was hypothesized that melanopsin phototransduction may be similar to *Limulus* and *Drosophila* phototransduction.

Similar to mammalian rods and cones, *Drosophila* phototransduction is initiated by light-mediated isomerization of 11-*cis*-3-hydroxyretinal to all-*trans*-3-hydroxyretinal. This results in the conformational change in *Drosophila* rhodopsin (*Rh*) and activation of a G_q protein (*dgg*)¹⁴¹. G_q then goes on to activate a phospholipase C (PLC) called *norpA*¹⁴², resulting in the hydrolysis of phosphatidylinositol (4,5)-bisphosphate (PIP₂) into inositol 1,4,5-trisphosphate (IP₃), diacylglycerol (DAG), and a proton. In many systems, IP₃ activates IP₃ receptors on the smooth endoplasmic reticulum (ER) to cause increases in intracellular calcium, but *Drosophila* rhabdomeres lack smooth ER. Instead, phototransduction appears to rely on decreases in DAG in the membrane that cause the opening of a cation channel called transient receptor potential (*trp*) and its homolog transient receptor potential-like (*trpl*)^{143–146}. *trp* and *trpl* open to allow the influx of sodium and calcium and lead to depolarization of the cell.

The melanopsin phototransduction pathway appears to be similar to *Drosophila* rhodopsin, although there are some notable distinctions (discussed at the end). The best evidence comes from studies of mouse mutants that lack *Plcb4* and *Trpc6/7*, the

homologs of *Drosophila norpA* and *trp*. M1 ipRGCs from *Plcb4*^{-/-} or *Trpc6*^{-/-}; *Trpc7*^{-/-} mice display a dramatically reduced (<1%) melanopsin photocurrent to flashes of light *in vitro*¹⁴⁷. This suggests that a PLCβ4-TRPC6/7 pathway accounts for the majority of the melanopsin phototransduction cascade, at least in M1 ipRGCs and to flashes of light (Fig 1.5).

This would indicate that G_q proteins would be required for the activation of PLCβ4. Indeed, melanopsin requires the use of a heterotrimeric G protein¹⁴⁸, though its precise identity is unknown. The mouse genome contains four distinct G_q family members: *Gnaq*, *Gnal1*, *Gnal4*, and *Gnal5*. Transcriptomic analysis of ipRGCs has detected multiple G_q proteins in addition to other heterotrimeric G proteins, although *Gnaq* and *Gnal1* appear to be the most abundant¹⁴⁸⁻¹⁵⁰. In support of *Gnaq* and *Gnal1*, their mRNA knockdown in a rodless/coneless mouse has similar effects on the PLR as knockdown of melanopsin mRNA¹⁵¹. However, *Gnaq*^{-/-}; *Gnal1*^{-/-} double knockout mice displayed no deficits in ipRGC physiology *in vitro* or in melanopsin-dependent behaviors¹⁴⁹. This suggests two possibilities: (1) GNAQ and GNA11 are the predominant G proteins in the melanopsin phototransduction cascade and when they are removed other G_q family genes can compensate or (2) other heterotrimeric G proteins are the capable of driving melanopsin phototransduction in their absence. Future studies of animals lacking all four G_q family genes in ipRGCs will be needed to clarify these differences.

In either case, PLCβ4 appears to provide the predominant drive for the M1 ipRGC photocurrent¹⁴⁷. This suggests that the IP₃/DAG/H⁺ pathway would be important for linking PLCβ4 to the TRPC6/7 channels. As in *Drosophila*, intracellular calcium stores appears to be dispensable for melanopsin phototransduction¹⁵², suggesting a

function for DAG. DAG is membrane-associated, and melanopsin phototransduction proceeds in excised patches of ipRGC membrane¹⁴⁸, implicating DAG or another membrane-associated molecule. However, acute application of DAG to the recording pipette does not induce a current¹⁴⁸ as it does in *Drosophila*. This leaves open the question of the second messenger in ipRGCs.

In *Drosophila*, while the generation of DAG is the key second messenger step, DAG *per se* appears not be critical. Rather, it is the resulting changes in membrane rigidity as well as local acidification from the generation of a proton that are critical^{143,146}. Therefore, the inability to generate a current in ipRGCs from exogenous DAG may be due to the absence of local acidification, but this idea is yet to be tested.

Ultimately, the majority of the current *in vitro* (at least in M1 ipRGCs) is due to TRPC6/7 channels. Of the TRPC family, ipRGCs express primarily TRPC3, TRPC6, and TRPC7. Early studies using pharmacology found that TRPC antagonists effectively blocked the melanopsin photocurrent¹⁵³. However, ipRGCs from individual *Trpc3*^{-/-}, *Trpc6*^{-/-}, or *Trpc7*^{-/-} mice still retained a melanopsin photocurrent (although the current in *Trpc6*^{-/-} ipRGCs was moderately reduced)¹⁵⁴. This suggested that other TRPC channels or TRPC3/6/7 in combination might be required. As addressed previously, M1 ipRGCs in *Trpc6/7*^{-/-} double mutants had virtually no photocurrent and were identical to *Trpc3/6/7*^{-/-} triple mutants¹⁴⁷. While it remains possible that the small residual current is due to another TRPC family member, it is more likely that some other unidentified pathway exists between melanopsin activation and ipRGC depolarization.

The vast majority of accumulated evidence suggests that a G_q-PLCβ4-TRPC6/7 pathway is the predominant phototransduction pathway in ipRGCs. However, a residual

photocurrent persists in the absence of this pathway (that is not present in melanopsin knockout ipRGCs) and to date no behavioral deficits have been reported in G_q , PLC β 4, or TRPC6/7 mutant animals^{147,149}. This suggests that at least one other pathway is capable of generating a current downstream of melanopsin. In support of this, melanopsin *in vitro* is capable of activating a wide variety of signaling pathways^{155,156}. In addition, M1 ipRGCs have been the most widely studied. Other ipRGC subtypes may use distinct phototransduction mechanisms. Each subtype has its own distinct electrophysiological response profile^{99,100,157,158}, implying there may be differences in the phototransduction pathway. The use of a non-conventional phototransduction pathway in non-M1 ipRGCs would explain the lack of PLR deficit in G_q mutant mice because the PLR likely utilizes non-M1 ipRGC input. Future studies, both *in vitro* and *in vivo*, are needed to address the melanopsin phototransduction pathways in other ipRGC subtypes.

The roles of rods, cones, and melanopsin phototransduction in the PLR

Now that it has become well established that ipRGCs are the main outputs from the retina for many non-spatial visual behaviors, it is critical to understand how. The first question is how light information is first detected for non-image forming visual behaviors. ipRGCs could simply serve as relay stations for rod and cone light detection, they could rely almost exclusively on melanopsin phototransduction with little synaptic input, or a combination of the two. The behaviors that are mediated by ipRGCs vary dramatically in their sensitivity, duration, and preference for different wavelengths of light¹⁵⁹, indicating that each behavior likely utilizes distinct photoreceptive mechanisms (and possibly distinct ipRGC subtypes). I will focus this section on the pupillary light reflex, because

its photoreceptive mechanisms have been studied most extensively and because it is the primary focus of my own work.

The pupillary light reflex is a simple visual behavior that is initiated within seconds of light onset (Fig. 1.6). The pupil is large in darkness, rapidly shrinks, and is capable of maintaining constriction indefinitely in continuous light. Its remarkable speed and stability are critical for allowing adaptation of the photoreceptors as well as supporting high visual acuity¹⁶⁰. In fact, the PLR is so critical for normal vision that it is broadly conserved in all major groups with camera eyes and even independently evolved with independent evolutionary arrivals of camera eyes evolved (Fig. 1.6).

The PLR in vertebrates is believed to utilize a simple neural circuit. Light is absorbed by the photoreceptors in the retina, which transduce that energy to electrical information. Light information is relayed from ipRGCs to the midbrain olivary pretectal nucleus (OPN), then to the Edinger-Westphal (EW) nucleus, then to the parasympathetic ciliary ganglion, whose neurons release acetylcholine on the iris muscle, causing pupil constriction⁶⁹. The circuit is generally drawn as a simple linear map, although there are many reasons to believe that it is not as simple as believed, such as the interconnectivity of the OPN and EW, its modulation by cognition and emotions¹⁶¹⁻¹⁶³, and bilateral asymmetry that I will discuss later.

However, I will focus this thesis most extensively on the initial steps of the PLR, the photoreceptors and their immediate synaptic partners. The photoreceptors driving the PLR have been investigated in depth for decades, although much controversy remains. This is likely due to a combination of an incomplete knowledge of the photoreceptors and the imprecise methods used to isolate their relative roles. The relatively recent discovery

of melanopsin (~15 years ago) precluded a full understanding of the photoreceptive mechanisms of the PLR in older studies. However, data from these early studies are still a rich characterization of the PLR under a variety of light conditions.

The PLR has been historically investigated in the most detail in primates including humans by both basic scientists interested in the PLR mechanisms and clinicians who use the PLR for diagnosis of retinal and central nervous system disorders¹⁶⁴. It was also believed to be a reliable readout of general photoreceptor function and was used by vision scientists interested in rod and cone function. We now know that this is not the case: the PLR follows a very specific circuit that may not hold for other rod/cone functions and features a multi-synaptic circuit that filters a lot of the information from rods and cones, preventing the ability of using it as a direct readout of their activity.

The most common techniques for studying the PLR have taken advantage of the distinct light detection and signaling properties of rods and cones. For instance, rods and cones have different absorbance spectra, permitting specific wavelengths of light to be preferentially absorbed by rods or cones. Additionally, they are preferentially located in distinct regions of the primate retina (rods in the periphery, cones in the central retina). Lastly, rods and cones have differences in their speed of signaling: rods are relatively slow and cones are fast. So for instance, a long wavelength, high frequency stimulus delivered to the central retina will much more effectively activate cones than rods. Then, this effect of this stimulus on the PLR can be compared to a stimulus designed to preferentially activate rods.

However, there will always be uncertainty about the physiological suitability of these artificial stimuli. Showing that rods or cones can drive a PLR in response to a stimulus designed to activate them does not answer the question of how the photoreceptors drive the PLR in the environment. As a result, a variety of incompatible models have been proposed over the years, including rod-only models^{165,166}, mixed rod-cone models¹⁶⁷⁻¹⁶⁹, and cone-only models¹⁷⁰⁻¹⁷². Since the discovery of melanopsin, it is now taken into account when designing stimuli and the models have updated to include cone-melanopsin^{173,174} and rod-melanopsin¹⁷⁵. In all cases, there is no consensus model of the role of the different photoreceptors in the PLR.

More recent studies have taken advantage of genetic mutant animals that allow specific manipulation of the photoreceptors. For instance, both mouse models and human subjects that lack the rod and cone photoreceptor function still retain a PLR at bright light intensities with relatively slow kinetics^{74,79,111,176,177}, implicating melanopsin. In converse experiments, melanopsin knockout mice displayed a decrease in maximal pupil constriction at bright light intensities⁸⁷. Collectively, these experiments have unambiguously shown that melanopsin plays a role in the PLR at bright light intensities. Extending these studies to include mouse models that specifically silence either rods or cones is critical for understanding the full retinal control of the PLR.

Recent studies have taken a partial step in this direction using transgenic mouse models that allow better spectral separation of photoreceptor activation. A mouse model that features a cone opsin with greater sensitivity to red light was revealed to have an enhanced PLR in response to red light¹⁷⁸, leading to a model in which cones and melanopsin can recapitulate the entirety of the PLR. Additionally, using UV light to

preferentially activate the short wavelength cones (S cones) in a melanopsin knockout background (*Opn4^{-/-}*) revealed fast fluctuations in pupil size to an oscillating UV stimulus, implying that S cones could drive the PLR¹⁷⁹. Collectively, these studies have led to a model in which cones are the predominant photoreceptors for the PLR^{178,180}. However, this remains to be tested with mouse mutant lines that block rod or cone function.

An alternative approach to manipulating the photoreceptors is descriptive study of the PLR. For instance, the PLR is significantly less sensitive than the sensitivity of rods and is close to the sensitivity of cones, suggesting that cones may be more important for the PLR. However, the PLR is not a simple readout of photoreceptor activity. The OPN is refractory to RGC input at low light intensities¹⁷⁹, suggesting that RGC input needs to be particularly strong for OPN activation and PLR. Additionally, it is unknown how reliable synaptic transmission is in any other part of the PLR circuit.

Instead of using threshold sensitivity, many groups have utilized wavelength sensitivity to determine the photoreceptor input, referred to as an action spectrum. Because each photoreceptor has a distinct peak and pattern of sensitivity to wavelength, the pattern of wavelength sensitivity of the PLR should match that of the photoreceptor that drives it. However, decades of action spectra in a variety of species have not settled on the photoreceptors involved because the results have covered virtually the entire visible spectrum, from peaks that are <400 nm to >560 nm^{168,181,182}. This appears to be predominantly due to inconsistencies in the criteria used to determine sensitivity (e.g. threshold vs. EC₅₀) or the different background intensities (full dark adaptation or varying levels of light adaptation), although it may reflect distinct mechanisms in different vertebrate species.

In conclusion, the specific roles of rods, cones, and melanopsin in the PLR are contentious with decades of history. However, I believe the current availability of mouse mutant models to silence specific photoreceptors types makes the answer within reach, which I will address in Chapter 3 of this thesis.

Intrinsic pupillary light reflex in mammals

In addition to difficulties in separating the roles of rods and cones (and now melanopsin), virtually every previous PLR study in mammals has ignored the possibility of a photoreceptive iris muscle and assumed that the retina drove all PLR. However, the earliest recorded studies of the PLR mechanisms that I am aware of (from the nineteenth century) were conducted in the isolated iris muscle of non-mammalian vertebrates, which is robustly photosensitive *in vitro*^{183–185}. Subsequent studies have implicated a rhodopsin-based phototransduction cascade in iris^{186,187}, although these studies were largely conducted before the age of molecular genetics and sequencing, and rhodopsin has yet to be identified with certainty as the photopigment in non-mammalian vertebrate iris. In fact, one study has proposed that the embryonic chick iris uses cryptochrome-based phototransduction¹⁸⁸.

Despite having an intrinsic PLR, non-mammalian vertebrate iris muscles also receive neuronal input from parasympathetic and sympathetic neurons^{189,190}. Despite this, their intrinsic response is so robust that it is widely assumed that there is very little role for neural input in their PLR¹⁸⁶. This is supported by the fact that many non-mammalian vertebrates have either a very weak or no consensual PLR in the unilluminated eye¹⁹¹, which must be driven solely by the neural circuit. However, this question of intrinsic

versus neuronal input is yet to be addressed in sufficient detail in non-mammalian vertebrates.

Since the discovery of an intrinsic PLR in non-mammalian vertebrates, decades of studies of the mammalian iris muscle failed to find intrinsic phototransduction. This led to the conclusion that the entirety of the mammalian PLR is from a neural mechanism, and precipitated the studies of rods and cones discussed previously. However, recent studies have drawn attention to the fact that many mammalian species (including mouse) have a photosensitive iris muscle, which is capable of driving an intrinsic PLR both *in vitro* and *in vivo*^{147,192–195}.

It is not clear why animals would use both a neural circuit and intrinsic phototransduction for the PLR. One proposed reason is to allow animals to maintain pupil constriction at bright light intensities at which the pupil is so small that it allows very little light to reach the retina¹⁴⁷. Additionally, intrinsic iris phototransduction has been proposed to enhance pupil constriction on the side of the body exposed to brighter light (referred to as bilateral asymmetry)¹⁴⁷. Because the PLR uses brain circuitry, it allows light information from one retina to reach both eyes. Therefore, there is both a ‘direct PLR’ on the illuminated side and a ‘consensual PLR’ on the unilluminated side. However, the direct PLR in mouse is more sensitive than the consensual PLR¹⁴⁷. This bilateral asymmetry is thought to arise because the brain circuitry presumably activates both iris muscles similarly and activation of the iris muscle on the illuminated side enhances pupil constriction¹⁴⁷. While this bilateral asymmetry does not exist in humans¹⁹⁶, it would be especially valuable for species that have laterally placed eyes such as mouse. To date, the mechanisms mediating bilateral asymmetry in the PLR are unknown.

It was recently identified that the mouse iris muscle uses melanopsin for phototransduction¹⁴⁷. However, melanopsin in the iris muscle appears to use a slightly different phototransduction cascade than in ipRGCs. In iris, melanopsin drives an intracellular calcium pathway, whereas ipRGC melanopsin uses a TRPC6/7 transduction cascade (as covered earlier)¹⁴⁷. Additionally, in support of the idea that the iris muscle mediates bilateral asymmetry in the PLR and is critical for maintaining the PLR in bright light, melanopsin knockout mice have a weaker PLR bilateral asymmetry than wildtype¹⁴⁷ and do not achieve full pupil constriction at bright light intensities^{87,147}. However, the role of melanopsin in the iris muscle and retina for the PLR has yet to be disentangled.

In summary, the PLR is a critical visual behavior, but its precise photoreceptive mechanisms have been surprisingly difficult to settle. This is both due to experimental inconsistencies as well as imprecise techniques for isolating a single photoreceptor type. In this thesis, I have attempted to resolve these issues by using a variety of specific mutant mouse lines, pharmacology, chemogenetic tools, transsynaptic viral tracing, and surgical techniques to reveal the photoreceptors and circuits in the PLR and to quantify their contributions.

Contents of this thesis

This thesis is based on my work studying the mechanisms of the pupillary light reflex (PLR) in mouse. Despite being an apparently simple behavior, its cellular and circuit mechanisms have remained unclear for decades. In the data presented here, I have focused on the first steps in the PLR: (1) whether light is detected primarily by the iris

and/or retina, (2) what specific photoreceptors in the retina are utilized, and (3) the retinal circuits connecting the rods/cones to ipRGCs to drive the PLR.

Chapter 2 addresses the relative roles of iris and retina phototransduction in driving the PLR. I will show that in mice, the retina drives virtually all PLR, with minimal contribution from iris phototransduction. I will show that this is due to melanopsin expression in the iris at low levels and in a small number of cells. I will then show that the retina drives the PLR using a bilaterally asymmetric brain circuit mediated by the Brn3b-positive ipRGCs.

Chapter 3 is then focused on which retinal photoreceptors are critical for the PLR. I will show that despite common beliefs, cones are only minimally involved in the PLR due to their rapid light adaptation. Instead, I will show that rod function is both necessary and sufficient for the full sensitivity of the PLR. At bright light intensities, I will show that melanopsin phototransduction augments rod input to the PLR to stabilize pupil size.

Chapter 4 then addresses the retinal circuits connecting rods to ipRGCs to drive the PLR. I will show that viral circuit tracing techniques identify the rod bipolar cell as presynaptic to ipRGCs, despite a general belief that rod bipolar cells do not contact RGCs. I will then show that rods drive the PLR using an ON bipolar cell that does not require the conventional rods circuits, implicating a functional role for the rod bipolar cell to ipRGC circuit in the PLR.

Chapter 5 takes a slight divergence from studies of the PLR. There, I address the retinal circuit mechanisms that allow light to acutely control body temperature and general activity. I find that Brn3b-positive ipRGCs, using their melanopsin phototransduction cascade, mediate the acute effects of light on body temperature.

These studies provide thorough coverage of the initial steps in the PLR, from the detection by the photoreceptors to output circuits from the retina.

Figures

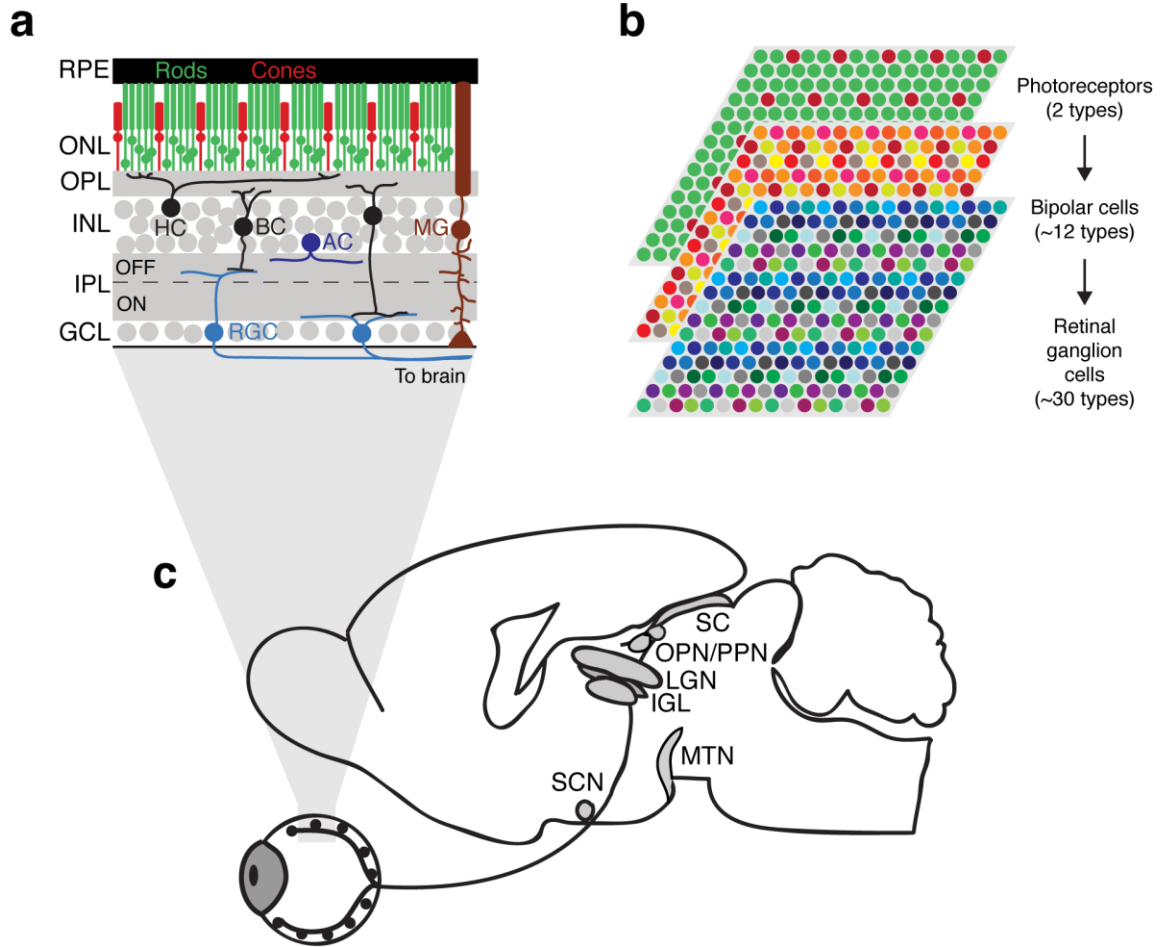


Figure 1.1: Basic structure of the visual system.

(a) The major cell types of the retina, including the rods and cones in the outer nuclear layer (ONL). Rods and cones form synaptic connections with horizontal cells (HC) and bipolar cells (BC) in the outer plexiform layer (OPL). Horizontal cells and bipolar cells have their cell bodies in the inner nuclear layer (INL) with the amacrine cells (AC). Bipolar cells and amacrine cells form synapses with retinal ganglion cells (RGC) in the inner plexiform layer (IPL). Retinal ganglion cells have their cell bodies in the ganglion cell layer (GCL) and send their axons to the brain. Müller glia (MG) extend along all three layers of the retina and are supporting cells. (b) A diagrammatic flow of visual information shows the progressively complex transformation of visual information from photoreceptors to bipolar cells to RGCs. (c) The major RGC projections to the brain, including the suprachiasmatic nucleus (SCN), lateral geniculate nucleus (LGN) and intergeniculate leaflet (IGL), olivary and posterior pretectal nuclei (OPN and PPN), superior colliculus (SC), and medial terminal nucleus (MTN). Note: there are many other minor projections from RGCs as well as a few major projections encompassing the accessory optic system that could not be added for space reasons.

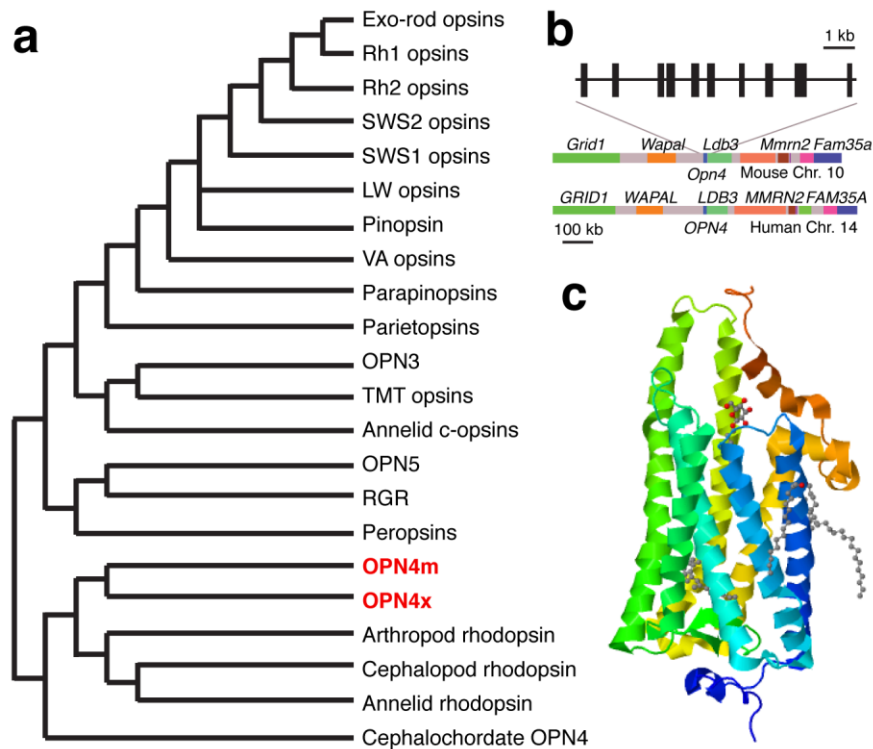


Figure 1.2: Evolutionary and genomic relationships of melanopsin.

(a) Evolutionary tree of opsin genes in animals. Melanopsin families cluster with the invertebrate opsins and are distantly related to the rod and cone opsins. Tree is adapted from Davies et al. 2010¹⁹⁷. Note: the branch lengths are of arbitrary distance, tree only show qualitative relationships. (b) Chromosomal synteny between mouse chromosome 10 and human chromosome 14, the chromosomes that contain melanopsin. The expanded view shows the gene structure of mouse melanopsin displaying exons as black bars. Both chromosome and gene structure are based on NCBI Gene Database gene ID 30044 and 94233. (c) Crystal structure of a C-terminal truncation of rhodopsin from the Japanese flying squid (*Todarodes pacificus*). Melanopsin structure is assumed to be highly similar, but no structure of melanopsin has been reported to date. Extracellular surface (N-terminus) is oriented downwards and intracellular surface (C-terminus) is oriented upwards. Structure is reprinted from the RCSB Protein Data Bank (ID: 2Z73) as originally published from Murakami and Kouyama 2008¹⁹⁸.

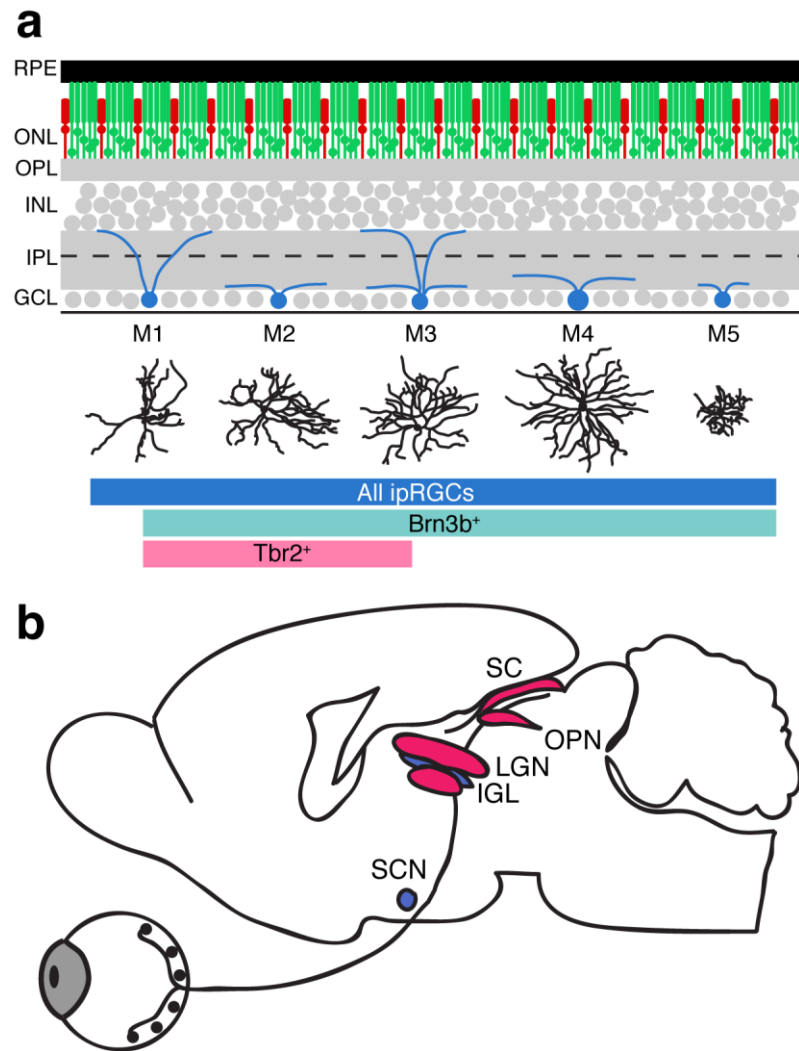


Figure 1.3: Diversity and central projections of ipRGCs.

(a) ipRGCs are located in the ganglion cell layer (blue) and comprise at least 5 distinct subtypes: M1–M5. Subtypes can be classified morphologically by soma size, dendritic morphology (including total dendrite length and dendritic field area) and stratification depth. Additionally, subtypes can be partially separated genetically by the expression of *Brn3b* (all subtypes except SCN-projecting M1 cells) and *Tbr2* (M1, M2, and M3, except SCN-projecting M1 cells). Above: vertical sections of the retina in cartoon form. Below: Whole-mount tracings of the entire dendritic tree of actual mouse ipRGC subtypes to relative scale^{70,99}. (b) Cartoon depicting prominent central targets of ipRGCs, including brain areas mediating circadian functions (SCN and IGL), midbrain regions involved in reflexive behaviors (OPN and SC), and image-forming centers (LGN). Areas receiving

predominantly M1 innervation are colored blue, while areas receiving predominantly non-M1 innervation are in red. Abbreviations: SCN- suprachiasmatic nucleus, IGL- intergeniculate leaflet, OPN- olivary pretectal nucleus, SC- superior colliculus, LGN- lateral geniculate nucleus. Model is based on Hattar et al.⁸⁴; please see this paper for details on more central projections.

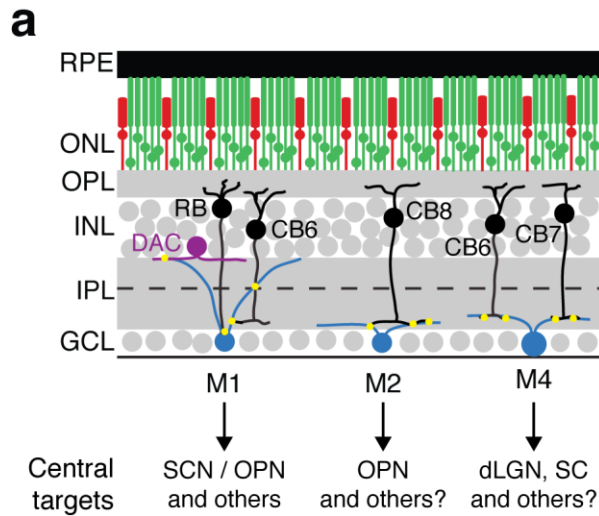


Figure 1.4: Distinct inputs and outputs to different ipRGC subtypes.

Each ipRGC subtype receives distinct input from the inner retina and sends that information to distinct brain regions. M1 ipRGCs are proposed to receive input from rod bipolar cells (RB) on their soma, type 6 cone bipolar cells (CB6) on their dendrites, and dopaminergic amacrine cells (DAC) on their distal dendrites. M1 ipRGCs then project to at least the SCN, and then send axonal collateral projects to the OPN or almost a dozen other regions (Diego Fernandez, Shih-Kuo Chen, unpublished data). M2 ipRGCs are believed to get input from type 8 cone bipolar cells (CB8), although their outputs are less clear. They at least project to the OPN and not the SCN, but it is unknown if they project elsewhere as well. The M4 ipRGCs receive input from type 6 and type 7 cone bipolar cells (CB6 and CB7) on their dendrites and then project to at least the dLGN and SC, although they may project other places as well.

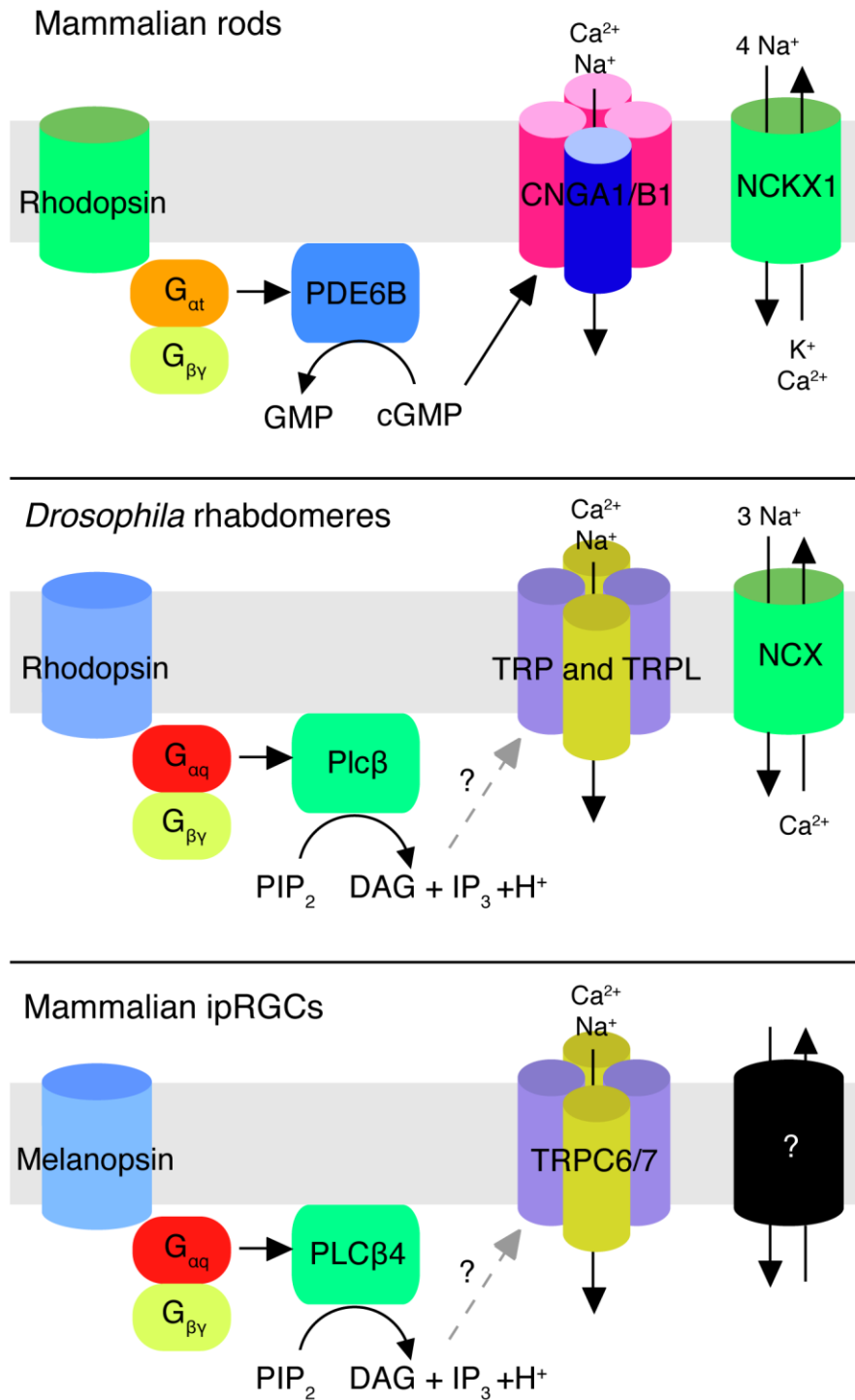


Figure 1.5: Phototransduction in ipRGCs closely resembles *Drosophila* rhabdomeres.

Comparison of phototransduction in mammalian rods, *Drosophila* rhabdomeres, and mammalian ipRGCs. Mammalian rods use a G_i pathway and a cyclic nucleotide-gated channel (CNGA1/B1) to hyperpolarize in response to light. Both *Drosophila* rhodopsin and mammalian melanopsin use a G_q pathway and a transient receptor potential (TRP) channel to depolarize in response to light. While both mammalian rods and *Drosophila* rhabdomeres are known to utilize a calcium exchanger to reset the resting calcium concentration in the cytoplasm following phototransduction, no such channel has yet been investigated in ipRGCs, though it is believed to be present.

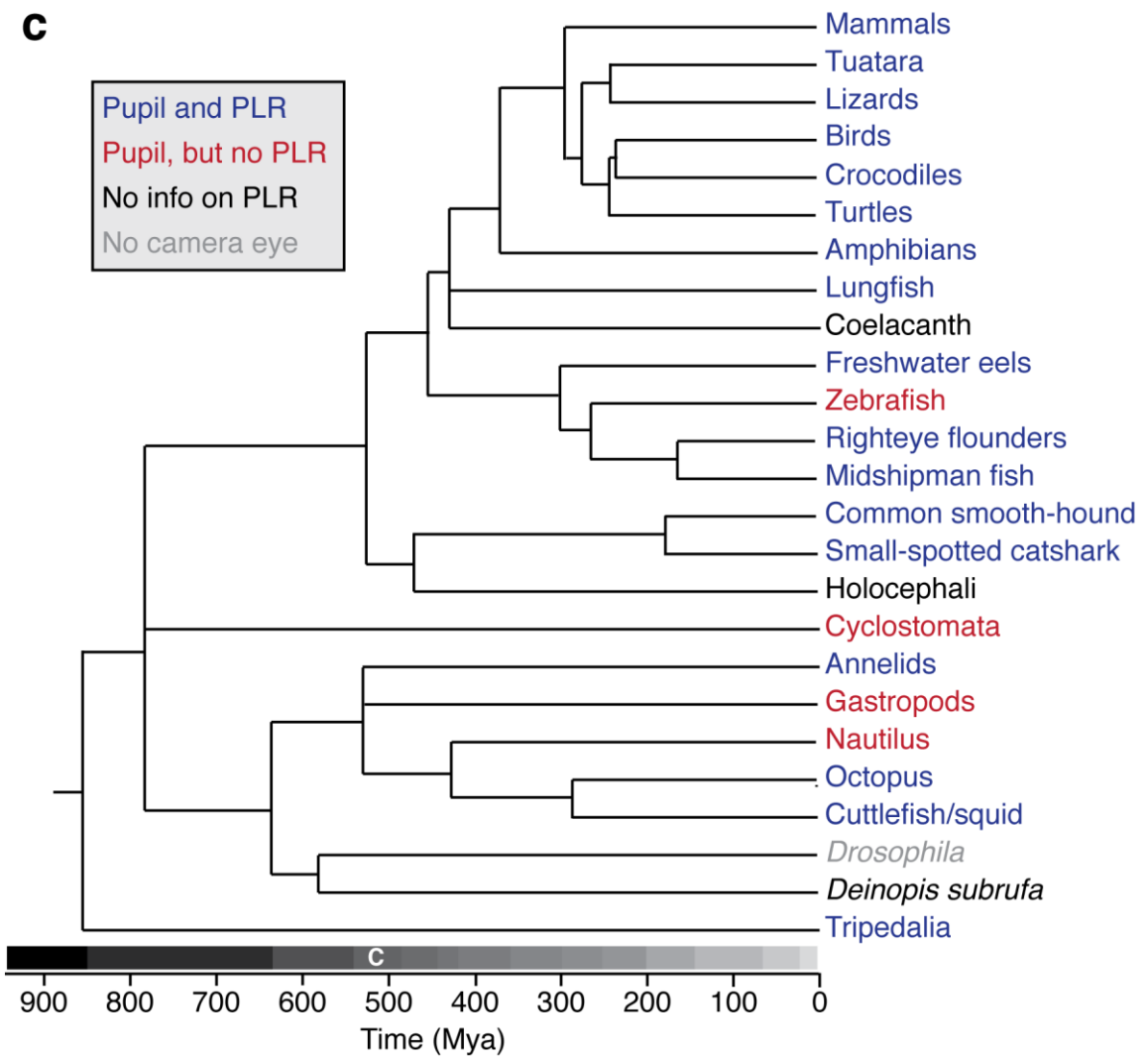
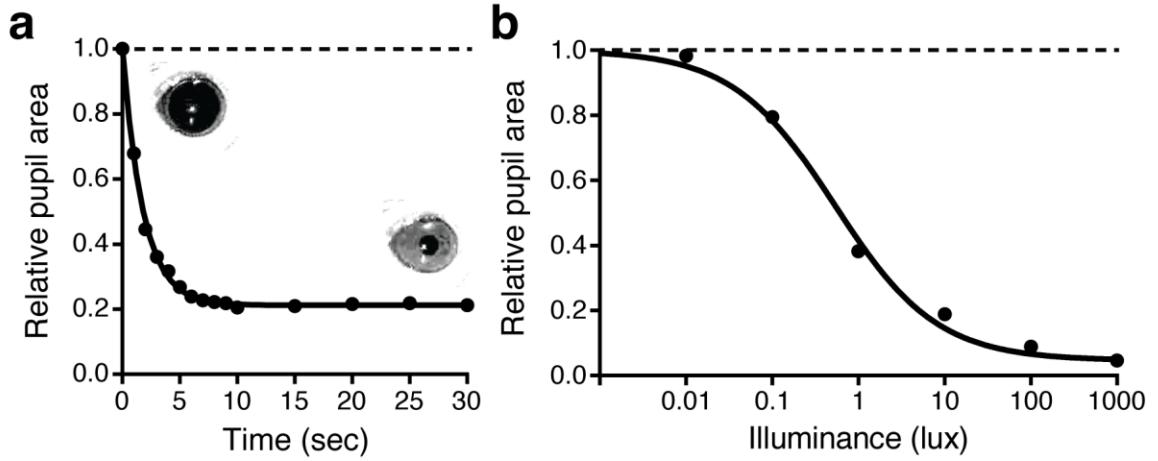


Figure 1.6: Characteristics and evolutionary conservation of PLR.

(a) The PLR is initiated rapidly, within one second, and stable for the entirety of a 30-second light pulse (shown here is a 10 lux stimulation). Data is shown as a relative size to the resting pupil size in darkness. (b) The PLR is tuned to the precise environmental light intensity, with greater constriction at higher light intensities. (c) An evolutionary tree showing the presence or absence of the pupil and PLR in a variety of animals. Many animals with a camera eye have a pupil that can be modulated by light (blue), while some have lost the ability to modulate the pupil size with light (red), some have a camera eye but there is no available information on whether there is a pupil or PLR (black), or have no camera eye (gray). Note that when a camera eye has evolved independently from the lineage that gave rise to mammals—as in both octopus and *Tripedalia*—a PLR has also evolved with it. This highlights the broad utility of the PLR in regulating the light reaching the retina. The distance on the x-axis is the median estimated evolutionary distance from TimeTree.org. Each gray/black box represents a different epoch in Earth’s geological history. The C represents the Cambrian period.

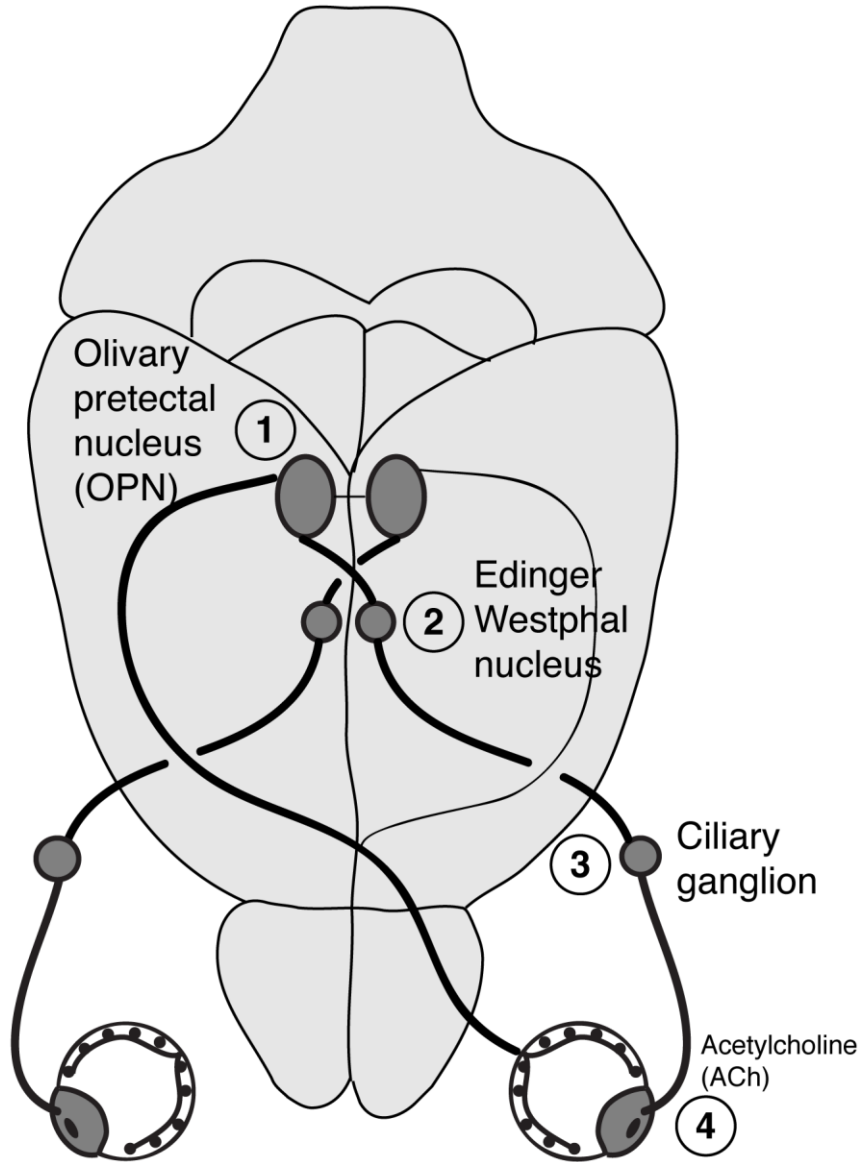


Figure 1.7: Light activation of one eye travels bilaterally through PLR brain circuitry.

The PLR is initiated by activation the retina, which sends information to both the ipsilateral and contralateral OPN (1), though ipsilateral projections in mouse are minor, which then send information to both the opposite OPN as well as to the contralateral Edinger Westphal nucleus (2). From the Edinger Westphal are projections to the ciliary ganglion (3), which are parasympathetic neurons sending cholinergic projections to the iris muscle (4). This brain circuitry allows activation of both iris muscles from the

activation of one retina. Note: the relative strengths of most inputs are unknown and are drawn as lines of the same thickness.

Chapter 2

Differentiating the contributions of retina and iris phototransduction to controlling pupil size

This chapter is based on a manuscript in revision:

Rupp AC, Schmidt TM, Bray ER, Somasundaram P, Hiriyanna S, Yungheer BJ, Tufford A, Cui Y, Simon MI, Wu Z, Badea TC, Robinson PR, Cayouette M, Wess J, Birnbaumer L, Park KK, Hattar S. Melanopsin-expressing cells of the retina, not iris, mediate the pupillary light reflex.

Abstract

Vertebrates possess multiple photosensitive tissues that integrate their intrinsic photosensitivity with neuronal input about the light environment. The iris muscle controls pupil size via the pupillary light reflex (PLR), integrating its intrinsic melanopsin-based photosensitivity with extrinsic neuronal input originating in the retina. However, how iris and retina light detection are coordinated for the PLR is essentially unknown. We report here that the mouse PLR predominantly utilizes retina input from melanopsin-expressing intrinsically photosensitive retinal ganglion cells (ipRGCs). We uncover that ipRGCs utilize a bilateral asymmetric brain circuit. In contrast, very few cells in the iris express melanopsin, making the mouse intrinsic PLR extremely insensitive with no apparent contribution to the PLR. Animals lacking melanopsin phototransduction specifically in the retina have similar deficits in the PLR as global melanopsin knockout. In contrast, animals with melanopsin expression exclusively in ipRGCs display a normal PLR. These results identify melanopsin-expressing ipRGCs of the retina as the specific source of light detection for the PLR.

Introduction

Vertebrates utilize environmental light information to regulate many physiological functions such as alignment of circadian rhythms to the light/dark cycle, control of pupil size, and seasonal modulation of reproduction. Light detection is mediated by a variety of tissues throughout the body, most famous among them the retina, pineal gland, parietal eye, and iris muscle^{147,192,193,199–203}. In addition to being light sensitive, all of these tissues also receive light information from neuronal input^{189,199,204,205}. However, the contributions of intrinsic versus neuronal light detection to their physiological functions remain a mystery.

In mammals, the situation is simpler, with only confirmed two photosensitive tissues: the retina and iris muscle (notwithstanding other disputed claims^{206,207}). Retina and iris light detection both result in a reduction in pupil size, referred to as the pupillary light reflex (PLR). The iris muscle must integrate light information from both sources to precisely control pupil size for high visual acuity¹⁶⁰. Additionally, unlike circadian photoentrainment or seasonal behaviors, the PLR is rapidly initiated and can be easily quantified. Therefore, we reasoned that the mammalian PLR is a useful model for addressing the roles of intrinsic versus neuronal input in regulating a specific visual function.

While the intrinsic drive to the PLR is relatively well characterized in aquatic animals such as amphibians and fish^{185–187,208}, much less is known about the mammalian intrinsic PLR. In fact, until recently it was widely believed that mammals possessed no intrinsic PLR and that all of their PLR is driven by the retina-brain circuitry¹⁸⁹. Despite

this, a few studies have observed light-mediated contraction of the mammalian iris muscle *in vitro*^{147,192–195} as well as a neuronal-independent PLR *in vivo*^{147,193,194}.

A recent breakthrough was the identification of melanopsin as the photopigment mediating the iris intrinsic PLR in mice¹⁴⁷. Melanopsin has previously been characterized as the photopigment in the intrinsically photosensitive retinal ganglion cells (ipRGCs) that mediate the retinal input to the PLR^{79,82,83,87,95,97}. Melanopsin is critical for the PLR: melanopsin knockout mice lack the ability to achieve full pupil constriction in response to bright light^{87,147}. However, the expression of melanopsin in both iris and retina makes it difficult to interpret how melanopsin controls pupil size.

One hypothesized function for melanopsin phototransduction in the iris is mediating bilateral asymmetry in the PLR. Light presented to one eye drives both a direct PLR in the illuminated (ipsilateral) eye and a consensual PLR in the unilluminated (contralateral) eye. The direct PLR in mice is more sensitive than the consensual PLR¹⁴⁷, although the mechanisms underlying this asymmetry are unclear. It has recently been proposed that if the iris has an intrinsic phototransduction cascade and the output of the PLR brain circuitry were equal to both eyes, the intrinsic PLR of one eye would sum with the neuronal input to enhance constriction on the illuminated side¹⁴⁷. In support of this model, melanopsin knockout mice have a weaker PLR bilateral asymmetry than wildtype¹⁴⁷. However, the separation of melanopsin function in the retina and iris is critical for interpreting these results.

Here, to address the relative roles of the retina and iris phototransduction in the PLR and in driving its bilateral asymmetry, we used a variety of approaches to isolate only the intrinsic or only the retina-brain input. We find that the mouse PLR appears to

be exclusively mediated by the retina. A subpopulation of ipRGCs is both necessary and sufficient for the bilateral asymmetry of the PLR using the brain circuitry. In contrast, we find that very few cells in the iris muscle express melanopsin at a very low level. This results in extreme insensitivity of the intrinsic PLR that is neither necessary nor sufficient for normal PLR function. Removing melanopsin phototransduction specifically from the retina results in a loss in maximal pupil constriction, whereas rescue of melanopsin specifically in the retina of melanopsin knockout mice restores maximal pupil constriction. These data indicate that melanopsin phototransduction in the retina, not iris, is critical for its role in the PLR.

Results

The intrinsic PLR operates exclusively at very bright light intensities

We first wanted to identify the sufficiency of the intrinsic PLR by isolating the intrinsic PLR from neuronal input *in vivo*. To do so, we performed either unilateral optic nerve transection to remove output from the retina to brain or atropine application to block parasympathetic input to the muscarinic acetylcholine receptors on the iris (Fig. 2.1a). Following optic nerve transection, we observed a severe loss in the PLR of the illuminated eye (direct PLR), with only weak and incomplete pupil constriction at very bright light intensities (Fig. 2.1b), resulting in a dramatic decrease in sensitivity (mean EC_{50} for Control eye = 10.9 log photons/cm²/s, Transection = 15.8 log photons/cm²/s; $P < 0.001$, paired two-tailed t test). We confirmed that optic nerve transection successfully blocked output from the retina and atropine blocked input to the iris, as assessed by a lack of consensual PLR (data not shown). Similar to optic nerve transection, acute application

of atropine also resulted in a dramatic loss in PLR sensitivity (Fig. 2.1c; mean EC_{50} for PBS = 10.7 log photons/cm²/s, Atropine = 16.7 log photons/cm²/s; $P < 0.001$, paired two-tailed t test) and only partial pupil constriction. The sensitivities measured here are very similar to the intrinsic PLR sensitivities of mice and other mammals *in vitro*¹⁴⁷, and in total indicate that the intrinsic PLR is extremely insensitive compared to the retina-brain input. Even at light intensities corresponding to sunlight (≥ 16 log photons/cm²/s), the intrinsic PLR only drives the equivalent amount of pupil constriction as that driven by the retina-brain circuitry by moonlight (~ 11 log photons/cm²/s).

We then genetically isolated the intrinsic PLR by measuring the PLR of mice lacking the two major G_q-coupled muscarinic acetylcholine receptors (mAChR) on the iris muscle (M1 and M3 mAChRs). Mice lacking the M3 mAChR alone (*Chrm3*^{-/-}) have no PLR at moderate light intensities (Fig. 2.2a, 13.0 log photons/cm²/s), but retain an incomplete PLR at bright light intensities (Fig. 2.2a, 15.4 log photons/cm²/s), as previously reported²⁰⁹. However, M1/M3 mAChR double mutants (*Chrm1*^{-/-}; *Chrm3*^{-/-}) had no measurable PLR at bright light intensities (15.4 log photons/cm²/s) (Fig. 2.1d), indistinguishable from atropine treatment (Fig. 2.1c). These results demonstrate that the PLR acts predominantly through cholinergic signaling to M1/M3 mAChR in the iris. Collectively, isolating the intrinsic PLR through surgical, pharmacological, or genetic means, we find that the intrinsic PLR only partially constricts the pupil, and only at extremely bright light intensities at which the PLR in intact animals has reached saturation, suggesting that the intrinsic PLR does not contribute to the PLR when the retina-brain circuit is intact.

Limiting amounts of melanopsin in the iris muscle

We hypothesized that low melanopsin levels in iris could contribute to the observed insensitivity of the intrinsic PLR. To test this, we performed immunofluorescence for melanopsin in albino mouse iris. While we observed a robust signal compared to our no primary antibody control (Fig. 2.3a,b), this signal persisted in melanopsin knockout iris despite a complete absence of the melanopsin protein (Fig. 2c–f), suggesting that melanopsin protein is at levels that are undetectable over background.

Due to the undetectable levels of melanopsin, we mated melanopsin-Cre mice (*Opn4^{Cre}*) to a ubiquitous fluorescent reporter under a general promoter (*ROSA^{Synaptophysin-tdTomato}*) to permanently label iris cells that have ever expressed melanopsin (Fig. 2.4a). We observed that a tiny fraction of cells in the iris sphincter muscle were tdTomato-positive (Fig. 2.4b,c: occupying $\sim 1.7\% \pm 0.5\%$ (SEM) of the total iris sphincter area; 7.0 ± 2.0 (SEM) total cells per iris sphincter muscle, $n = 4$ mice), in marked contrast to the dense tdTomato labeling in the retina (Fig. 2.4d). Unexpectedly, we also saw many cells in the iris dilator muscle labeled (Fig. 2.4e)—always more than in the sphincter—which is counterintuitive because activation of the dilator muscle leads to pupil dilation. This suggests that a combination of very low levels of melanopsin in the iris, very few cells in the iris sphincter expressing melanopsin, and expression of melanopsin in the iris dilator could contribute to the extreme insensitivity of the intrinsic PLR.

This suggests that melanopsin levels could contribute to the intrinsic PLR sensitivity. To test this, we compared the intrinsic PLR in wildtype mice (2 copies of melanopsin) to melanopsin heterozygous mice (1 copy of melanopsin) and melanopsin knockout mice (0 copies of melanopsin). We show partial disruption of the PLR in

melanopsin knockout mice (*Opn4*^{-/-}) after vehicle treatment (PBS, Fig. 2.4f) and a complete absence of the direct PLR following atropine treatment (Atropine, Fig. 2.4g), because melanopsin is required for the intrinsic PLR^{147,194}. Intriguingly, we found that the intrinsic PLR following atropine application was essentially eliminated in melanopsin heterozygous mice (*Opn4*^{+/-}) that still retain one copy of the melanopsin gene (Fig. 2.4g). Importantly, these mice had a normal PLR in the absence of atropine administration (PBS, Fig. 2.4f), demonstrating that the intrinsic PLR is dispensable for normal PLR function. Collectively, these data suggest that melanopsin is present at limiting amounts in the iris muscle and that the intrinsic PLR may not contribute to the magnitude of the PLR.

Modulation of the strength of the intrinsic PLR

A previous report found that blockade of all neural firing in the eye resulted in an enhancement of the intrinsic photosensitivity¹⁴⁷. Therefore, we wondered how the neural circuit could affect the intrinsic PLR. To test this, we blocked the neuronal input to the iris muscle for 7 days using atropine. Following daily atropine administration, we observed an enhancement of the direct PLR every day, although it never reached levels in the vehicle-treated eye (Fig. 2.5a). This suggests that animals have a mechanism to measure the amount of input to the iris and can adapt accordingly to strengthen the intrinsic PLR.

To determine if atropine is interpreted as loss of input to the iris or loss of output from the retina, we performed unilateral optic nerve transection and followed the response of the direct PLR for seven days. To our surprise, the injured eye did not show enhancement of PLR, but instead rapidly lost the direct PLR within 3–4 days of transection (Fig. 2.5b), opposite to the effect of atropine. This decay in response also

occurred following optic nerve crush, indicating that this result is not specific to one method of blocking retinal output (Fig. 2.6). Additionally, to be sure that this effect is specific to the iris muscle phototransduction and is not non-specifically modulating the PLR, we performed the daily atropine administration in melanopsin knockout animals and never saw a PLR (Fig. 2.7). This suggests a complex interplay between the retina-brain circuitry and the intrinsic PLR to modulate its strength.

While optic nerve transection and atropine administration both isolate the intrinsic PLR from the neural circuitry, they do so through opposite means. Optic nerve transection blocks output from the transected eye, while atropine administration blocks input to the treated eye. This means that for the seven days of treatment, the iris of the transected eye received neuronal input from the contralateral eye, whereas the iris that was treated with atropine received no input from either eye.

To determine the epistatic relationship between optic nerve transection and atropine treatment, we performed optic nerve transection with or without daily atropine administration. Treatment with atropine following optic nerve transection resulted in a slowly enhanced direct PLR, opposite to transection plus vehicle treatment (Fig. 2.5c). This suggests that the loss of all input to the iris is capable of altering the sensitivity of the intrinsic PLR, even when loss of retinal output would normally attenuate the intrinsic PLR. These experiments show that mice may possess mechanism(s) to detect the strength of input from the PLR brain circuitry and modulate the intrinsic PLR in accord.

Melanopsin phototransduction in the retina, but not iris, is required for the PLR

Melanopsin is required for maximal PLR at bright light intensities, but not lower light intensities^{87,147}. However, it is unknown if melanopsin in the iris or retina is

responsible. It has been suggested that iridic melanopsin would be particularly important for driving the PLR at bright light intensities when a small pupil would limit the total light reaching the retina¹⁴⁷. To determine if the PLR at bright light intensities requires melanopsin in retina or iris, we took advantage of the fact that melanopsin in the retina and iris use distinct phototransduction pathways: Melanopsin in the M1 subtype of ipRGCs that is most important for the PLR⁹⁵ predominantly utilizes a G_q-PLCβ4-TRPC6/7 pathway, while melanopsin in the iris utilizes a G_q-PLCβ4-intracellular calcium pathway¹⁴⁷ (though the requirement for G_q in iris and retina remains presumed but unproven)¹⁴⁹ (Fig. 2.7a). *Plcb4*^{-/-} mice have severely diminished phototransduction in both iris and M1 ipRGC phototransduction, whereas *Trpc6/7*^{-/-} mice have normal iris phototransduction, but essentially no M1 ipRGC phototransduction¹⁴⁷. Therefore, *Plcb4*^{-/-} mice should phenocopy global melanopsin knockout, whereas *Trpc6/7*^{-/-} mice are tissue-specific knockouts of melanopsin phototransduction in the retina.

We confirmed that global melanopsin knockout mice (*Opn4*^{-/-}) display a deficit in maximal direct PLR (Fig. 2.8b), as previously reported¹⁴⁷. However, it should be noted that the maximal pupil constriction deficit is small, showing that even rod/cone input through ipRGCs can largely compensate for the loss of melanopsin in both retina and iris. Surprisingly, we found that *Plcb4*^{-/-} mice appeared to have a deficit in maximal constriction that was less severe than melanopsin knockout (Fig. 2.8c), though it is statistically indistinguishable (*Plcb4*^{-/-} v. *Opn4*^{-/-}: $P = 0.070$ by two-tailed t test). In contrast, *Trpc6/7*^{-/-} mice display a deficit in maximal direct PLR that appears identical to melanopsin knockout (Fig. 2.8d; *Trpc6/7*^{-/-} v. *Opn4*^{-/-}: $P = 0.156$ by two-tailed t test). These mouse lines had previously been tested *in vitro* for melanopsin phototransduction

in retina and iris¹⁴⁷, making these results the first *in vivo* evidence of the specific components of the melanopsin phototransduction pathway. Importantly, *Trpc6/7*^{-/-} mice retain an intrinsic PLR after atropine treatment similar to control animals (Fig. 2.9a). This result indicates that melanopsin in the retina is specifically required for driving a maximal PLR, even in the presence of iris phototransduction.

In a converse experiment, we removed melanopsin from the iris but retained it in the retina. To do so, we infected the retina of melanopsin knockout mice (*Opn4*^{Cre/Cre}) with an AAV that expresses melanopsin in a Cre-dependent manner (Fig. 2.8e, AAV-DIO-mRuby-P2A-Opn4). We confirmed that the virus did not infect the iris muscle (Fig. 2.8e) and that the intrinsic PLR was still lacking after melanopsin restoration in the retina (Fig. 2.9b), demonstrating that this method specifically restores melanopsin in the retina while leaving melanopsin absent from the iris. Following restoration of melanopsin in ipRGCs of one retina, we observed a full rescue of the direct PLR compared to the opposite, uninfected eye (Fig. 2.8f). This provides further evidence that removal of iris phototransduction has no effect on the PLR. Importantly, exogenous melanopsin expression did not enhance the sensitivity of the PLR, because we saw no differences in PLR at lower light intensities (Fig. 2.8g). To test the hypothesis that iridic melanopsin is important for maintaining small pupil sizes across the day¹⁴⁷, we monitored the pupil size of mice with melanopsin rescued in the retina (*Opn4*^{Cre/Cre} with AAV-DIO-Opn4) under bright light across the day. We found that melanopsin's exclusive presence in the retina is capable of maintaining small pupil sizes for at least twelve hours in bright light (Fig. 2.9c). Collectively, our results indicate that melanopsin-expressing ipRGCs are the

primary drivers of the PLR, while iris phototransduction is dispensable for the PLR even at bright light intensities.

Brn3b-positive ipRGCs are required for PLR bilateral asymmetry

One proposed function of iris phototransduction is to generate bilateral asymmetry in the PLR (i.e. greater constriction on the illuminated side)¹⁴⁷. However, our experiments thus far have shown that the retina represents the predominant input to the PLR, raising the possibility that instead, the retina mediates bilateral asymmetry in PLR.

To test if ipRGCs alone could mediate bilateral asymmetry in the PLR, we sought to activate only the ipRGCs without activating the iris. To do so, we infected one retina of melanopsin-Cre mice (*Opn4^{Cre/+}*) with an adeno-associated virus that expresses a Cre-dependent G_q-coupled DREADD (AAV-DIO-hM3D(G_q)-mCherry), restricting expression to ipRGCs. Importantly, the virus did not infect the iris muscle (Fig. 2.10a), allowing us to activate only the ipRGCs of one retina in darkness using the selective DREADD agonist clozapine N-oxide (CNO)²¹⁰ and observe pupil constriction in both eyes. After infection, we saw the expression of mCherry in multiple subtypes of ipRGCs, including Brn3b-negative ipRGCs and M1 ipRGCs (Fig. 2.11 a–e), though M1 ipRGCs appeared to express mCherry at the lowest level.

Following intraperitoneal injection of CNO, we observed robust pupil constriction in both eyes, with greater constriction on the infected side (Fig. 2.10b), indicating that ipRGCs alone can drive bilateral asymmetry in PLR. To confirm that this effect is not due to the presence of melanopsin in the iris, we performed the same experiment in melanopsin knockout mice (*Opn4^{Cre/Cre}*) and again observed robust bilateral asymmetry in PLR by activating the retina alone (Fig. 2.11f).

Recently, we and others have proposed that ipRGCs might mediate the direct PLR independent of the brain^{194,195,211,212} to drive bilateral asymmetry. This is based on several observations: (1) a subpopulation of ipRGCs survives optic nerve transection²¹³ (Fig. 2.12a–c), (2) ipRGCs located in the retinal periphery send projections into the ciliary body/iris complex¹⁹⁴ (Fig. 2.12d) and not to the optic disc²¹⁴, (3) the intrinsic PLR slowly degrades over seven days following optic nerve transection (Fig. 2.5b) or optic nerve crush (Fig. 2.6), and (4) the intrinsic PLR is defective in animals lacking rod phototransduction¹⁹⁵.

To address this direct retina to iris connection, we performed several experiments: First, we again expressed a G_q-coupled DREADD in ipRGCs and showed that the pupil constriction in response to CNO was absent following either optic nerve transection (Fig. 2.13a) or atropine application (Fig. 2.13b). Second, the PLR was absent following atropine application in mice with melanopsin restored exclusively in the retina (Fig. 2.9b). Third, we were unable to locate any putative synaptic release sites from ipRGCs in iris or ciliary body using the albino *Opn4^{Cre/+}; ROSA^{Synaptophysin-tdTomato/+}* mouse line (Fig. 2.4a). These results strongly suggest that ipRGCs require the conventional brain circuitry to drive the direct PLR. However, we cannot rule out the possibility that a unique subpopulation of ipRGCs mediates the PLR independent of the brain and was not infected by either AAV that expresses either DREADD or melanopsin. Regardless, these data show that the retina-brain circuitry is sufficient for generating bilateral asymmetry in the PLR and that any functional contribution of ipRGCs independent of the brain is minimal.

Additionally, we find that bilateral asymmetry is specifically mediated by the Brn3b-positive M1 ipRGCs that mediate the consensual PLR^{95,105}, providing further evidence for ipRGCs using the brain circuitry for the PLR bilateral asymmetry. When we injected mice lacking the Brn3b-positive ipRGCs (Brn3b-DTA: *Opn4*^{Cre/+}; *Brn3b*^{DTA/+})¹⁰⁵ with the same Cre-dependent G_q-coupled DREADD virus (Fig. 2.11e), we observed minimal pupil constriction following CNO administration with no bilateral asymmetry (Fig. 2.10c), indicating Brn3b-positive ipRGCs are required for the bilateral asymmetry in the PLR. Additionally, when we infected aDTA mice (*Opn4*^{aDTA/aDTA})⁹⁵ that lack the M1 ipRGCs but retain non-M1 ipRGCs with a similar G_q-coupled DREADD AAV that is not Cre-dependent (AAV-hM3D(G_q)) (Fig. 2.14b), we saw minimal PLR and no bilateral asymmetry (Fig. 2.10d, Fig. 2.14d), despite robust bilateral asymmetry in wildtype controls (Fig. 2.14c). These results demonstrate that activation of ipRGCs alone can generate robust bilateral asymmetry using the brain circuitry without iris phototransduction.

Additionally, not only are Brn3b-positive ipRGCs sufficient for bilateral asymmetry, they are also required. When we tested the direct and consensual PLR in control mice (*Opn4*^{Cre/+}) across a range of light intensities, we observed a robust bilateral asymmetry across ~4 log-units (Fig. 2.10e). In contrast, when we tested both the direct and consensual PLR in Brn3b-DTA mice (*Opn4*^{Cre/+}; *Brn3b*^{DTA/+}), we observed essentially no PLR in either eye until very bright light intensities (Fig. 2.10f), similar to optic nerve transection or atropine treatment (Fig. 2.1). The greatest bilateral asymmetry in control mice occurred at relatively low light intensities at which the Brn3b-positive cells are required for the PLR (Fig. 2.10e, f). At bright light intensities when Brn3b-DTA

mice retain partial PLR, there is no bilateral asymmetry in control mice. Therefore, this indicates that Brn3b-positive ipRGCs are both necessary and sufficient for normal bilateral asymmetry in the PLR.

Despite a normal requirement for Brn3b-positive ipRGCs, Brn3b-DTA mice displayed a more robust direct PLR in bright light, although they did not reach wildtype levels (Fig. 2.15a, *Opn4*^{Cre/+} vs. *Opn4*^{Cre/+}; *Brn3b*^{DTA/+} $P = 0.007$ by one-way ANOVA with Sidak's post-test). To test if the iris muscle phototransduction mediates this direct PLR in Brn3b-DTA mice, we blocked the neuronal input using atropine. Atropine administration largely abolished the direct PLR in both Brn3b-DTA and controls, resulting in minor direct PLR in both lines (Fig. 2.15b). Additionally, the direct PLR in Brn3b-DTA mice was effectively lost following additional knockout of melanopsin (*Opn4*^{Cre/Cre}; *Brn3b*^{DTA/+}) (Fig. 2.15c), suggesting that the direct PLR in Brn3b-DTA mice is due to iris muscle phototransduction. Interestingly, the consensual PLR in Brn3b-DTA mice lacking melanopsin was also impaired compared to Brn3b-DTA mice ($P < 0.001$ by two-tailed t test; compare Fig. 2.15a with 2.15c), implying that the remaining Brn3b-negative ipRGCs have a unique requirement for melanopsin. Together, these results confirm that the Brn3b-positive ipRGCs mediate the neuronal PLR¹⁰⁵, but that at bright light intensities the iris muscle can enhance a small direct PLR in their absence.

Remarkably, the extent of PLR bilateral asymmetry across vertebrates is correlated with the ratio of contralateral and ipsilateral retinal projections to the brain²¹⁵. ~90% of RGC projections in mouse go to the contralateral hemisphere, and mice have moderate bilateral asymmetry. Species with roughly equal ipsi-/contralateral projections such as humans have no bilateral asymmetry¹⁹⁶, and species with all contralateral

projections have no consensual PLR at all. In total, these results show that the entirety of the PLR can be recapitulated by the activity of the Brn3b-positive M1 ipRGCs using a bilateral asymmetric brain circuit, and demonstrate that iris phototransduction does not contribute to the PLR in mice.

Discussion

The possibility of a photosensitive iris muscle in mammals and its role in the pupillary light reflex has been of considerable debate for decades¹⁸⁹. We confirm here that there is a melanopsin-dependent PLR in mammals that is independent of the conventional PLR retina-brain circuitry, implicating the iris muscle phototransduction. However, we show that this iris muscle phototransduction does not appear to contribute to normal PLR function and is only observable in the absence of the retina-brain PLR. Even in non-mammalian vertebrates—whose robust intrinsic PLR has been the primary target of study—the iris muscle receives neuronal input that drives the PLR¹⁸⁹. Therefore, it remains unclear how important the intrinsic photosensitivity is in defining pupil size or PLR sensitivity in any species.

The uncertainty in the roles of the iris and retina is due to the inability to specifically silence phototransduction exclusively in either tissue and compare the resulting PLR *in vivo*, even in non-mammalian vertebrates. The identification of melanopsin as the photopigment in the mouse iris muscle and its use of different signal transduction pathways in iris and retina¹⁴⁷ allowed us to specifically delete melanopsin phototransduction in the iris muscle or retina and determine its effect on the PLR *in vivo*. We ultimately found that the role of melanopsin in the PLR is exclusively through the ipRGCs of the retina.

We find here that melanopsin dosage is critical for the intrinsic PLR (Fig. 2.4). The primate iris muscle expresses melanopsin, but they have no intrinsic PLR *in vitro* or following optic nerve transection¹⁴⁷. Even animals that have an intrinsic PLR *in vitro*, such as dogs and albino rats¹⁴⁷, lack a PLR following blockade of the retina-brain circuitry^{193,216}. These findings, in combination with our results, indicate that the presence of melanopsin in the iris and even an intrinsic PLR *in vitro* are not reliable predictors of a role for intrinsic iris photosensitivity in the PLR.

Perhaps the most surprising finding of this work is that ipRGCs mediate the PLR using a bilateral asymmetric circuit. While we have no clear anatomical basis for this finding, bilateral asymmetry exists at multiple levels of the PLR brain circuit. ipRGCs project to both the ipsilateral and contralateral OPN⁹⁹, with unknown relative strengths. Additionally, each OPN projects to many brain regions on both its ipsilateral and contralateral side, with a wide variety of relative strengths. Even each OPN sends a weak projection to the opposite OPN. It is currently unclear how important each of these projections is in determining the bilateral asymmetry and will be interesting to investigate this circuitry in more quantitative detail in the future.

Why does the PLR have bilateral asymmetry or bilaterality at all? The most likely benefit of a bilateral PLR is to ensure that eyes that receive different amounts of light constrict their pupils to different degrees. Because pupil size is so finely tuned for high visual acuity at each light intensity¹⁶⁰, it would be beneficial to allow each eye to largely independently regulate its own pupil size. In agreement, animals whose eyes likely receive very different light intensities because they are more laterally placed, such as

mouse and shark, have a relatively weak consensual PLR^{147,217}. However, species with forward-facing eyes such as humans have identical direct and consensual PLR¹⁹⁶.

While we believe it is unlikely that melanopsin phototransduction in the iris contributes to the PLR, we cannot rule out the possibility that it might contribute to other functions. Activated melanopsin couples to G_q signaling proteins, which modulate a variety of signal transduction cascades through their effects on intracellular calcium. Additionally, when melanopsin is exogenously expressed in non-neuronal cells, its phototransduction cascade can regulate gene expression through Ca²⁺ signaling and activation of the transcription factor NFAT²¹⁸. Therefore, the presence of melanopsin in the iris muscle might serve a physiological function separate from the PLR.

Methods

Animal husbandry

C57Bl/6 x Sv129 hybrid mice were used in all experiments and were housed according to guidelines from the Animal Care and Use Committee of Johns Hopkins University. Male and female mice age 2–8 months were housed in plastic translucent cages with steel-lined lids in an open room. Ambient room temperature and humidity were monitored daily and tightly controlled. Food and water were available *ad libitum*. All mice were maintained in a 12hr:12hr light-dark cycle for the entirety of their lives with a light intensity around 500 lux during the day.

Pupillometry

All mice were dark-adapted for at least 30 minutes prior to any experiments and all PLR experiments were performed between Zeitgeber times (ZT) 2 and 10. Mice were

exposed to a 474-nm LED bulb (SuperBrightLEDs) that was directed to one eye using the gooseneck arms of a dissecting microscope light source. Light intensity was adjusted by applying neutral density filters (Roscolux) that reduced intensity by 12.5%. The photon flux was measured using a luminometer (SolarLight) and converted from W/m^2 to $photons/cm^2/sec$.

Videos of the eye were taken using a Sony Handycam (DCR-HC96) mounted on a tripod a fixed distance from the mouse. Manual focus was maintained on the camera to ensure that only one focal plane existed for each mouse and that therefore variable distance from the camera should not contribute to differences in relative pupil area throughout the video. Pupil size was first recorded under dim red light and the endogenous infrared light source of the camera to capture the dark-adapted pupil size. Following at least 5 seconds of recording in dark, the pupil was continuously recorded for at least 30 seconds of a light step stimulus. All pupil images presented in the paper were cropped to a fixed square area (generally 100 x 100 pixels) surrounding the eye using GNU Image Manipulation Program (GIMP). The images were made grayscale and then brightness and contrast were adjusted to enhance visibility of the pupil and exported as PNG files.

Data analysis

Videos were transferred from the camera to a computer as Audio Video Interleave (AVI) files and individual frames were taken using VLC media player (www.videolan.org/vlc/) and saved in portable network graphics format (PNG). Images were taken in the dark, at 5 seconds, and at least 30 seconds following stimulus onset. Pupil area was then quantified manually in ImageJ (<http://rsbweb.nih.gov/ij/>) software.

First, the image was enlarged to 300% normal size. Then, the image was converted to grayscale and brightness and contrast were adjusted so as to confine the borders of the input channel (black → white) to the edges of the pixel intensity histogram. The pupil area was measured in pixels using the oval tool in which the 4 cardinal points of the oval were touching their respective edges of the pupil. The relative pupil area was calculated using LibreOffice Calc or Microsoft Excel in which the area during the light stimulus was divided by the area prior to lights onset. The minimum relative pupil size was used for all genotypes.

The intensity-response curve was fit using a variable slope sigmoidal dose-response curve in Graphpad Prism 6. The top and bottom of the fit were constrained to 1.0 and between 0 and 0.10, respectively, to ensure the EC₅₀ for each genotype was represented by similar curves. The sensitivity for each genotype or treatment was calculated using the same process of fitting each individual animal's data points with a sigmoidal dose-response curve to generate EC₅₀.

Optic nerve transection and crush

Optic nerve transection and crush surgeries were performed by Kevin Park, Ben Yungher, and Eric Bray of the University of Miami. Unilateral optic nerve crush was performed on WT mice of a mixed C57Bl/6 x Sv129 background. Unilateral and bilateral optic nerve transections were performed on F1 C57Bl/6 x Sv129 mice purchased from Jackson Labs.

Atropine application

0.1% atropine solution was prepared by dissolving atropine sulfite salt monohydrate (Sigma A0257) in phosphate buffered saline (PBS). After at least 30

minutes of dark adaptation, 1 μ l of atropine solution was applied to the cornea using a pipettor. Animals were returned to the cage for at least 5 minutes to allow the atropine to dissolve into the eye. For control experiments, PBS was applied instead of atropine solution. One application of atropine was effective at blocking the contralateral PLR for many hours of testing and was partially effective 24 hours later. Therefore, only one application of atropine was applied per day of experiments even if using multiple light intensities.

Statistical analysis

All statistical tests were performed in Graphpad Prism 6. Specific statistical comparisons are listed in the figure legends. Because the EC₅₀ data appears to be a normal distribution on a log scale (log-normal distribution), all statistical tests and data analysis involving EC₅₀ were performed on the log transformed data set.

Viral infection

Mice were anesthetized by intraperitoneal injection of avertin (2, 2, 2-Tribromoethanol) and placed under a stereo microscope. 0.5–1 μ l AAV-DIO-hM3DG_q-mCherry (4.6×10^{12} viral particles/ml, Roth lab, UNC Vector Core) or 0.5 μ l AAV-DIO-mRuby-P2A-Opn4 (kindly provided by Preethi Somasundaram and Phyllis Robinson, University of Maryland, Baltimore County) was placed on a piece of Parafilm and drawn into a 10- μ l microcapillary tube (Sigma P0674) that had been pulled to a needle (Sutter Instruments, Model P-2000). The loaded needle was then placed in the holster of a pico-injector (Harvard Apparatus PLI-90). The needle punctured the eye posterior to the ora serrata and air pressure was used to drive the viral solution into the vitreous chamber of the eye to ensure delivery specifically to the retina. Mice recovered from surgery on a

heating pad until they woke from anesthesia. All PLR experiments and confocal imaging were done at least 3 weeks following viral injection.

Confocal microscopy

Mice that had been infected with the AAV were anesthetized with avertin and then euthanized using cervical dislocation. The eyes were removed and the retinas were dissected in PBS and then fixed in 4% paraformaldehyde for 1–2 hours on ice. The retinas were then washed in PBS at least three times before either mounting on a microscope slide (Fisher) in Fluoromount (Sigma) with DAPI (2-(4-amidinophenyl)-1H-indole-6-carboxamide) or preparing for immunofluorescence. Immunofluorescence was performed in 4% goat serum with antibody concentrations as follows: anti-melanopsin 1:1000 (Advanced Targeting Systems), anti-Brn3a 1:500. Secondary antibodies include: Goat anti-rabbit 488 1:1000, goat anti-rabbit 546 1:1000, goat anti-mouse IgG H+L 546 1:1000. Images were taken on a Zeiss LSM 710 confocal microscope using a 20X objective. After imaging, images were made grayscale, background subtracted, and brightness and contrast were adjusted in FIJI (<http://fiji.sc>) for the image presented in the chapter.

Figures

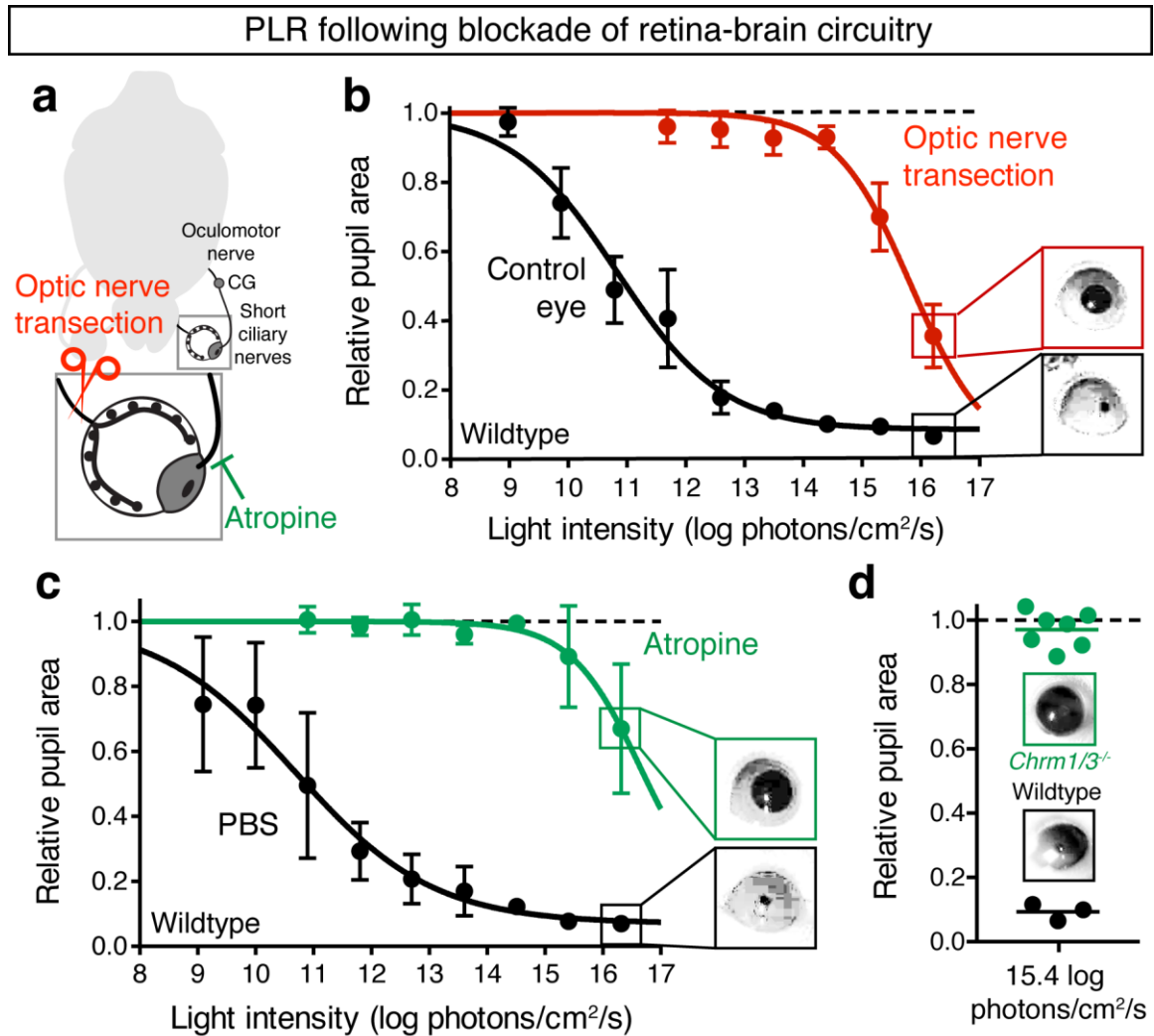


Figure 2.1: The intrinsic PLR operates exclusively at bright light intensities.

(a) Diagram showing the strategy to isolate the intrinsic PLR from retina-brain circuitry by cutting the optic nerve (Optic nerve transection) or blocking the mAChR on the iris muscle (Atropine). The oculomotor nerve sends a branch to the ciliary ganglion (CG), which then innervates the iris muscle by the short ciliary nerves. The short ciliary nerves are cholinergic parasympathetic fibers, and their inputs to the iris can be blocked with mAChR antagonists such as atropine. (b) Intensity-response curve of unilateral optic nerve transection in wildtype mice versus control, untransected eye ($n = 8$ mice). Mean \pm 95% confidence intervals (CI). (c) Intensity-response curve of wildtype mice following

unilateral atropine administration versus vehicle (PBS) eye ($n = 4$ mice). Mean \pm 95% CI.
(d) M1/M3 mAChR double knockout mice ($Chrm1^{-/-}; Chrm3^{-/-}$, $n = 7$) have no measurable pupil constriction at 15.4 log photons/cm²/s compared to wildtype controls ($n = 3$). Line is mean and data points are individual mice.

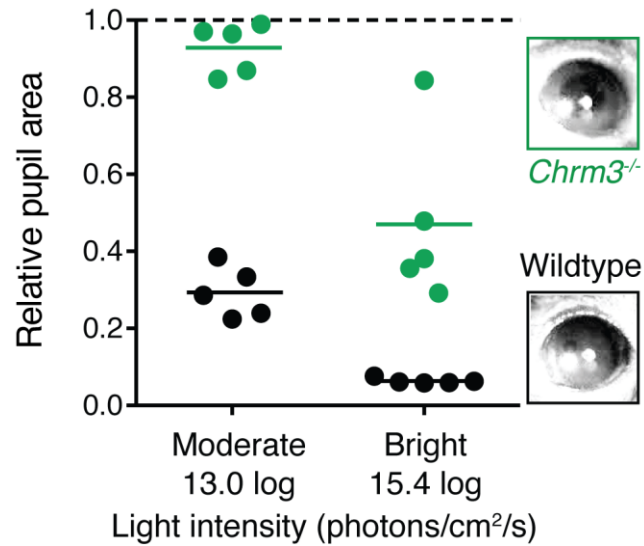


Figure 2.2: M3 mAChR are required for a normal PLR.

M3 mAChR knockout mice (*Chrm3^{-/-}*, green, $n = 5$) have a deficit in maximal pupil constriction at both a moderate (13.0 log photons/cm²/s) and bright (15.4 log photons/cm²/s) compared to wildtype controls (black, $n = 5$). Line indicates mean, data points are individual mice. For both moderate and bright light, WT *v.* *Chrm3^{-/-}*: $P < 0.001$ by two-way repeated measures ANOVA with Sidak's post-test.

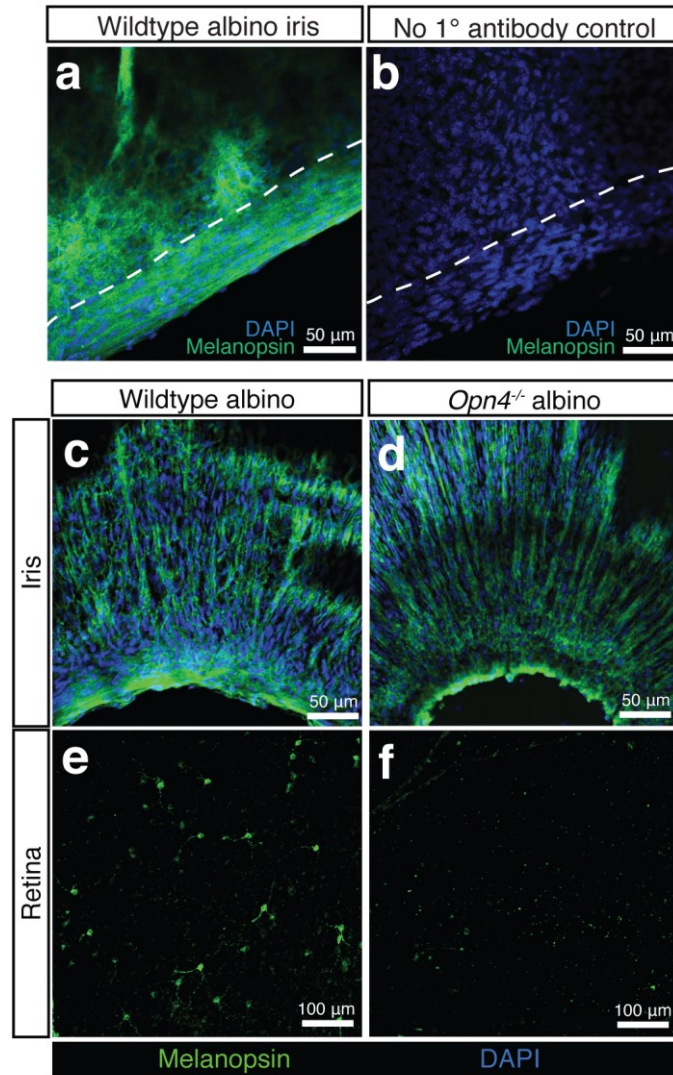


Figure 2.3: Melanopsin immunofluorescence in albino iris.

(a) Melanopsin immunofluorescence (green) generates a robust signal in albino iris that is absent in (b) albino iris stained with a no primary antibody control. The dotted line refers to the division between the iris sphincter and iris dilator muscles. (c–f) Melanopsin immunofluorescence is observed in the iris of albino (c) wildtype and (d) melanopsin knockout (*Opn4^{-/-}*), though it is only detectable in the (e) wildtype and not (f) melanopsin knockout retina.

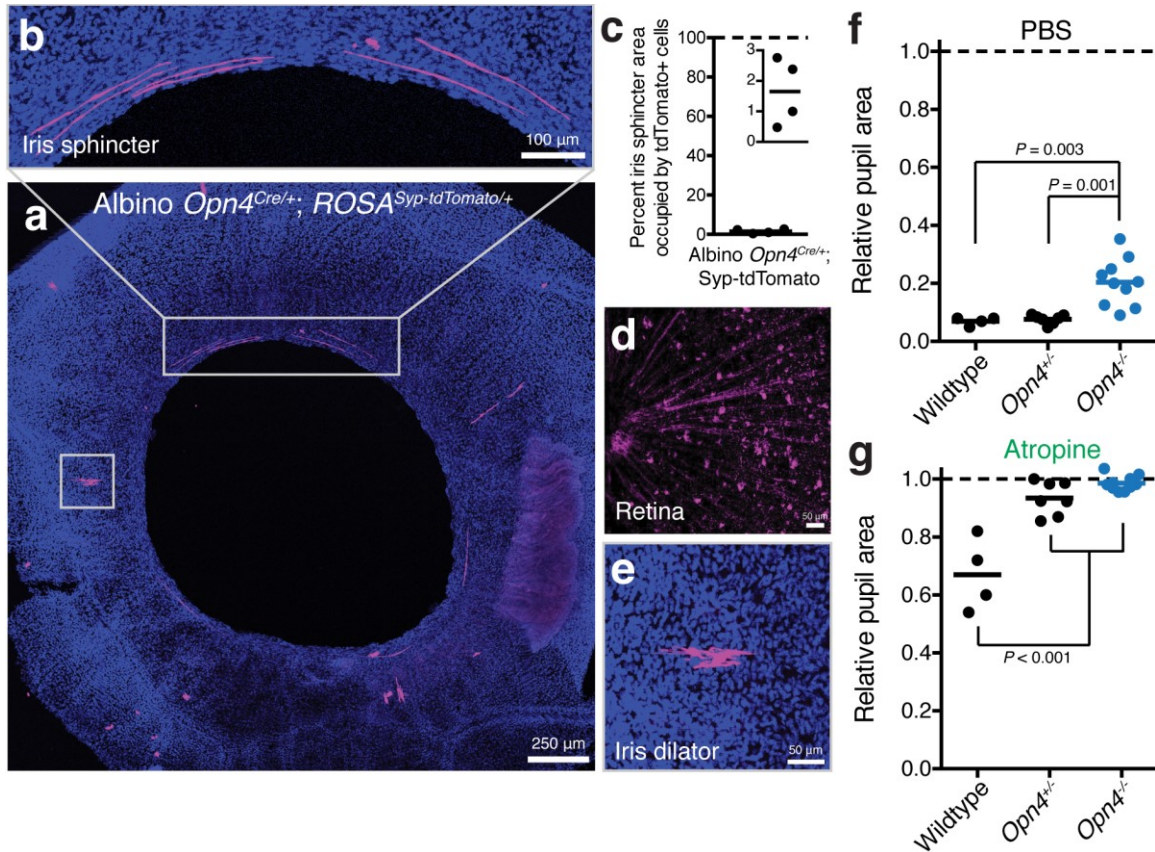


Figure 2.4: Melanopsin pervasiveness contributes to PLR insensitivity.

(a) Whole mount of albino iris with a melanopsin reporter (*Opn4^{Cre/+}; ROSA^{Synaptophysin-tdTomato/+}*) identifies very few cells in the iris muscle that express melanopsin. Most tdTomato⁺ cells are in the iris dilator muscle (e), as opposed to the iris sphincter muscle (b). (c) tdTomato⁺ cells only encompass about 1.7% of the total iris sphincter area. (d) Robust Syp-tdTomato labeling is seen in the retina. (f,g) Melanopsin knockout mice (*Opn4^{-/-}*) display defects in direct PLR at 16.3 log photons/cm²/s in response to (f) PBS administration and no pupil constriction in response to (g) atropine. WT *n* = 4 (replotted from 2.1c), *Opn4^{+/-}* *n* = 7, *Opn4^{-/-}* *n* = 10. *P* values calculated by one-way ANOVA followed by Sidak's post-test.

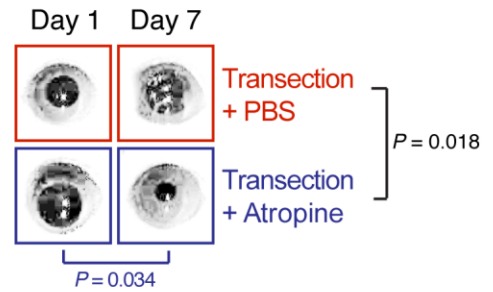
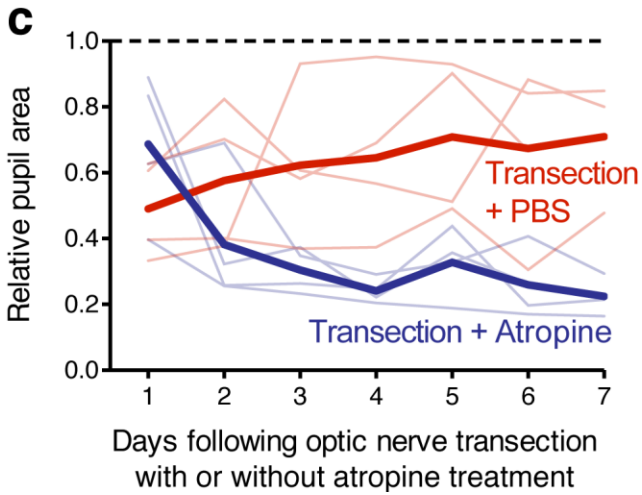
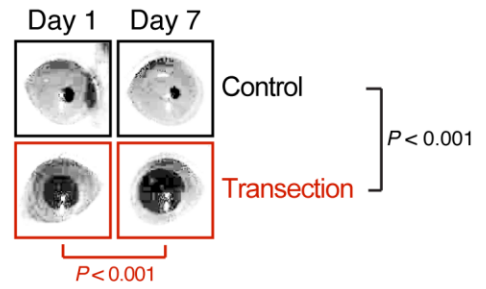
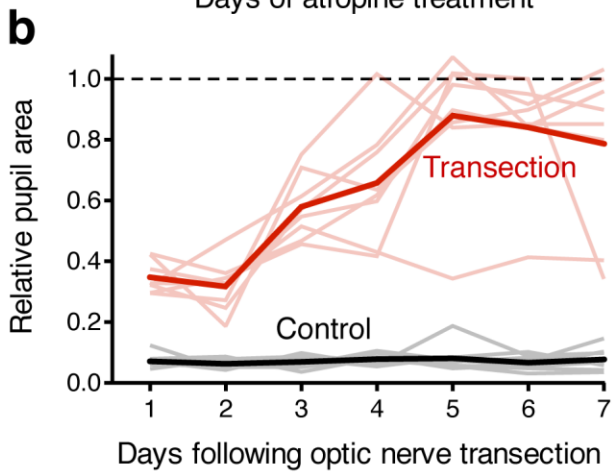
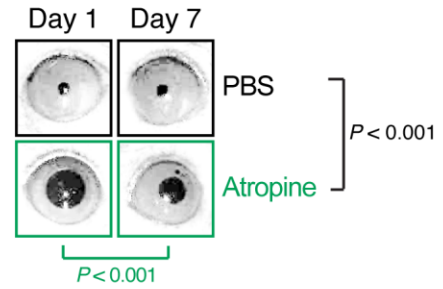
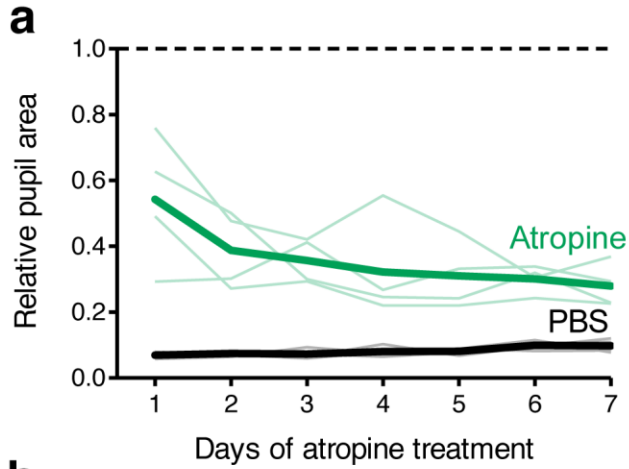


Figure 2.5: Modulation of intrinsic PLR strength over time.

(a) Persistent blockade of input to the iris muscle of one eye by atropine administration for 7 days (green, $n = 4$) enhances the intrinsic PLR. However, at day 7 the intrinsic PLR is still less effective than the control eye (PBS, black). Dark line is mean, light lines are individual mice. (b) Unilateral optic nerve transection (red, $n = 7$) decreases the intrinsic PLR over 7 days compared to day 1. Black lines represent the uninjured control eyes. (c) Transection with atropine administration (blue, $n = 4$) enhances the intrinsic PLR, while transection with vehicle administration (red, $n = 4$) decreases the intrinsic PLR. All statistical comparisons were determined by two-way ANOVA followed by Sidak's post-test. Light intensity for all experiments is $15.4 \log \text{ photons/cm}^2/\text{s}$.

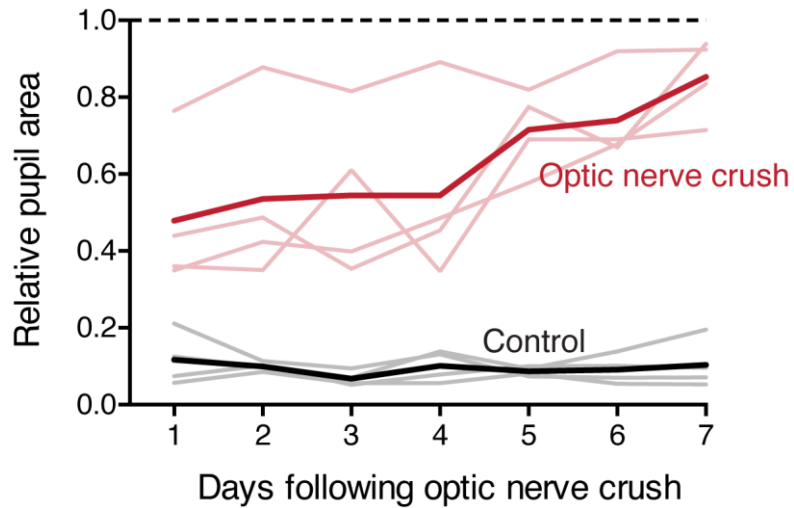


Figure 2.6: Optic nerve crush leads to a reduction in intrinsic PLR over time.

Unilateral optic nerve crush measured daily for 7 days following injury leads to a loss in direct PLR (15.4 log photons/cm²/s), $n = 4$ wildtype mice (Optic nerve crush Day 1 vs. Day 7: $P < 0.001$ by one-way ANOVA followed by Sidak's post-test). The direct PLR on the injured side is significantly worse than control ($P < 0.001$ by two-way repeated measures ANOVA with Sidak's post-test).

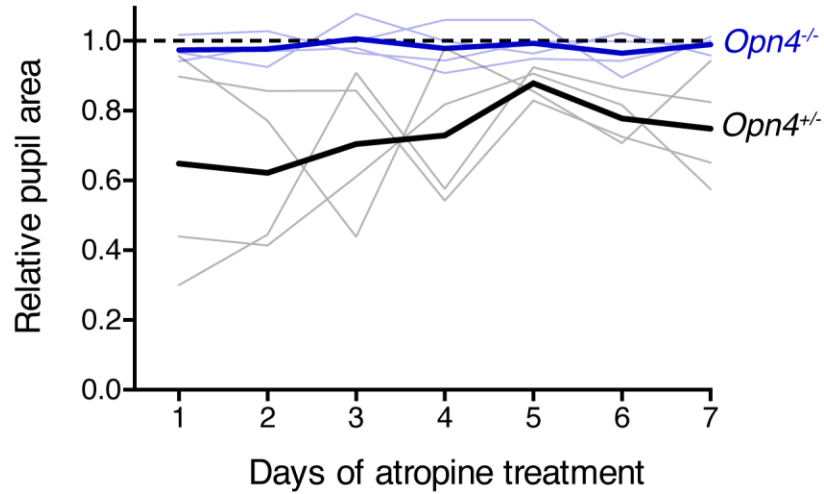
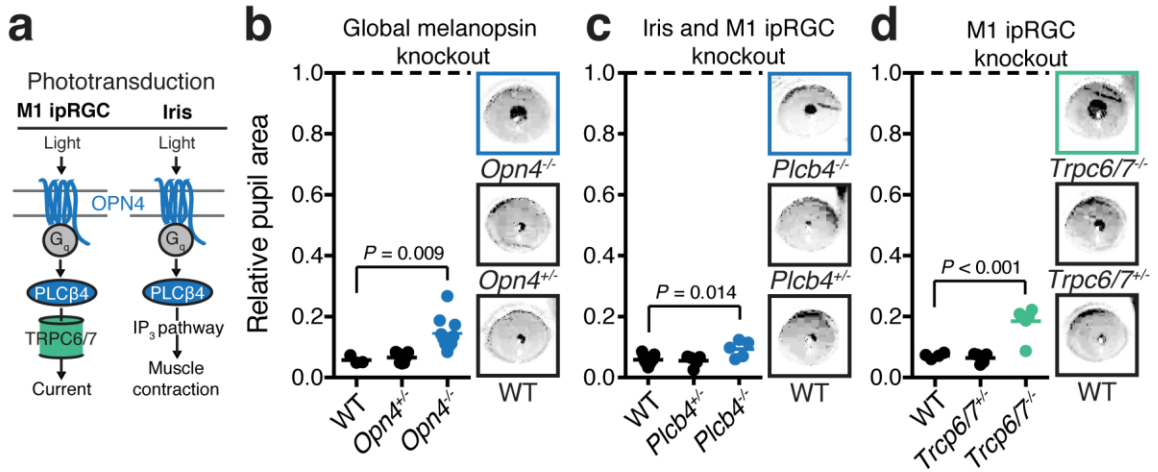


Figure 2.7: Enhancement of PLR by atropine requires melanopsin.

Performing daily atropine administration in melanopsin knockout mice ($n = 4$, blue line, *Opn4^{-/-}*) results in no enhancement of the PLR over 7 days. The same effect was absent in melanopsin heterozygous mice ($n = 4$, black line, *Opn4^{+/-}*), suggesting that a critical amount of melanopsin is required for PLR enhancement by atropine. Dark, thick lines represent the mean for each genotype; thin, transparent lines represent each mouse. Light intensity is 15.4 log photons/cm²/s.

Removal of melanopsin phototransduction exclusively from retina



Restoration of melanopsin exclusively in ipRGCs of melanopsin knockout

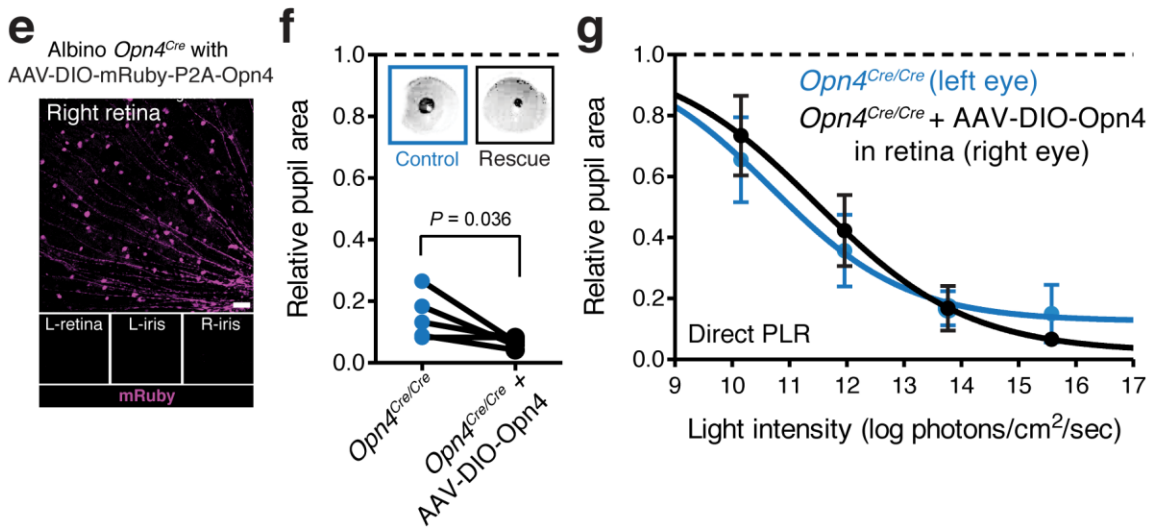


Figure 2.8: Melanopsin knockout in the retina, not iris, causes PLR deficits.

(a) Diagram of phototransduction pathways in retina and iris. Note that ipRGCs utilize TRPC6/7 channels while the iris does not. (b) Melanopsin knockout mice (*Opn4*^{-/-}, *n* = 10) have a defect in maximal direct PLR compared to wildtype (*n* = 3) and littermate heterozygous control mice (*Opn4*^{+/-}, *n* = 7). (c) *Plcb4* knockout mice (*Plcb4*^{-/-}, *n* = 5) also have a deficit in maximal direct PLR compared to littermate wildtype (*n* = 9) and heterozygous controls (*Plcb4*^{+/-}, *n* = 5) (d) *Trpc6/7* double knockout mice (*Trpc6/7*^{-/-}, *n* = 6) also have a defect in maximal direct PLR compared to WT (*n* = 4) and littermate *Trpc6*^{+/-} or *Trpc6*^{+/-}; *Trpc7*^{+/-} heterozygous controls (*Trpc6/7*^{+/-}, *n* = 5). Statistical tests for **b–d** are one-way ANOVA followed by Sidak's post-test and all light intensities are 16.3 log photons/cm²/s. (e) Viral infection of AAV-DIO-mRuby-P2A-*Opn4* in albino *Opn4*^{Cre} shows expression of the mRuby reporter in just the retina of one eye, leaving melanopsin absent in both iris muscles (L-iris, R-iris) and opposite retina (L-retina). (f) Enhancement of the PLR at bright light (15.4 log photons/cm²/s) after rescue of melanopsin in just the right retina compared to the left eye that still lacks melanopsin. Statistical test is paired one-tailed *t* test, *n* = 5 mice. (g) Intensity-response curve of the direct PLR in melanopsin knockout mice with one retina with restored melanopsin expression (black) versus the opposite control eye (blue) shows a specific enhancement of PLR at bright light intensities and no difference in sensitivity. Data is mean ± 95% CI for *n* = 5 mice.

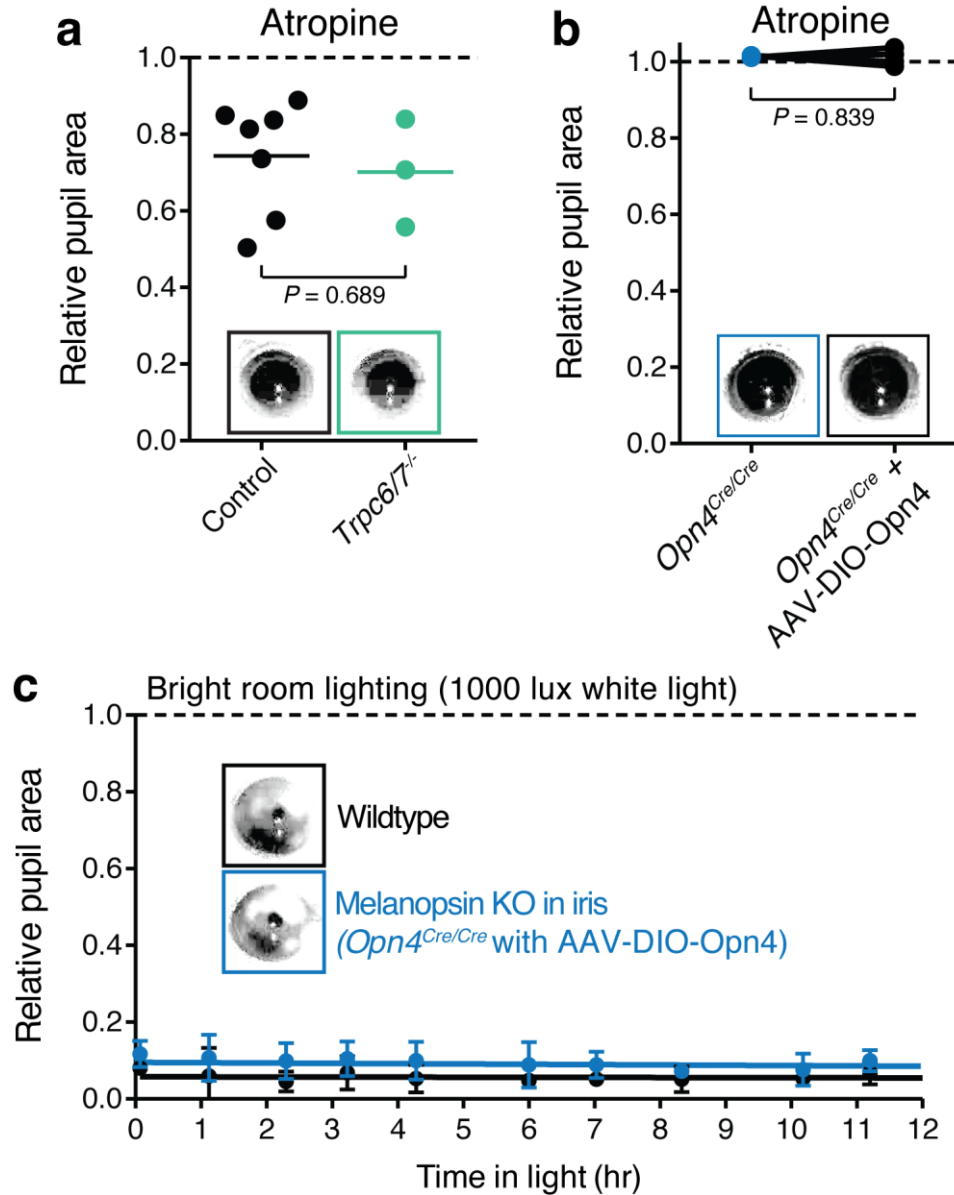


Figure 2.9: Differentiating melanopsin's role in iris and retina.

(a) Atropine application does not block the PLR in $Trpc6/7^{-/-}$ mice ($n = 3$) and littermate controls ($n = 7$), indicating the intrinsic PLR is intact after the removal of M1 ipRGC phototransduction. Littermate controls are mixtures of single $Trpc6$ or $Trpc7$ single homozygous or heterozygous mutants in varying combinations. Statistical test is two-tailed t test. (b) The intrinsic PLR remains abolished in melanopsin knockout mice ($Opn4^{Cre/Cre}$) after viral restoration of melanopsin only in ipRGCs (AAV-DIO-Opn4). Left eye is control while right eye was infected with virus, $n = 4$. Statistical test is paired

two-tailed t test. (c) Wildtype (black, $n = 3$) and mice with melanopsin removed from the iris ($Opn4^{Cre/Cre}$ with AAV-DIO-Opn4, blue, $n = 4$) were kept under relatively bright room lighting (1000 lux) for 12 hours corresponding to their circadian day and their pupil size was monitored at various times. Mice lacking melanopsin in iris were able to maintain small pupil sizes across the day. By repeated-measures two-way ANOVA followed by Sidak's post test, there is a slight deficit in melanopsin iris knockout mice ($P = 0.045$), but the effect size is very small and not physiologically relevant and presumably reflects the fact that melanopsin was restored in only one retina and not in all cells in that retina. Data is mean \pm 95% CI and line is linear regression.

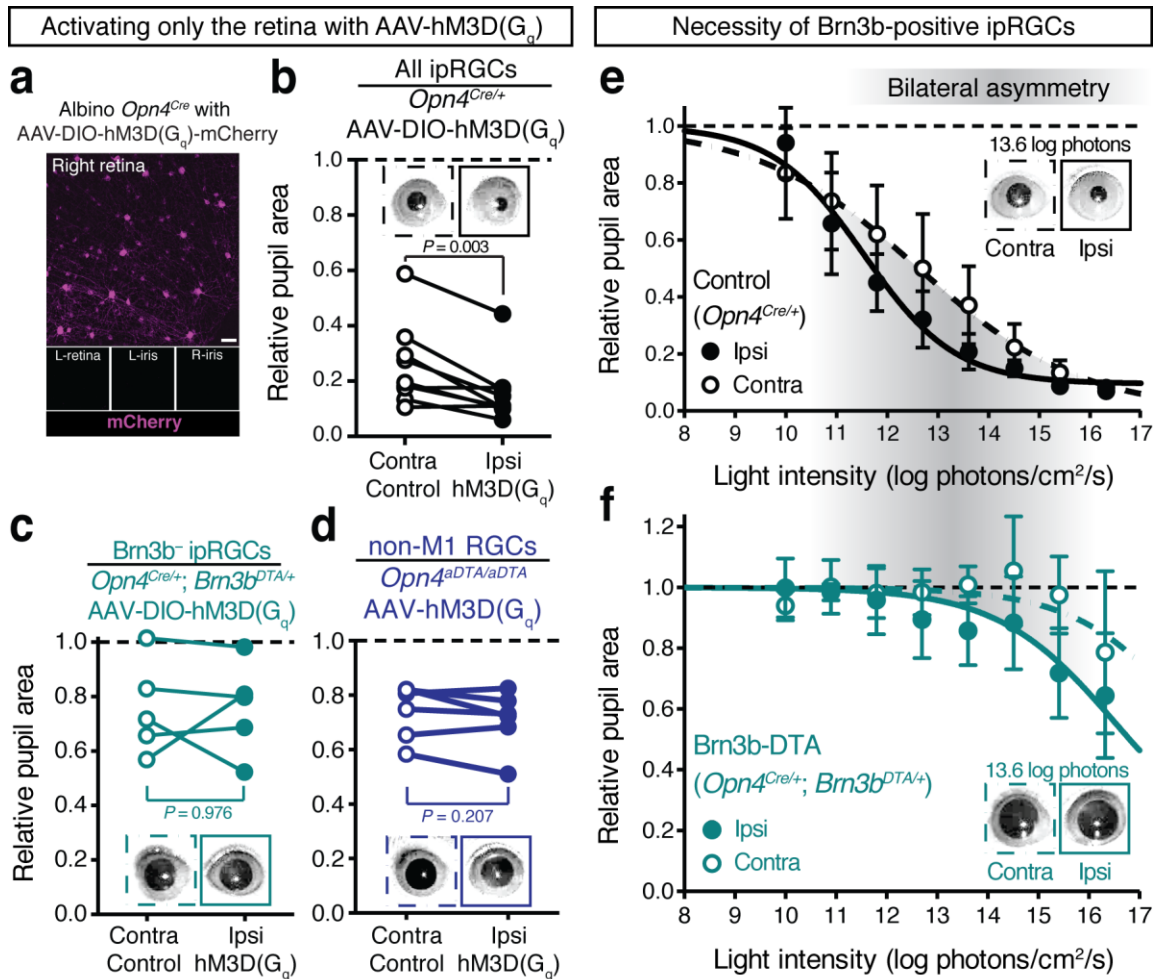


Figure 2.10: Brn3b-positive ipRGCs are both necessary and sufficient for bilateral asymmetry in the PLR.

(a) Injection of an AAV expressing a Cre-dependent hM3D(G_q)-mCherry in only the right eye of albino *Opn4^{Cre/+}* mice shows infection of just the right retina, with the left retina and both left and right irises uninfected. Scale bar = 50 μm. (b) Intraperitoneal injection of CNO in darkness drives a robust bilateral asymmetry in PLR when only activating the ipRGCs of one retina (*Opn4^{Cre/+}* with AAV-DIO-hM3D(G_q), *n* = 8). (c, d) The magnitude and bilateral asymmetry in PLR after CNO are abolished following genetic ablation of the (c) Brn3b-positive ipRGCs (*Opn4^{Cre/+}*; *Brn3b^{DTA/+}*, *n* = 5) or (d) the M1 ipRGCs (*Opn4^{aDTA/aDTA}*, *n* = 6). Statistical tests in b–d are paired two-tailed *t* tests. (e, f) Intensity-response curves of the direct (closed circles, ipsilateral eye) and consensual (open circles, contralateral eye) for (e) control (*Opn4^{Cre/+}*, *n* = 5) and (f) Brn3b-DTA mice (*Opn4^{Cre/+}*; *Brn3b^{DTA/+}*, *n* = 5). Mean ± 95% CI. Note that the

intensities at which the PLR in control mice shows robust bilateral asymmetry (shaded area) require Brn3b-positive ipRGCs.

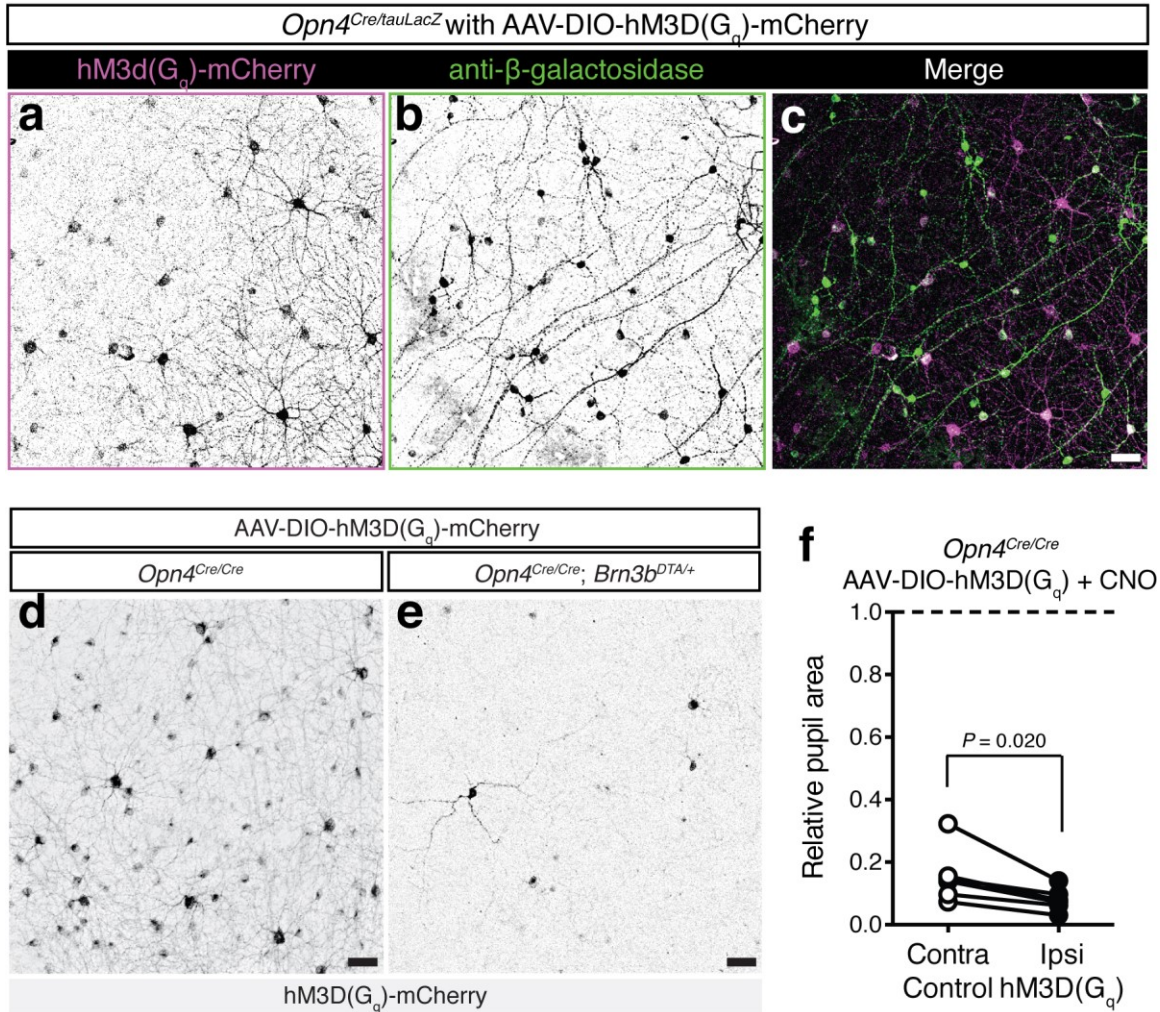


Figure 2.11: Infection of multiple ipRGC subtypes with AAV-DIO-hM3D(G_q).

(a–c) Injection of AAV-DIO-hM3D(G_q) into the vitreous of melanopsin-Cre mice that also have a LacZ cassette to preferentially label M1 ipRGCs (*Opn4^{Cre/tauLacZ}*). mCherry expression (a) can be seen in a variety of RGCs with different morphologies, corresponding to different ipRGC subtypes. Immunofluorescence for beta-galactosidase (b) preferentially labels M1 ipRGCs, revealing that many of them express mCherry, though not all (see merge in c). (d, e) Additionally, Brn3b-negative ipRGCs are labeled by the virus, as revealed by mCherry expression in Brn3b-DTA mice (*Opn4^{Cre/Cre}; Brn3b^{DTA/+}*) (e). Though the number of cells labeled is far below that of control mice (*Opn4^{Cre/Cre}*) (d) because the Brn3b-positive ipRGCs are killed by the DTA transgene. (f) Bilateral asymmetry by unilateral infection of AAV-DIO-hM3D(G_q) persists in melanopsin knockout mice (*Opn4^{Cre/Cre}*, *n* = 6), indicating that iris muscle melanopsin is

not required for the retina to drive bilateral asymmetry. Statistical test is paired two-tailed t test. Scale bars = 50 μm .

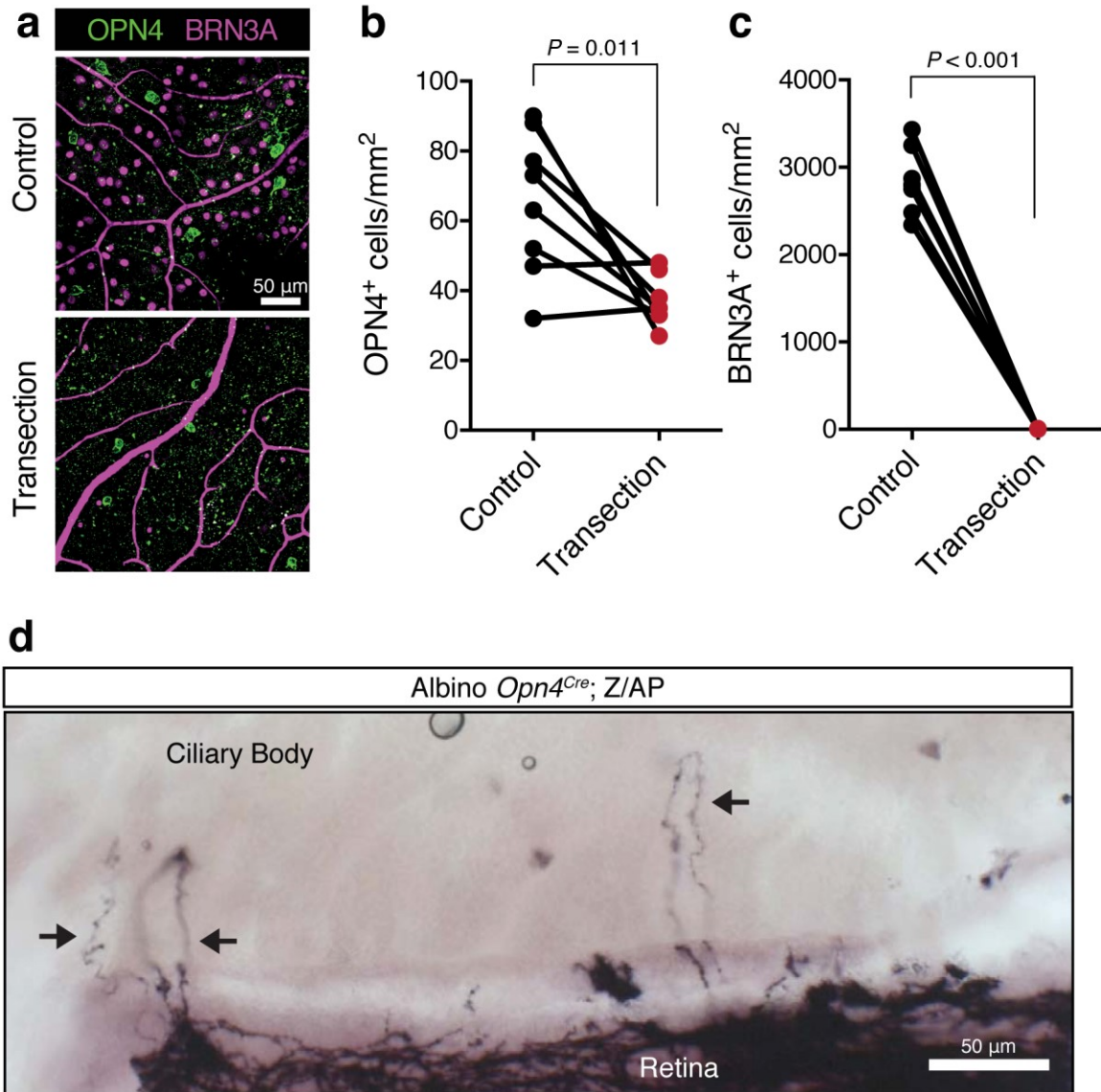


Figure 2.12: Evidence for ipRGC involvement in the intrinsic PLR.

(a) Immunofluorescence for ipRGCs (OPN4, green) and conventional RGCs (BRN3A, magenta) following unilateral optic nerve transection. Control eye is the contralateral eye. (b) Some OPN4⁺ cells are lost following optic nerve transection, many survive, especially compared to (c) BRN3A⁺ cells. Statistical tests are paired two-tailed *t* test. (d) Alkaline phosphatase staining in the retina and attached ciliary body of P14 albino *Opn4^{Cre/+}; Z/AP* mice. Processes from ipRGCs can be seen exiting the retinal periphery and entering the ciliary body.

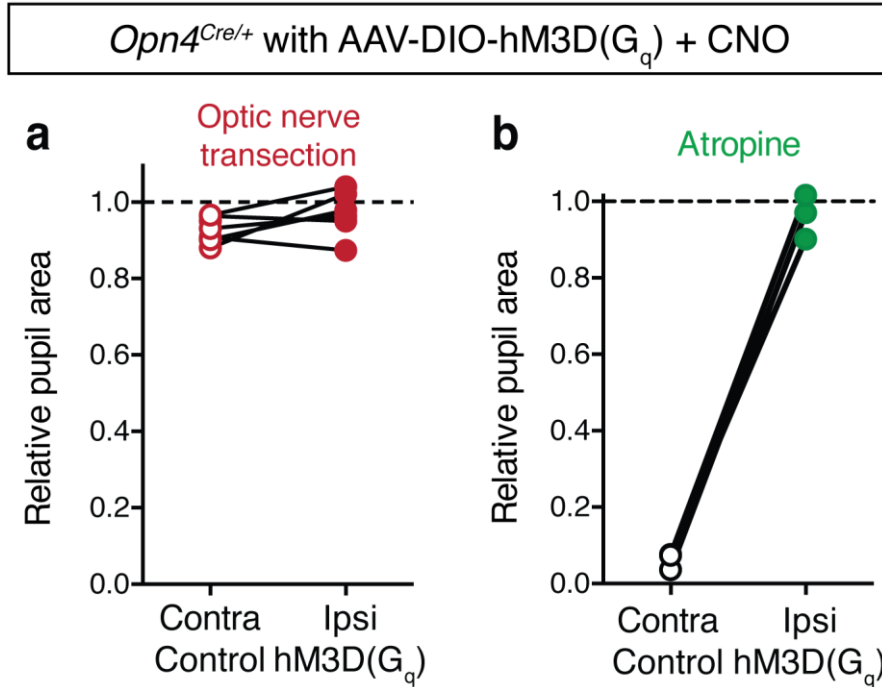


Figure 2.13: ipRGCs require brain circuitry to drive the PLR.

PLR following CNO administration in *Opn4^{Cre/+}* mice injected with AAV-DIO-hM3D(G_q) is abolished following (a) unilateral optic nerve transection ($n = 7$) and (b) unilateral atropine application ($n = 3$). In both cases, optic nerve transection and atropine application were performed on the ipsilateral eye that received viral infection.

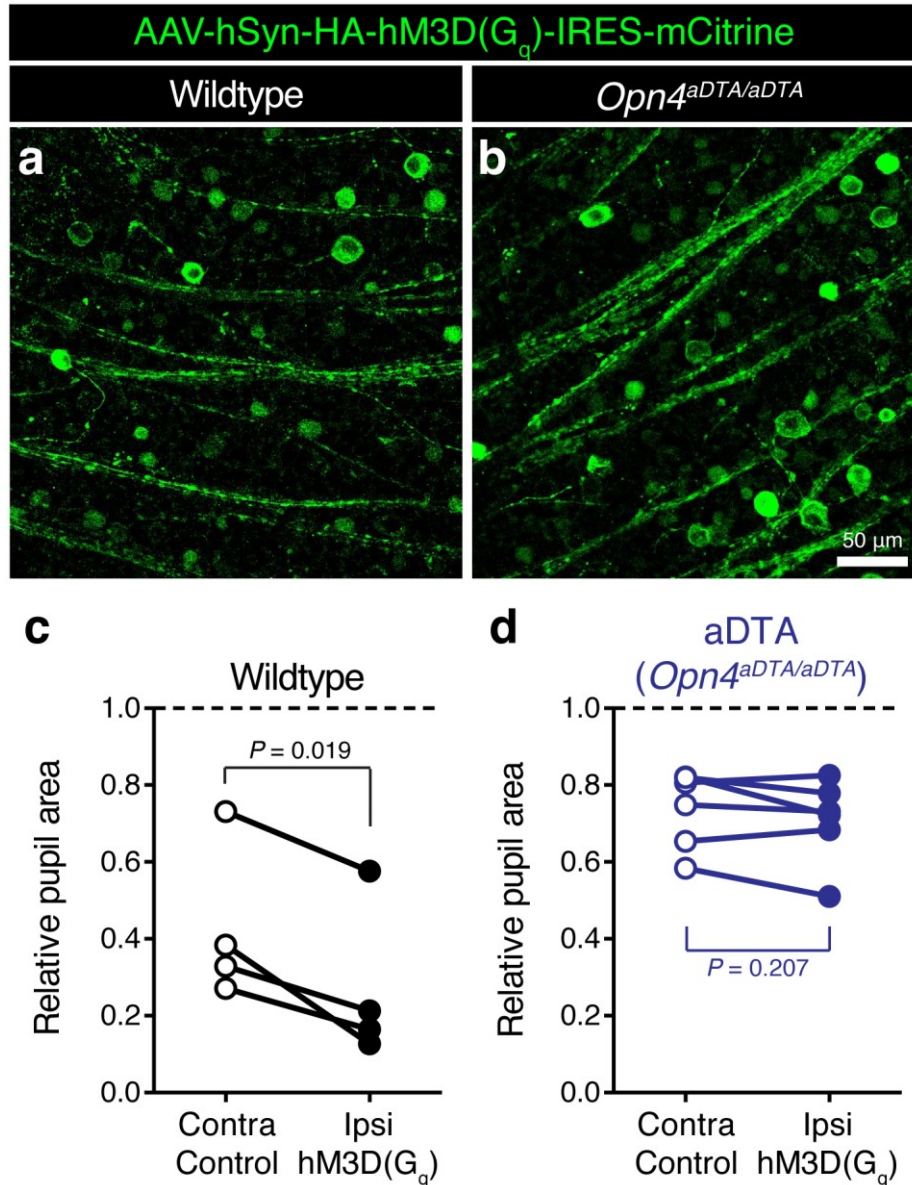


Figure 2.14: Mice lacking M1 ipRGCs lack PLR bilateral asymmetry.

(a, b) mCitrine fluorescence in the ganglion cell layer following infection of AAV-hSyn-HA-hM3D(G_q)-IRES-mCitrine in the retina of either (a) wildtype or (b) mice lacking the M1 ipRGCs (aDTA: *Opn4^{aDTA/aDTA}*). Many different cell types are infected in both mouse lines. (c) Wildtype mice ($n = 4$) expressing AAV-hM3D(G_q) in one retina show PLR bilateral asymmetry with greater constriction on the infected side following injection of CNO. (d) After ablation of the M1 ipRGCs (aDTA: *Opn4^{aDTA/aDTA}*, $n = 6$), a residual PLR is present with reduced magnitude following CNO injection (WT v. aDTA $P = 0.012$ for Contra and $P < 0.001$ for Ipsi by two-way repeated measures ANOVA followed by

Sidak's post test), though it has no bilateral asymmetry; replotted from Fig. 2.10d. Statistical tests for P values reported on the graphs are paired two-tailed t tests.

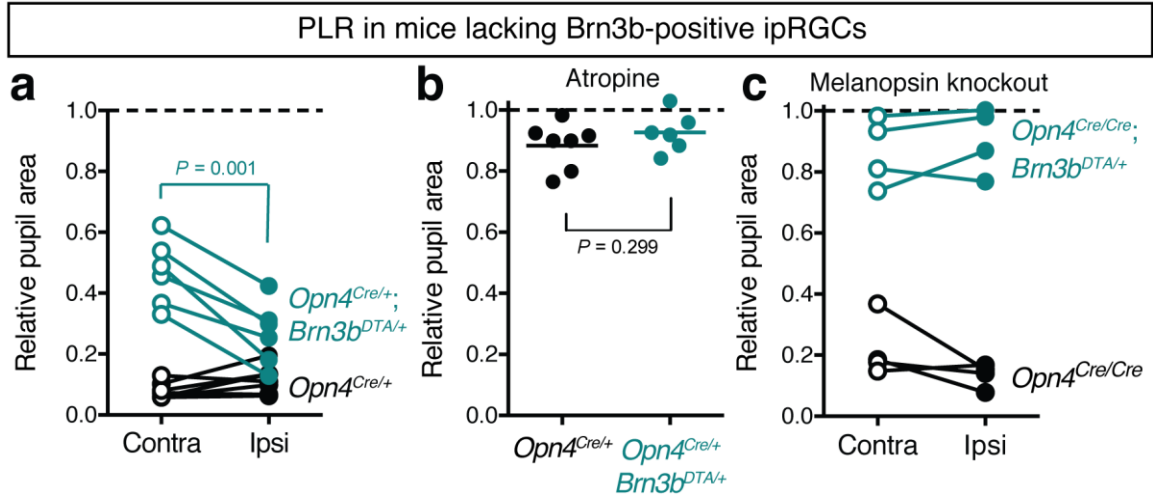


Figure 2.15: Enhanced direct over consensual PLR occurs in Brn3b-DTA mice at bright light intensities.

(a) The direct PLR is enhanced in Brn3b-DTA mice (*Opn4^{Cre/+}; Brn3b^{DTA/+}*) compared to the consensual PLR ($P = 0.001$ by one-way ANOVA followed by Sidak's post-test). (b) The robust direct PLR is largely abolished in both Brn3b-DTA ($n = 6$) and control mice ($n = 7$) following atropine administration. $P = 0.299$ by two-tailed t test. (c) Removal of melanopsin in Brn3b-DTA mice (*Opn4^{Cre/Cre}; Brn3b^{DTA/+}*, $n = 4$) abolishes the enhancement of the direct PLR, but it is retained in control mice (*Opn4^{Cre/Cre}*, $n = 4$). All light intensities are $16.3 \text{ log photons/cm}^2/\text{s}$.

Chapter 3

Rods mediate the rapid pupillary light reflex

This chapter is based on a manuscript currently in submission:

Keenan WT[†], **Rupp AC[†]**, Somasundaram P, Hiriyanna S, Wu Z, Badea TC, Robinson PR, Hattar S. A visual circuit uses discrete mechanisms to support transient and sustained pupil constriction.

[†] Denotes equal contribution

Abstract

Light-dependent changes in pupil size are critical for vision. The pupil rapidly closes or opens following changes in luminance and maintains a consistent pupil size during steady light. Despite a century of research, the quantitative contribution of light detection by rods, cones, and melanopsin to the pupillary light reflex (PLR) across environmental light intensities and timescales remains unclear. Here we report differential requirements for distinct photoreceptive systems for rapid versus sustained pupil constriction. Rods, which are required for vision only at low light intensities, are the predominant contributors to the PLR at all light intensities for rapid responses. However, within minutes of light onset, the PLR switches to a melanopsin-based response for prolonged light stimulation (at least 12 hours). Thus, we report complementary roles for rod and melanopsin phototransduction in driving a critical visual behavior across time and light intensity.

Introduction

The pupillary light reflex (PLR) converts luminance information to pupil size across the day to limit the light reaching the retina. With increases in background light intensity, the PLR drives precise decreases in pupil size rapidly that are accurately tuned for high visual acuity¹⁶⁰. The PLR is also widely used as a diagnostic in clinical evaluations of retina and brain function¹⁶⁴. Therefore, it is essential to understand the precise mechanisms allowing the PLR to drive the optimal pupil size at different light intensities.

The mammalian retina contains three photoreceptor types: rods, cones, and melanopsin-expressing intrinsically photosensitive retinal ganglion cells (ipRGCs). These photoreceptors are responsible for driving the PLR⁸⁸. The precise contribution of individual photoreceptors to the PLR, however, has remained controversial despite decades of work^{79,87,165,167–169,173–179,181,182,219–221}. Previous studies have taken advantage of the different light detection properties of each photoreceptor type to deliver stimuli that activate one photoreceptor to a greater extent than others^{169,173–175,178,179,182,220–222}. These studies have unequivocally shown that rods, cones, and melanopsin phototransduction are each capable of driving the PLR under unique spectral stimuli, but their precise contributions to the PLR under environmental conditions of variable intensity and duration is essentially unknown.

Light input for the PLR is relayed through ipRGCs^{95,97}, which integrate their endogenous melanopsin phototransduction cascade with indirect light information from rods and cones^{70,83,88}. Removing melanopsin results in only minor PLR deficits due to the fact that rod and cone light input reaches ipRGCs^{87,95}. Additionally, blind patients and

mice lacking rod and cone function still retain a PLR, but only at bright light intensities^{79,111,177}. This, in combination with the previous findings that all photoreceptors are capable of driving the PLR, suggests that there may be redundancy in photoreceptor input to the PLR. This raises an intriguing evolutionary question: why do ipRGCs require light input from different sources if each input alone is capable of driving the PLR?

To quantitatively determine the role of the different photoreceptors in driving the PLR, it is necessary to specifically silence individual photoreceptor types and to measure the PLR under more natural conditions. Here, we used an array of well-established mouse mutant lines that block rod, cone, or ipRGC phototransduction pathways to study the PLR. We show that rapid activation of the PLR predominantly utilizes rods, with minimal contribution from cones and melanopsin phototransduction. However, rod contributions are unstable at bright light intensities, where instead the less sensitive melanopsin phototransduction provides stable light detection for the PLR. Surprisingly, we find minimal involvement of cone photoreceptors. These findings uncover a mechanism of complementary stimulus encoding by different cell types that allows a sensory system to be sensitive to small changes in intensity but yet relay stable sensory information.

Results

Experimental PLR setup to mimic the natural environment

To measure the pupillary light reflex under ‘environmental’ conditions, we used broad-spectrum white light (‘daylight’) directed from above a mouse’s head (Fig. 3.1). Using this approach, we measured a rapid induction of the PLR in wildtype mice within

seconds that was maintained for the entire 30-second stimulus. Wildtype mice initiate the PLR at relatively low light intensities ~ 0.001 lux, corresponding to a cloudy night, and reach saturation ~ 1000 lux, corresponding to a bright office building or dawn/dusk on a bright day. In all cases, pupil constriction was maintained for the entire 30 seconds, although at dimmer intensities there was a moderate decrease in constriction.

PLR action spectrum matches rhodopsin/melanopsin spectrum

To characterize the photoreceptor input to the mouse PLR, we generated an action spectrum. We produced a full intensity-response curve for five distinct narrow wavelength lights for wildtype mice (Fig. 3.2). As previously reported, we found that blue (474-nm light) was the most sensitive, with green (526-nm) and ultraviolet (400-nm) light about one log-unit less sensitive than blue light. Finally, the PLR in response to long wavelength light (orange (590-nm) and red light (626-nm)) was even less sensitive. Plotting the relative sensitivity of the PLR to each wavelength against the relative sensitivity of each photoreceptor, we find that the PLR sensitivity most closely matches the sensitivity of melanopsin/rhodopsin, with little overlap with either of the cone opsins (Fig. 3.2). This suggests that rod and melanopsin phototransduction account for the majority of the PLR.

Rod phototransduction is required for the rapid PLR

To directly test if rod and melanopsin phototransduction are required for the PLR, we used genetic mutant mouse lines that lack critical components of each individual cell type's phototransduction cascade while leaving the function of the other photoreceptors intact (Fig. 3.3). We refer to mice lacking functional cones as cone knockout, lacking functional rods as rod knockout, and lacking functional melanopsin as melanopsin

knockout. We tested a variety of mutant mouse lines to corroborate our findings. Specifically, we used mice with distinct mutations of critical phototransduction machinery or complete ablation of cell bodies (rod knockouts: *Gnat1*^{-/-} and Rod-DTA; cone knockouts: *Cnga3*^{-/-}, *Gnat2*^{-/-}, and Cone-DTA) (Fig. 3.3)^{22,23,223–225}. In addition, we removed phototransduction in ipRGCs using melanopsin knockout mice (*Opn4*^{-/-}) (Fig. 3.3)^{83,99}.

Importantly, all of these mutant mouse lines have been extensively tested for visual function. Rod sensitivity and function is unchanged in cone mutant animals and cone sensitivity and function is unchanged in rod mutant animals^{22,223,226–230}. For ipRGCs, electrophysiological recordings show functional rod input in cone mutants and functional cone input in rod mutants²³¹. Additionally, all of the mutant lines used in this paper have similar pupil sizes in darkness (Fig. 3.3b). Therefore, these mouse lines allow precise separation of rod, cone, and melanopsin activation while leaving the function of the other photoreceptors intact.

When we tested the rapid PLR of rod, cone, and melanopsin mutant mice (Fig. 3.4a), we were surprised that rod knockout mice displayed no pupil constriction at a moderate light intensity that drives robust constriction in wildtype mice (10 lux, Fig. 3.4b). In contrast, cone knockout and melanopsin knockout mice were indistinguishable from wildtype in pupil constriction amplitude and kinetics (Fig. 3.4b). When we determined the full intensity-response relationship, all cone knockout and melanopsin knockout animals displayed pupil constriction that was indistinguishable from wildtype animals at all light intensities (Fig. 3.4c, d). In fact, Cone-DTA mice had a more sensitive PLR than wildtype (Fig. 3.4c, d). In contrast with cone and melanopsin mutant mice, rod

knockout mice show virtually no pupil constriction until the light intensity becomes relatively bright (i.e. >10 lux, Fig. 3.4c, d). This results in rod knockout mice displaying a >2-log unit decrease in sensitivity (Fig. 3.4d; mean EC₅₀ for WT = 0.17 lux, *Gnat1*^{-/-} = 57.5 lux, Rod-DTA = 52.5 lux). These results indicate that rod function is required for a normal rapid PLR.

These results were unexpected due to the previous published reports indicating the importance of cones in driving the rapid PLR^{178,179}. Mice lack a long-wavelength opsin, making them less sensitive to red light than humans. However, in a transgenic mouse model in which the mouse green cone opsin is replaced by the human red cone opsin, mouse cones become more sensitive to red light (*Opn1mw^{red}*)²³². Using this mouse model and stimulating the PLR using red light, a previous study found an enhancement of the PLR in the red-sensitive cone line compared to wildtype animals¹⁷⁸, suggesting that cones provide strong input to the PLR. Due to the conflict in conclusions with our results from Fig. 3.4c, we wanted to confirm these previous findings using the same mouse model (*Opn1mw^{red}*). However, using this mouse model and stimulating the rapid PLR with red light, we measured no difference in magnitude or sensitivity of the PLR between cone transgenic mice and wildtype littermate controls (Fig. 3.4e, f). In fact, when we mated this mouse line to the rod knockout line (*Gnat1*^{-/-}; *Opn1mw^{red}*), we found that all rapid pupil constriction in response to red light occurs through rods, even when cones have enhanced sensitivity to red light (Fig. 3.4g). Overall, this supports our findings that cones are not the predominant input to the rapid PLR.

Recently, it has been proposed that short wavelength-sensitive cones (S cones) are particularly important for the PLR and other non-spatial behaviors^{172,179,233,234}. The red

cone opsin transgenic mouse line we used replaces the green cone opsin and will not affect the UV opsin²³². Therefore, we wondered if the reason we see minimal cone requirement for the PLR is because rods are much more sensitive than S cones to broad-spectrum white light. While our light source contains substantial UV light to activate S cones similar to sunlight (Fig. 3.1), their signal will be relatively swamped out by the robust activation of rods.

To test if S cones are involved in the PLR, we tested the PLR in the different retinal mutant lines to UV light (365 nm) that will enhance the relative activation of S cones compared to white light, while decreasing the relative rod activation. In this situation, we find that both cone and rod knockout mice show a decrease in sensitivity (Fig. 3.5). This result shows that when designing a stimulus to preferentially activate S cones, we see evidence of their involvement in the PLR. However, it underscores the fact that under natural conditions of broad-spectrum light, rod signals predominate over cone signals.

This result is also inconsistent with the previous observations that melanopsin knockout mice have a small deficit in PLR magnitude at high light intensities^{87,147,149,179}. We reasoned that the discrepancy could be due to a major difference between our and previous light stimulation protocols. In our stimulations, we use overhead white light simulating environmental light. Most PLR studies, including those of melanopsin knockout mice, stimulate a single eye with monochromatic light and observe constriction in the opposite eye. When we tested melanopsin knockout mice using the latter methodology (contralateral light), we observed the previously reported deficit in melanopsin knockout mice (Fig. 3.6). However, when we measured the PLR of the same

melanopsin knockout mice under our overhead paradigm simulating environmental light, there was no observable difference from wildtype animals (Fig. 3.6). These results suggest that melanopsin may be required specifically for the contralateral PLR and confirm our findings that melanopsin activation is not required for the rapid PLR under environmental conditions.

Collectively, these results indicate that rods are the only photoreceptors that are required for any aspect of the rapid PLR. Even at light intensities at which cones mediate spatial vision²²⁹, rod function is required for driving the rapid PLR.

Rods are sufficient for the full rapid PLR

We next wondered if rods are sufficient to drive rapid pupil constriction. To test this, we generated double mutants of cone and melanopsin phototransduction used previously (Cone mutants: *Cnga3*^{-/-}, *Gnat2*^{-/-}, and Cone-DTA, Melanopsin mutant: *Opn4*^{-/-})²²⁸. In these mouse lines, rods are the only functional photoreceptors in the retina ('rod-only'). These lines are referred to as rod-only 1, 2, and 3 depending on the cone mutation used (Fig. 3.7a). We found that rod-only lines 1 and 3 had identical rapid PLR to wildtype at all light intensities (Fig. 3.7b,c). This indicates that rods alone are sufficient for the rapid PLR at all light intensities, including bright intensities at which rods are presumably saturated for vision. Notably, while rod-only type 2 was generally similar to wildtype in sensitivity (Fig. 3.7c), this mouse line had a decrease in overall amplitude at all light intensities and high variability between and within animals (Fig. 3.7b). Regardless of the differences between RO2 and the other rod-only lines, all rod-only lines were either identical or similar to wildtype and indicate that rods are sufficient for the full PLR.

Though we have shown that rods provide the predominant input to the rapid PLR, the fact that animals lacking rod function (Fig. 3.4) or both rod and cone function^{79,111,176,177} retain a PLR at bright light intensities indicates that melanopsin in possible combination with cones is sufficient for the rapid PLR at bright light intensities. To define the sufficiency of cones and melanopsin, we generated double mutant mice as previously for the rod-only lines ('cone-only' CO: *Gnat1*^{-/-}; *Opn4*^{-/-}, 'melanopsin-only' lines: MO1 *Gnat1*^{-/-}; *Cnga3*^{-/-}, MO2 *Gnat1*^{-/-}; *Gnat2*^{-/-}, MO3 Rod-DTA; Cone-DTA).

As expected and in marked contrast to the rod-only animals, both cone-only and melanopsin-only mice had severe sensitivity defects in the rapid PLR (Fig. 3.7d,e; mean EC₅₀ for WT = 0.13 lux, MO1 = 182 lux, MO2 = 126 lux, MO3 = 141 lux, CO = 1233 lux, $P < 0.001$ for all 4 genotypes by one-way ANOVA with Sidak's post-test). However, melanopsin-only mice still retained a normal PLR at bright light intensities, in agreement with previous findings^{79,147,177}. Notably, melanopsin-only mice were indistinguishable from rod knockouts (Fig. 3.7e), providing further evidence that cones are dispensable for the rapid PLR, even in the absence of rod function. Furthermore, we found that cone-only animals had virtually no PLR at all light intensities up to 1000 lux, at which they achieved only partial constriction (Fig. 3.7d). This results in cone-only mice having a further sensitivity deficit compared to rod knockout (Fig. 3.7e; mean EC₅₀ for RKO = 64 lux, CO = 1233 lux, $P < 0.001$ by one-way ANOVA).

The 'rod-only', 'cone-only', and 'melanopsin-only' mouse lines also displayed differences in PLR kinetics indicative of those photoreceptor's signaling properties. 'Rod-only' mice display similar kinetics to wildtype animals with rapid (<1 s) onset of constriction which is maintained for the duration of the 30s stimulus (Fig. 3.7f). 'Cone-

only' mice displayed similar rapid (<1 s) onset of constriction but showed rapid decay back to baseline during the thirty-second stimulus, consistent with cone light adaptation (Fig. 3.7f). 'Melanopsin-only' mice show a small delay in onset (3–5 seconds), consistent with melanopsin's sluggish kinetics¹⁷⁷, but then show continued constriction throughout the 30 seconds (Fig. 3.7f). These results provide an explanation for why cones have minimal input to the PLR: their rapid adaptation that is integral for their role in spatial vision prohibits their ability to sustain pupil constriction for more than a few seconds.

Collectively, these results indicate that rods are the only photoreceptors that are both necessary and sufficient for the rapid PLR at light intensities encompassing the dynamic range of the rapid PLR (i.e. light intensities up to 100 lux). Therefore, rod activation is the key determinant of pupil size for rapid constriction. While rods are not required for the rapid PLR at very bright light intensities, the remaining contribution is predominantly from melanopsin, not cones, due to its stable signaling properties.

The photoreceptor contributions to the pupillary light reflex over time and intensity

These experiments allow us to generate a model of the distinct roles of each photoreceptor type in the PLR at all light intensities (Fig. 3.8, see Methods for detailed explanation). First, we generated a quantitative model of a wildtype mouse's pupil size at the entire range of environmental light intensities and times up to 30 seconds (Fig. 3.8a). Then, we constructed individual heat maps quantifying the degree of necessity or sufficiency of rod, cone, and melanopsin phototransduction across both light intensity and time. Finally, we took the maximum of necessity or sufficiency at each time and light intensity to create a merged heat map representing photoreceptor contributions (Fig. 3.8b,c). This heat map provides a comprehensive visualization of the relative contribution

of each photoreceptor type to the PLR at any particular time or environmental light intensity.

Discussion

We find that redundancy is minimal for the PLR; distinct components of the PLR are mediated by distinct photoreceptors. Using a battery of mouse mutant lines, we show that upon light stimulation, the pupil rapidly constricts using exclusively rod input at light intensities corresponding to night and dawn/dusk. At higher light intensities corresponding to day, both rods and melanopsin are capable of driving this rapid response, though melanopsin input is more sluggish and provides stability to the rod input. At even brighter intensities, cones begin to contribute weakly to the rapid PLR, though their signal rapidly adapts.

This complementary arrangement of photoreceptors for the PLR is analogous to conscious visual perception, which utilizes rods at dim light and cones at bright light. However, we find that for the rapid PLR, rods dominate responses at all light intensities, dim and bright, with little contribution from cones. This difference between spatial vision and the rapid PLR raises the possibility that ipRGCs receive different rod/cone input than conventional RGCs. In support of this possibility, all ipRGC subtypes receive sensitive rod input²³¹ and cone input to some subtypes is relatively weak¹⁰¹.

Although this possibility could explain our results, we believe there is a more fundamental explanation for the difference between spatial vision and rapid PLR. Namely, the PLR requires measurement of absolute light intensity whereas image vision requires measurement of relative differences. Rods, but not cones, provide signaling capabilities consistent with measuring absolute magnitude. Specifically, rods have limited light

adaptation capabilities and longer temporal integration compared to cones²³⁵.

Additionally, the vast majority of photoreceptors in the mammalian retina are rods and they are extremely sensitive under dark adaptation, and the predominant interneurons are the rod bipolar cells. While this circuitry largely pools rod signals by the time they reach retinal ganglion cells, it still has the consequence that rods and the rod circuitry are the predominant cells activated by any light stimulus. In agreement with this idea, the dark-adapted electroretinogram (ERG), which corresponds to rapid PLR is essentially only driven by rods²². This means that the requirement of rods in the rapid dark-adapted PLR is not specific to the ipRGCs circuit, but instead that detection of any increases in light intensity from darkness or low light levels is going to be predominantly driven by rods. For example, rod-based signals overwhelm cone-based signals to preclude full color discrimination and the speed of perception at mesopic light²³⁶, as occurs in the human peripheral retina.

While humans and other primates have a rod-dominated retina like the mouse, they also possess a fovea, which concentrates the rare cones in the retina. This raises the question of whether the rapid PLR in mice is applicable to the human PLR. In support, the primate dark-adapted rapid PLR action spectra match a rhodopsin spectrum^{175,181,182}. In addition, rod mutant humans display a similar sensitivity defect in the PLR as we measured in rod mutant mice¹⁶⁷. Therefore, rods are likely the predominant photoreceptors for the rapid PLR in humans.

The minimal cone contributions to the PLR we find here is unexpected given the previous studies showing cone input to the PLR^{178,179}. Notably, most of these previous studies have used dynamic stimuli to preferentially activate cones and have observed

matching changes in pupil size, indicating cones are capable of modulating pupil size¹⁷⁹. Cones are most effective at encoding dynamic changes in light intensity and not stable background luminance due to their rapid activation and adaptation. In support, we find that cone-only animals show rapid adaptation of pupil size in response to steady light (Fig. 3.7f). It is probable then that cones have no role in defining the absolute pupil size in the environment. Instead, we find it most likely that cones contribute to relatively small fluctuations around a mean pupil size that is defined by rod or melanopsin phototransduction.

Instead, we find that melanopsin provides robust input to the PLR at bright light intensities. Why is melanopsin involved if rods alone are sufficient for the PLR? One possibility is that the pupil sizes of rod-only animals are relatively unstable compared to wildtype or cone mutants. This suggests that melanopsin is involved in the PLR to provide stable pupil sizes at high light intensities when rods saturate and adapt.

Another more likely possibility is that melanopsin has not been maintained in the PLR circuit for its role in the rapid PLR. Melanopsin phototransduction is capable of signaling for many hours²³⁷, and the PLR also is stable for many hours¹⁷⁷. Notably, this stability of melanopsin for long-term signaling appears to be most important for maintaining pupil sizes after rods begin to light-adapt (Bill Keenan, data presented in the associated manuscript in preparation). Therefore, the minor role of melanopsin in the rapid induction of pupil constriction may simply be to initiate its real purpose: to stabilize the pupil across the day.

Methods

Animal husbandry

C57Bl/6 x Sv129 hybrid mice were used in all experiments and were housed according to guidelines from the Animal Care and Use Committee of Johns Hopkins University. Male and female mice age 2–8 months were housed in plastic translucent cages with steel-lined lids in an open room. Ambient room temperature and humidity were monitored daily and tightly controlled. Food and water were available *ad libitum*. All mice were maintained in a 12hr:12hr light-dark cycle for the entirety of their lives.

Pupillometry

Light intensity during the day was kept around 500 lux, except in the case of rod-only type 1 (*Cnga3^{-/-}; Opn4^{-/-}*) and rod-only type 3 (Cone-DTA; *Opn4^{-/-}*), which were maintained in a dim light-dark cycle. Photoentrainment is poor at bright light in both of these lines²²⁸ and we observed more variable pupil constriction when these lines were maintained in a bright light-dark cycle, presumably due to lack of photoentrainment. All mice were dark-adapted for at least 30 minutes prior to any experiments and all PLR experiments were performed between Zeitgeber times (ZT) 2 and 10.

Mice were restrained manually under a 10-, 13-, or 23-Watt compact fluorescent light bulb (GE Daylight FLE10HT3/2/D or Sylvania Daylight CF13EL and CF23EL) with a color temperature of 6500 K to simulate natural sunlight. The light intensity was measured using a light meter (EXTECH Foot Candle/Lux Light Meter, 401025) at the surface on which the mouse was held. The light meter was initially calibrated by EXTECH using a Tungsten 2856 K light source; because our experiments used a fluorescent bulb of 6500 K, all measured light intensities reported here may vary by

0.92–1.12 times the actual light intensity. Light intensity was adjusted by a combination of altering the distance of the light bulb(s) from the mouse and/or applying neutral density filters (Roscolux). The light meter is incapable of detecting light intensities below 1 lux, so one neutral density filter cutting the light intensity by 12.5% was applied to the bulb to estimate 1-log unit decreases in illumination below 1 lux. Light intensities above 500 lux required the use of multiple light bulbs.

For the monochromatic light PLR experiments, an LED light (SuperBrightLEDs) was housed in a microscope light source with fiber optic gooseneck arms to direct the light source to the mouse eye. For the experiments involving the *Opn1mw^{red}* mice, we used a 626-nm LED in this setup and directed light to both eyes simultaneously or to just one eye and measured the PLR in the illuminated eye (see figure legends). The photon flux was measured using a luminometer (SolarLight) and converted from W/m² to photons/cm²/sec. The light intensity was decreased by 12.5% using neutral density filters (Rosco).

Videos of the eye were taken using a Sony Handycam (DCR-HC96) mounted on a tripod a fixed distance from the mouse. Manual focus was maintained on the camera to ensure that only one focal plane existed for each mouse and that therefore variable distance from the camera should not contribute to differences in relative pupil area throughout the video. Pupil size was first recorded under dim red light and the endogenous infrared light source of the camera to capture the dark-adapted pupil size. Following at least 5 seconds of recording in dark, the pupil was continuously recorded for at least 30 seconds of a light step stimulus. For all sustained PLR, animals were kept in a cage for 60 minutes under the light stimulus. Animals were removed from the cage after

60 minutes and held in front of the camera for 30 seconds as for the rapid PLR. All pupil images presented in the paper were cropped to a fixed square area (generally 100 x 100 pixels) surrounding the eye using GNU Image Manipulation Program (GIMP). The images were made grayscale and then brightness and contrast were adjusted to enhance visibility of the pupil and exported as PNG files.

Data analysis

Videos were transferred from the camera to a computer as Audio Video Interleave (AVI) files and individual frames were taken using VLC media player (www.videolan.org/vlc/) and saved in portable network graphics format (PNG). Images were taken in the dark, at 5 seconds, and 30 seconds following stimulus onset. Pupil area was then quantified manually in ImageJ (<http://rsbweb.nih.gov/ij/>) software. First, the image was enlarged to 300% normal size. Then, the image was converted to grayscale and brightness and contrast were adjusted so as to confine the borders of the input channel (black → white) to the edges of the pixel intensity histogram. The pupil area was measured in pixels using the oval tool in which the 4 cardinal points of the oval were touching their respective edges of the pupil. The relative pupil area was calculated using LibreOffice Calc or Microsoft Excel in which the area during the light stimulus was divided by the area prior to lights onset. For the rapid PLR, the minimum relative pupil size of either 5 seconds or 30 seconds after stimulus was used for all genotypes.

The intensity-response curve was fit using a variable slope sigmoidal dose-response curve in Graphpad Prism 6. The top and bottom of the fit were constrained to 1.0 and between 0 and 0.10, respectively, to ensure the EC_{50} for each genotype was represented by similar curves. However, for the RO2 fit, the bottom was not constrained

to between 0 and 0.10 because their values converged on a larger number. The sensitivity for each genotype was calculated using the same process of fitting each individual animal's data points with a sigmoidal dose-response curve to generate EC₅₀.

Statistical analysis

All statistical tests were performed in Graphpad Prism 6. Specific statistical comparisons are listed in the figure captions. Because the EC₅₀ data appears to be a normal distribution on a log scale (log-normal distribution), all statistical tests and data analysis involving EC₅₀ were performed on the log transformed data set.

Heat map generation

The photoreceptor contribution heat map was generated by first creating estimated pupil size matrices for both the rapid and sustained PLR at every light intensity and time for wildtype mice (x axis = time, y axis = intensity). To do so, we applied the equation for a one-phase association:

$$(1) Y = Y0 + (Plateau - Y0) * (1 - e^{(-K*x)})$$

In our case, Y is the **relative pupil area** generated at **time**, x. For the WT rapid PLR heat map, Y_{0,rapid} is set to 1 for every light intensity and the K_{rapid} was extracted from the wildtype rapid constriction kinetics curve at 100 lux. The *Plateau_{rapid}* value at each light intensity is the rapid PLR value extracted from the WT rapid intensity-response curve fit. This allows us to generate a full matrix of WT pupil sizes at every intensity and time by knowing the final pupil size (*Plateau*) and the rate of constriction (*K*) based on experimental determination (Fig. X). This process was used to generate a matrix of relative pupil areas with the y-axis being light intensity varying logarithmically (0.001-

100,000 lux) and the x-axis being time varying linearly from 0 to 30 seconds using a custom MATLAB script.

The matrices generated for the wildtype mice were also done to the photoreceptor mutants. In order to determine necessity of a photoreceptor we subtracted rod (*Gnat1*^{-/-}), cone (*Gnat2*^{-/-}), or melanopsin (*Opn4*^{-/-}) knockout matrices from the wildtype matrix. This yields larger values for genotypes that are more required and also normalizes for the overall constriction in wildtype mice at that intensity (i.e. because rods are fully necessary at some dim intensities at which WT mice have minimal constriction, the necessity value attributed to rods is small despite their absolute necessity at that intensity). To determine sufficiency we used ‘rod-only’ (*Cnga3*^{-/-}; *Opn4*^{-/-}), ‘cone-only’ (*Gnat1*^{-/-}; *Opn4*^{-/-}) and ‘melanopsin-only’ (*Gnat1*^{-/-}; *Gnat2*^{-/-}) matrices.

Finally, in order to produce a graphical heat map, the pupil size matrices were uploaded to *Plotly* (<https://plot.ly>) for heat map generation. Pupil sizes are the z-values of the heat map and the z-range was set from 0 to maximal wildtype constriction (1 – 0.09 = 0.91).

Figures

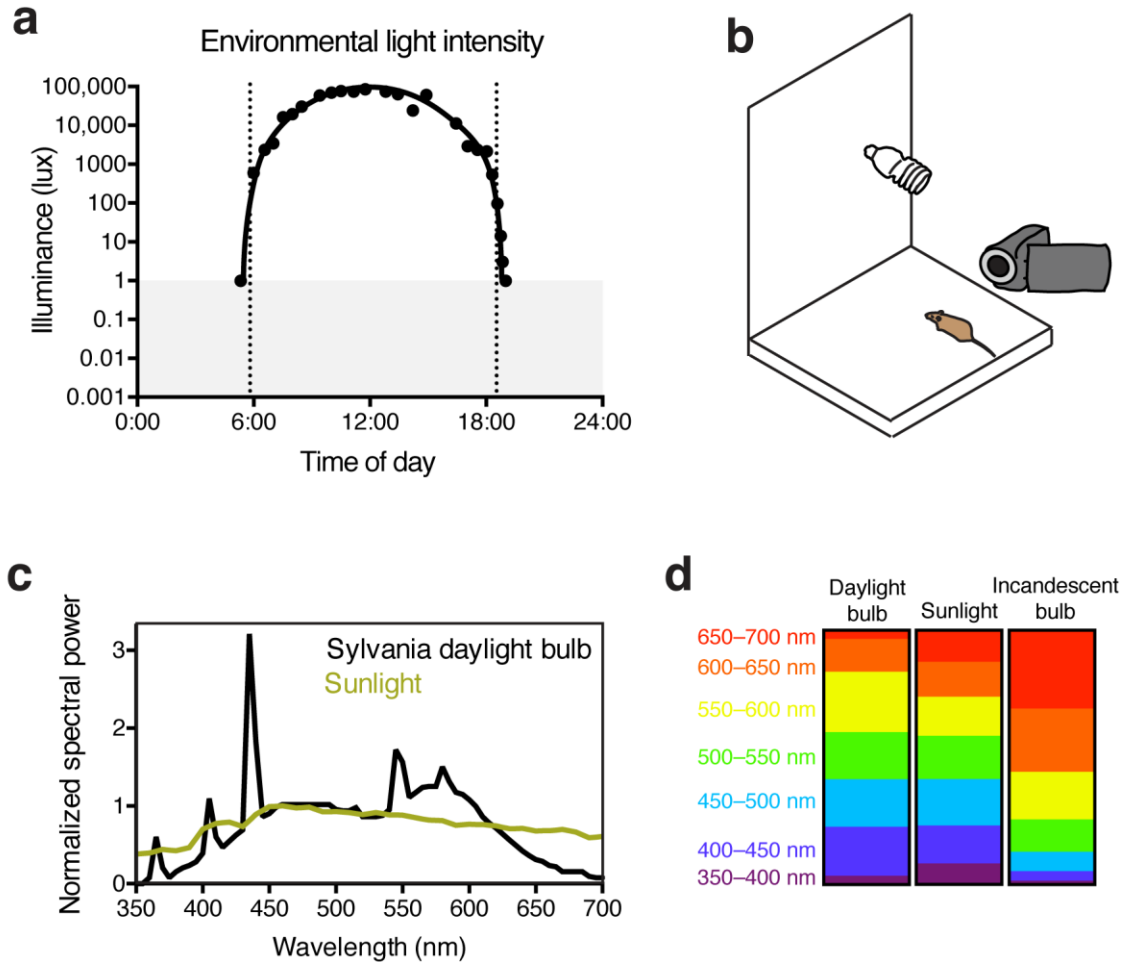


Figure 3.1: Experimental setup to mimic environmental light.

(a) Environmental light intensity measured in lux across one day (April 2, 2015) in Baltimore, Maryland, USA. The light meter used is unable to measure light intensities below 1 lux, indicated with the gray box. Dotted lines refer to the meteorological sunrise and sunset. Data is fit with a hand-drawn curve for ease of visualization. (b) Mice are unanesthetized and restrained by hand under a light bulb with a broad spectrum similar to sunlight (c). Breaking down the fraction of light into 50-nm bins for each light source, the daylight bulbs are very similar to sunlight across all wavelengths (d), while incandescent bulbs lack short wavelengths and are enriched in long wavelengths. Pupils are continuously recorded in darkness and light using an infrared video camera.

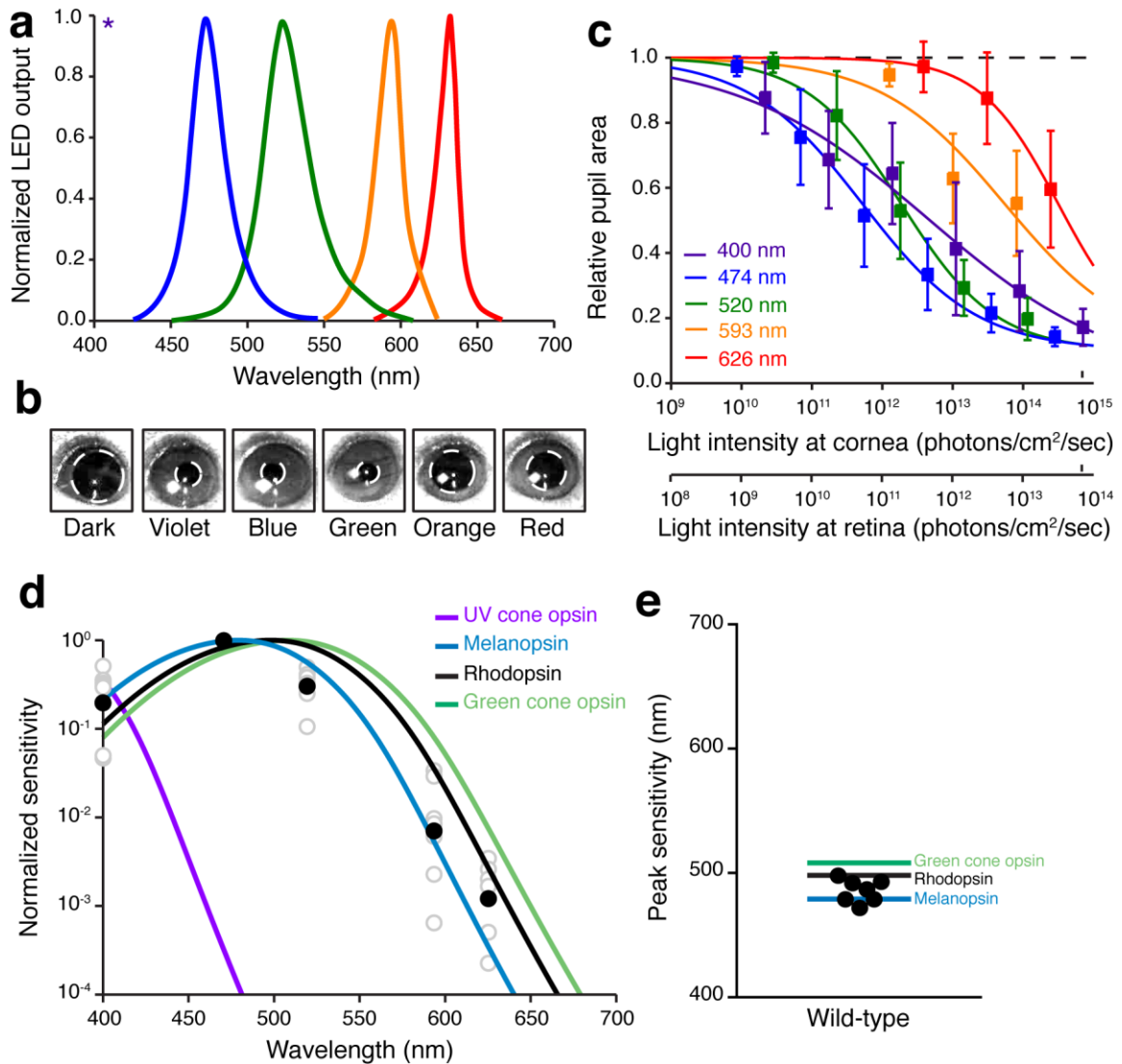


Figure 3.2: Action spectrum of the pupillary light reflex in wild-type mice matches rods and/or melanopsin.

(a) The output spectrum for the LED lights used in this experiment, as reported by the manufacturer. Violet LED output spectrum is unknown, as denoted by ‘*’, but is listed as 395 nm–405 nm. (b) Representative images from an individual wild-type mouse to each LED light at roughly equivalent photon flux light intensities ($\sim 10^{14}$ photons/cm²/sec). (c) Dose response relationship of the pupillary light reflex for each light used. Abscissa is reported in measured photons/cm²/sec as well as approximate light intensity reaching the retina based on the dark-adapted pupil size of 2.5 mm. (d) Sensitivity of the PLR in wild-type mice to each light based on the measured EC₅₀ and plotted as a normalized

sensitivity relative to the highest sensitivity light (black circles are average, gray circles from individual mice). Opsin nomograms representing mouse UV cone opsin (365 nm), melanopsin (480 nm), rhodopsin (498 nm), and green cone opsin (508 nm) are plotted for reference. (e) Maximal sensitivity of the modeled nomogram for each wild-type mouse. Nomogram was fit to the data using the least sum of squares method. Data is represented by mean \pm 95% CI.

a

Mouse line	Genotype	Effect on retinal function	Citations
Rod KO	<i>Gnat1</i> ^{-/-}	No rod phototransduction	Calvert et al. 2000
Rod-DTA	<i>rdta</i>	No rod cell bodies; cones present early in life	McCall et al. 1996
Cone KO1	<i>Cnga3</i> ^{-/-}	No cone phototransduction	Biel et al. 1999
Cone KO2	<i>Gnat2</i> ^{cpfl3/cpfl3}	No cone phototransduction	Chang et al. 2006
Cone-DTA	h.red DT-A	Ablation of all m-cones; >95% loss of s-cones	Soucy et al. 1998
Melanopsin KO	<i>Opn4</i> ^{-/-}	No melanopsin phototransduction	Hattar et al. 2002
Cone-only	<i>Gnat1</i> ^{-/-} ; <i>Opn4</i> ^{-/-}	No rod or melanopsin phototransduction	
Rod-only 1	<i>Cnga3</i> ^{-/-} ; <i>Opn4</i> ^{-/-}	No cone or melanopsin phototransduction	
Rod-only 2	<i>Gnat2</i> ^{-/-} ; <i>Opn4</i> ^{-/-}	No cone or melanopsin phototransduction	
Rod-only 3	h.red DT-A; <i>Opn4</i> ^{-/-}	No cone cell bodies nor melanopsin phototransduction	
Melanopsin-only 1	<i>Gnat1</i> ^{-/-} ; <i>Cnga3</i> ^{-/-}	No rod or cone phototransduction	
Melanopsin-only 2	<i>Gnat1</i> ^{-/-} ; <i>Gnat2</i> ^{-/-}	No rod or cone phototransduction	
Melanopsin-only 3	<i>rdta</i> ; h.red DT-A	No rod or cone cell bodies	
Red cone KI	<i>Opn1mw</i> ^{red}	Cones have shifted sensitivity to red	Smallwood et al. 2003
Red cone KI; Rod KO	<i>Opn1mw</i> ^{red} ; <i>Gnat1</i> ^{-/-}	Cones have shifted sensitivity to red, no rod phototransduction	

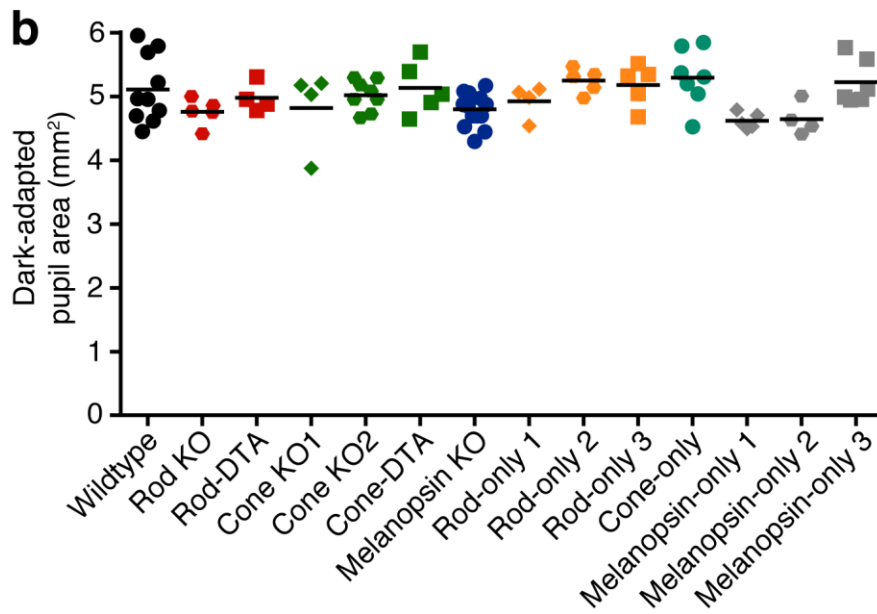


Figure 3.3: Mutant mouse lines used in this study.

(a) A table of the mutant mouse lines used in this study with their specific genotype, effect on retinal function, and original citation. (b) All mutant mouse lines have normal

resting pupil sizes, indicating no gross abnormalities in the PLR circuit at rest. No mouse line was significantly different from wildtype (determined by $P < 0.05$) using a one-way ANOVA with Sidak's post-test.

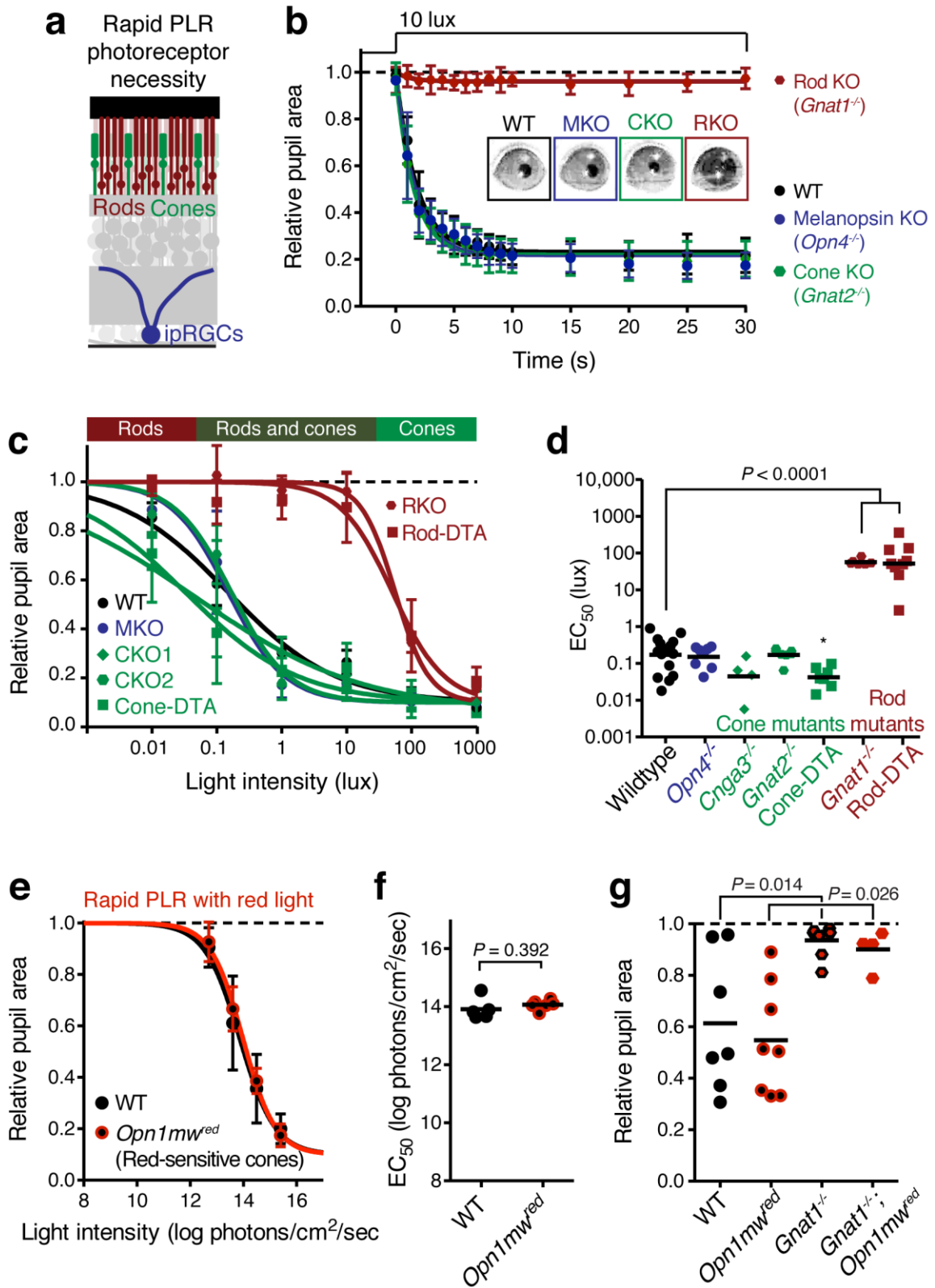


Figure 3.4: Rods are required for the rapid PLR.

(a) Diagram of the retina labeling the photoreceptors. For experiments in **b–d**, WT $n = 14$, *Opn4*^{-/-} $n = 8$, *Cnga3*^{-/-} $n = 4$, *Gnat2*^{-/-} $n = 7$, Cone-DTA $n = 7$, *Gnat1*^{-/-} $n = 6$, Rod-DTA $n = 9$. (b) PLR kinetics for a 10 lux 30-s light step (mean \pm 95% CI). While Melanopsin KO and Cone KO mice have normal kinetics, Rod KO mice have no PLR at all. (c) Intensity-response curves of the PLR in each of the photoreceptor mutant mouse lines (mean \pm 95% CI). The bar on top of the figure denotes the estimated sensitivities of rods and cones. (d) Rod mutant animals are the only mutants that display sensitivity (EC_{50}) deficits compared to WT ($P < 0.0001$ for both *Gnat1*^{-/-} and Rod-DTA). In fact, Cone-DTA mice are moderately more sensitive than WT (* $P = 0.011$). Points indicate individual mice, line indicates mean. Statistical significance determined using a one-way ANOVA with Sidak's post-test. (e) The PLR to red light (626-nm LED) is identical in mice with cones that are more sensitive to red light (*Opn1mw*^{red}, $n = 6$) compared to littermate WT ($n = 5$), mean \pm 95% CI. (f) Sensitivity (EC_{50}) from the curve fits in **e** shows no difference in between WT and *Opn1mw*^{red} mice ($P = 0.392$ by unpaired two-tailed t test). Points are individual mice, line is mean. (g) Removing rod function abolishes the PLR in response to red light (626-nm LED), even in mice with cones with enhanced sensitivity to red light. WT $n = 7$, *Opn1mw*^{red} $n = 8$, *Gnat1*^{-/-} $n = 8$, *Gnat1*^{-/-}; *Opn1mw*^{red} $n = 4$. Light intensity = 5×10^{14} photons/cm²/sec. Statistical significance determined using a one-way ANOVA with Sidak's post-test.

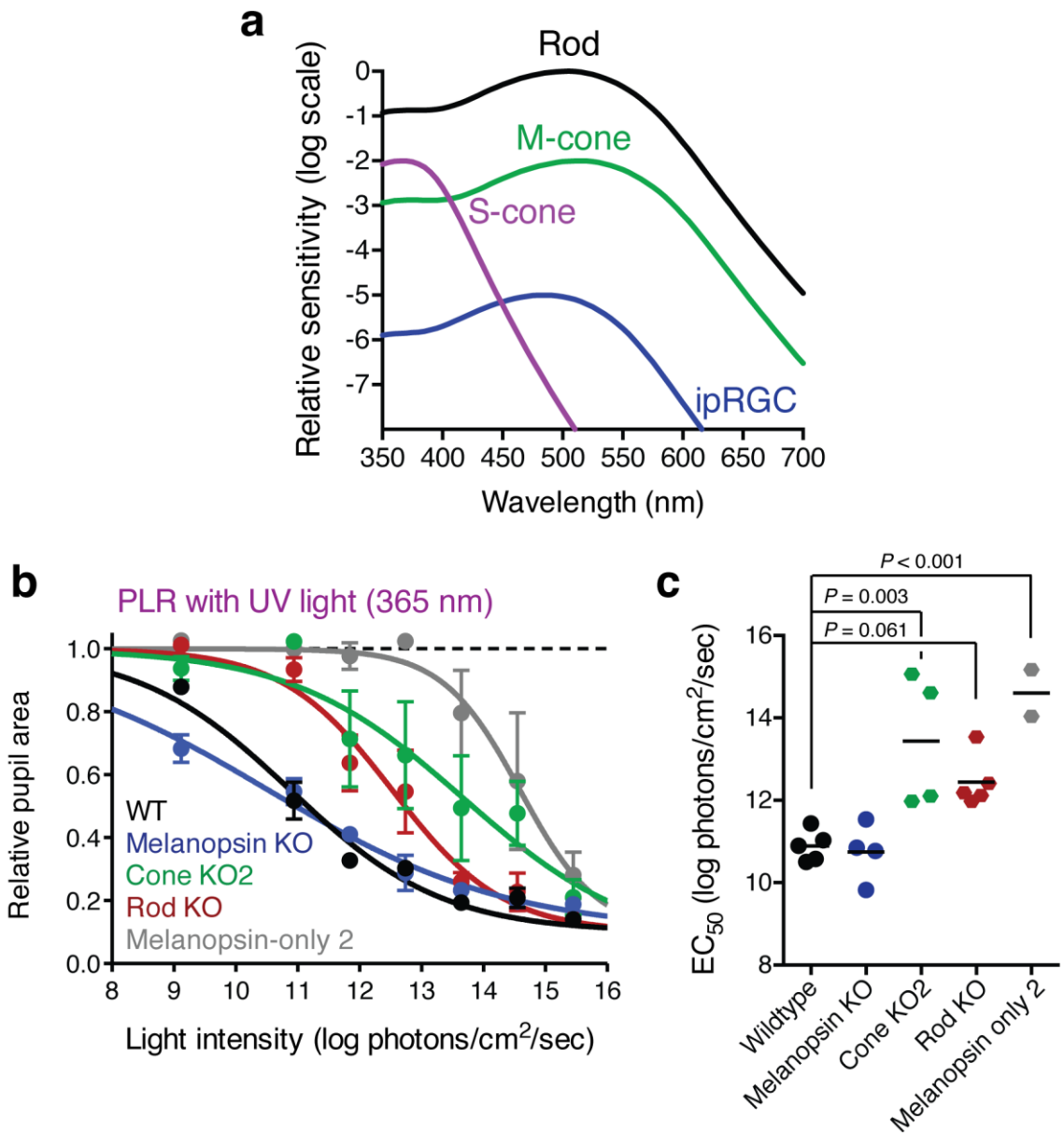


Figure 3.5: Both cones and rods are required for the PLR to UV light.

(a) Relative sensitivities of the different photoreceptors to light of different wavelengths, normalized to rod sensitivity. Note that at most wavelengths, rods are dramatically more sensitive than the other photoreceptors, while at UV the S-cones reach rod sensitivity. (b) Intensity-response curve of the PLR to UV light (365-nm LED). Melanopsin KO mice (blue, $n = 4$) are identical to WT (black, $n = 5$) at all light intensities. However, both Cone KO2 (green, $n = 4$) and Rod KO mice (red, $n = 5$) have sensitivity deficits in the

PLR. Mice lacking both rod and cone function (Melanopsin-only 2, gray, $n = 2$) are even more insensitive. Data is mean \pm SEM. (c) Sensitivities are quantified as EC₅₀. Statistical comparisons are one-way ANOVA followed by Sidak's post-test.

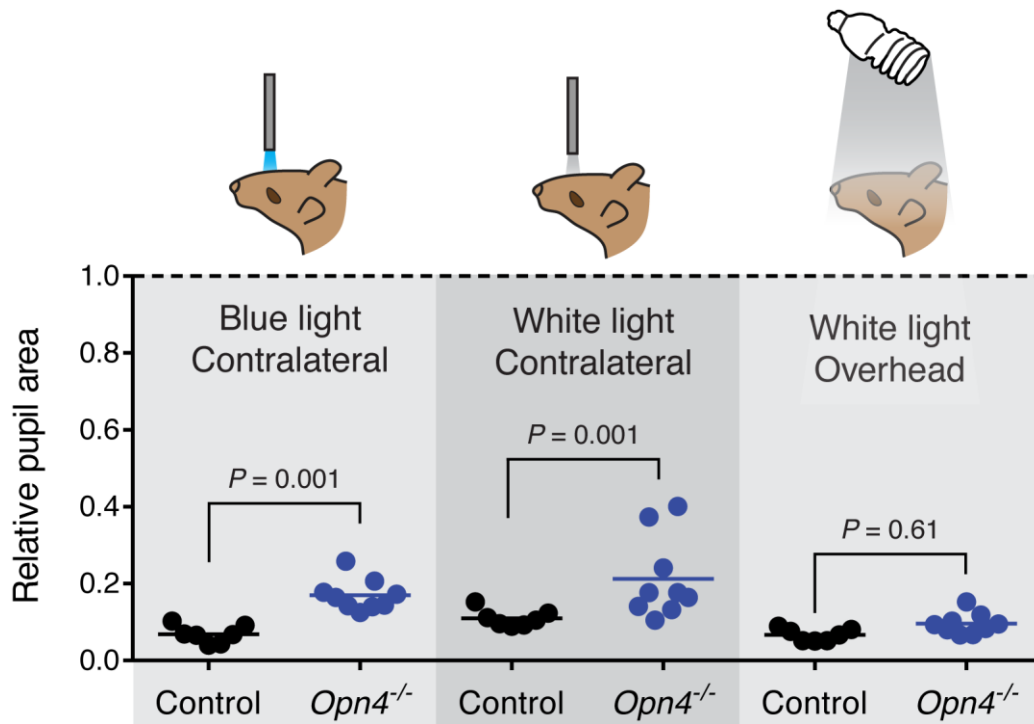


Figure 3.6: Melanopsin is not required for rapid PLR in response to environmentally relevant overhead light.

Rapid PLR determined under three different experimental light conditions. (Left) Blue (474-nm) LED light presented to contralateral eye. (Middle) White halogen light presented to contralateral eye. (Right) White compact fluorescent light presented overhead to both eyes. Statistical significance determined by one-way ANOVA followed by Sidak's post-test. No difference observed when light presented overhead. Control (black, *Opn4*^{+/-}) $n = 7$ and Melanopsin KO (blue, *Opn4*^{-/-}) $n = 9$.

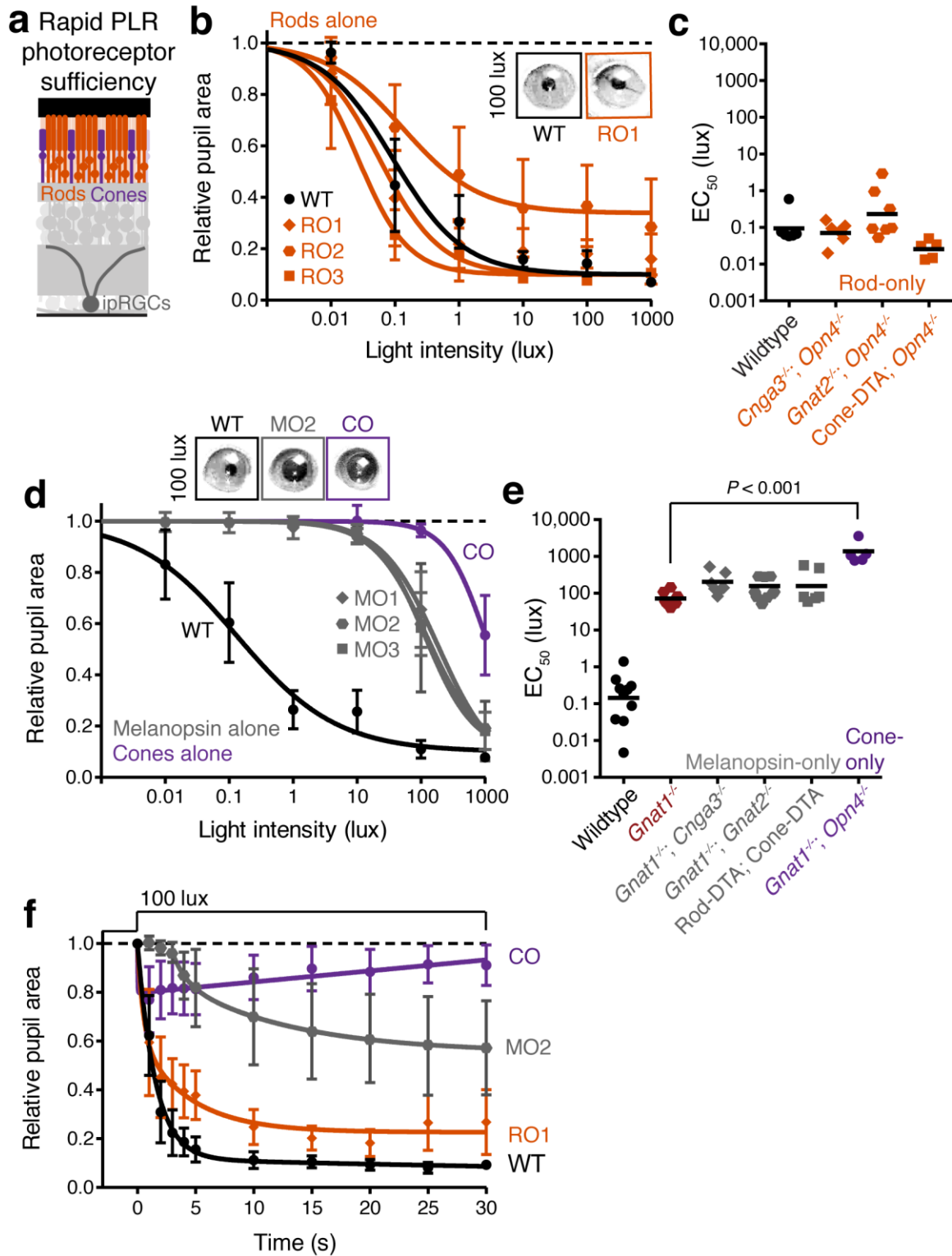


Figure 3.7: Rods are the only photoreceptors that are sufficient for the full rapid PLR.

(a) Multiple mouse lines with rods as the only functional photoreceptors. For the experiments in **b** and **c**: WT $n = 6$, Rod-only type 1 (RO1: *Cnga3*^{-/-}; *Opn4*^{-/-}) $n = 6$, Rod-only type 2 (RO2: *Gnat2*^{-/-}; *Opn4*^{-/-}) $n = 8$, Rod-only type 3 (RO3: Cone-DTA; *Opn4*^{-/-}) $n = 5$. (b) Intensity-response curve of the PLR in all of the rod-only lines, which are all similar to wild-type at all light intensities (mean \pm 95% CI). (c) Sensitivity (EC₅₀) in each of the mutant lines. No statistical differences were observed between the mouse lines (compared to WT, RO1 $P = 0.956$, RO2 $P = 0.340$, RO3 $P = 0.141$ using a one-way ANOVA with Sidak's post-test), although the RO2 line had more variability and trended toward lower sensitivity. Line indicates mean. (d, e) Multiple mouse lines with ipRGCs as the only functional photoreceptors (melanopsin-only) or a mouse line with cones as the only functional photoreceptors (cone-only). For the experiments in **d** and **e**: WT $n = 9$, *Gnat1*^{-/-} $n = 10$ (6 points replotted from Fig. 3.4), Melanopsin-only type 1 (MO1: *Gnat1*^{-/-}; *Cnga3*^{-/-}) $n = 7$, Melanopsin-only type 2 (MO2: *Gnat1*^{-/-}; *Gnat2*^{-/-}) $n = 9$, Melanopsin-only type 3 (MO3: Rod-DTA; Cone-DTA) $n = 6$, Cone-only (*Gnat1*^{-/-}; *Opn4*^{-/-}) $n = 6$. (d) Intensity-response curve of the PLR in all of the melanopsin-only lines and in the cone-only mouse line (mean \pm 95% CI). (f) EC₅₀ in each of the lines. All mutant lines are less sensitive than WT ($P < 0.001$) by >2 log units. Cone-only (*Gnat1*^{-/-}; *Opn4*^{-/-}) mice are additionally less sensitive than Rod KO (*Gnat1*^{-/-}) mice ($P < 0.001$), but no melanopsin-only line is significantly different from Rod KO (Compared to RKO: MO1 $P = 0.201$, MO2 $P = 0.625$, MO3 $P = 0.591$). All statistics are one-way ANOVA with Sidak's post-test, line indicates mean. (g) Kinetics of PLR in each of the 'only' lines at 100 lux, a light intensity at which all lines respond but show differences in magnitude. Rod-only mice (RO1) have both fast and relatively sustained kinetics, while cone-only (CO) mice have fast but transient responses and melanopsin-only (MO2) mice have slow but sustained signaling. Mean \pm 95% CI, sample size for each group is same as used in intensity-response experiments.

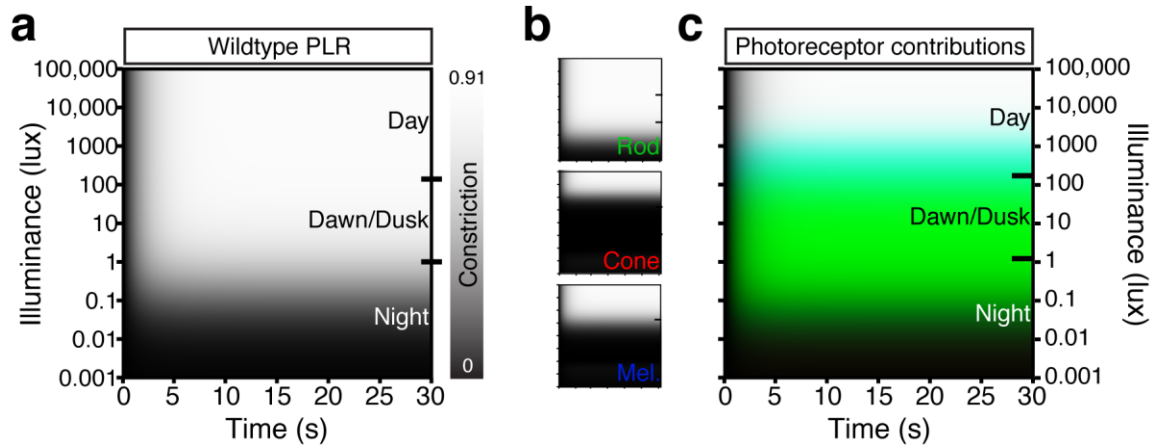


Figure 3.8: The photoreceptor contribution landscape of the pupillary light reflex.

(a) Heat map of the PLR as duration and intensity vary. Increasing intensity indicates increasing pupil constriction (black = 0 or no constriction, white = 0.91 the maximum mean constriction achieved by wildtype mice). Night, dawn/dusk, and daytime light intensities indicated by ticks on right side of plot. (b) Heat maps of individual photoreceptor contributions. Top to bottom: rod (green), cone (red), melanopsin (blue). Each photoreceptor contribution heat map is a combination of necessity (individual photoreceptor transduction knockouts) and sufficiency (“photoreceptor-only”) heat maps. Necessity and sufficiency were combined by taking the maximum value of either at each point. (c) Merged and colored heat maps of individual photoreceptor contributions from b. Green indicates rod contributions. Red indicates cone contributions. Blue indicates melanopsin contributions. See Methods for details on heat map generation.

Chapter 4

Rods use a non-conventional retinal circuit to drive the pupillary light reflex

This chapter is based on a manuscript currently in preparation:

Rupp AC, Ramakrishnan C, Deisseroth K, and Hattar S. A novel rod circuit drives the pupillary light reflex.

Abstract

The retina utilizes distinct parallel neural circuits for relaying various features of the visual world. Signals from rod photoreceptors are relayed in parallel circuits encoding distinct visual information. In all known rod circuits, connexin36 (Cx36)-containing gap junctions are required for rod signal transmission to retinal ganglion cells (RGCs), the projection neurons of the retina. Here we identify a novel retinal circuit that transmits rod signals to RGCs in the absence of Cx36. A subtype of RGCs—intrinsically photosensitive retinal ganglion cells (ipRGCs)—receives robust rod light information to drive the pupillary light reflex (PLR). However, the rod-driven PLR persists in *Cx36*^{-/-} mice. We use viral circuit tracing to show that rod bipolar cells, which were believed to never contact RGCs, make presumptive synaptic contacts with ipRGCs to drive the PLR, a circuit that would not require Cx36. This novel circuit has implications for understanding information flow in the retina and how different RGC subclasses encode the visual world.

Introduction

Precise neuronal circuits mediate the generation of a variety of behaviors from a limited number of sensory inputs. This is widely apparent in the retina, where parallel circuits encode distinct features of the visual world¹³. The output cells of the retina, the retinal ganglion cells (RGCs) exist in approximately thirty subtypes, differing in the visual information they encode, their presynaptic inputs, and synaptic targets in the brain⁵⁴. This allows a diversity of information about the visual world to be sent to the brain from the light absorption patterns of only two classes of classical photoreceptor cells, rods and cones.

To generate their specialized visual responses, each RGC subtype must receive unique presynaptic inputs. This is accomplished in part through the diversification of the excitatory interneurons—bipolar cells—that connect rods and cones to the RGCs. Approximately thirteen bipolar cell types exist with different connection patterns and light responses⁴⁷. Of these thirteen, the most abundant is dedicated to receiving exclusively light information from rods, called the rod bipolar cell²³⁸; the others receive cone input and are referred to as cone bipolar cells. However, while all cone bipolar cells directly synapse on RGCs, rod bipolar cells synapse instead on AII amacrine cells that then relay their light information to cone bipolar cells and ultimately to RGCs^{239,240}. This circuit utilizes connexin36-containing gap junctions between AII amacrine and cone bipolar cells²⁴¹. In agreement, connexin36 knockout mice have no known rod signals in RGCs^{242,243}.

Ultimately, the AII amacrine cell circuit is thought to be important for enhancing the signal to noise ratio of rod signals at dim light intensities. However, not all visual

functions require precise dim light detection. One major class of RGCs is the intrinsically photosensitive retinal ganglion cells (ipRGCs). ipRGCs are unique in that they do not require spatial visual information, but instead are dedicated for measuring ambient light intensity for subconscious visual functions such as pupillary light reflex and circadian photoentrainment^{70,95,237}. Additionally, these functions are relatively insensitive compared to the conscious perception of single photons²⁴⁴. Therefore, the presynaptic circuits for ipRGCs are likely to be distinct from the conventional circuits mediating spatial visual information.

Here, we investigated the circuits linking rods to ipRGCs. Using viral circuit tracing upstream of ipRGCs, we show that rod bipolar cells are presynaptic to ipRGCs. We then show that rods are capable of driving the PLR independent of connexin36-containing gap junctions, although they require ON bipolar cell function. These results indicate that a Cx36-independent ON circuit allows rod signals to reach ipRGCs and implicate a direct rod bipolar cell synaptic connection.

Results

Anatomical identification of cell types upstream of ipRGCs

To identify the cell types upstream of ipRGCs, we employed a transsynaptic viral tracing strategy to specifically label cells presynaptic to ipRGCs. To do so, we used two adeno-associated virus (AAV) injected into the vitreous of a mouse line that expresses Cre in ipRGCs (*Opn4^{Cre}*). The first AAV expresses a wheat germ agglutinin-Flp (WGA-Flp) fusion protein in the presence of Cre (AAV-DIO-WGA-Flp). WGA is a transsynaptic protein that travels retrograde, with some anterograde capacity²⁴⁵ (though

ipRGCs do make anterograde connections with dopaminergic neurons in the retina^{246,247}, this should be negligible relative to their presynaptic inputs). WGA will carry the Flp recombinase to cells upstream of ipRGCs. The second AAV carries a Flp-dependent (fd) yellow fluorescent protein (YFP), marking the cells that are Flp+ with YFP (AAV-fd-YFP) (Fig. 4.1a).

After injection of both AAVs, we observed a variety of YFP+ cells in the retina (Fig 4.1b,c). Importantly, injections of both viruses in wildtype mice lacking Cre never produced a fluorescent cell (data not shown), indicating that all cells labeled are specific to ipRGCs. The predominant cells were in the ganglion cell layer, representing ipRGCs that were infected with both viruses. In addition, the next two most abundant categories were Müller glia and a variety of amacrine cells. The robust Müller glia labeling has been previously reported to be specific to circuits upstream of ipRGCs¹²⁷, confirming the specificity of our method. Importantly, we never observed labeling of rods and cones and only rarely horizontal cells, implying there is limited capacity of the transsynaptic transfer of WGA to label cells multiple synapses away from ipRGCs.

We also observed labeling of bipolar cells, although much fewer than amacrine cells. This robust amacrine cell labeling is consistent with previous reports that the M1 subtype of ipRGCs receives relatively weak excitatory input, but strong inhibitory input¹¹⁸. When we quantified the types of bipolar cells labeled, we found that the majority were rod bipolar cells ($n = 10/12$ from 4 mice). A prediction from the conventional circuit diagram of the retina is that rod bipolar cell labeling should never be enriched over cone bipolar cells because rod signals must always pass through cone bipolar cells before

reaching RGCs²⁴⁸. This data suggests that rod bipolar cells may be directly presynaptic to ipRGCs.

This possibility has an anatomical basis, as rod bipolar cells have their synaptic terminals deep in the inner plexiform layer (IPL), close to RGC soma and proximal dendrites. In fact, when we label rod bipolar cell synaptic release sites using a genetically encoded presynaptic marker (*Pcp2-Cre; ROSA^{Synaptophysin-tdTomato/+}*), we find that release sites are absent along the axon shaft of rod bipolar cells and are concentrated in an area directly apposed to ipRGC somas and proximal dendrites (Fig. 4.2a).

The possibility has been proposed that M1 ipRGCs in rat receive direct ribbon synaptic input from rod bipolar cells on their soma. To test this, we fluorescently labeled all postsynaptic densities on ipRGCs by crossing a Cre-dependent *Psd95^{mVenus}* mouse line²⁴⁹ with the *Opn4^{Cre}* line. Importantly, the *Psd95^{mVenus}* line expresses a PSD95-mVenus fusion protein from the endogenous *Psd95* locus and cells expressing it are electrophysiologically normal²⁴⁹.

We observed many postsynaptic densities on the soma of M1 ipRGCs, identified by their melanopsin immunoreactivity and dendrites that stratify in the outermost IPL. However, when we co-stained for presynaptic ribbon synapses (anti-CtBP2) and rod bipolar cells (anti-PKCa), we found that colocalization of all three markers did not occur above random levels (Fig. 4.2). This suggests that M1 ipRGCs might not receive rod bipolar cell ribbon synapses on their soma. However, we cannot rule out the possibility that M1 ipRGCs receive non-ribbon input from rod bipolar cells or ribbon input on their dendrites or that non-M1 ipRGCs receive direct rod bipolar synapses^{63,139,250}.

A Cx36-independent rod ON circuit mediates the PLR

To test if a direct rod bipolar cell to ipRGC circuit is functional, we tested the pupillary light reflex (PLR) in mice lacking the conventional rod circuits (Fig. 4.3a). We have previously found rod function is required for the PLR at light intensities up to ~10 lux, as shown in the previous chapter.

To determine how rod signals reach ipRGCs, we silenced ON bipolar cells, including the rod bipolar cell, using a mouse line lacking the TRPM1 cation channel in ON bipolar cells (*Trpm1*^{-/-})²⁹. *Trpm1*^{-/-} mice phenocopy the defects in the PLR seen in rod transducin knockout mice (*Gnat1*^{-/-}), with no PLR until the light intensity reaches >10 lux (Fig. 4.3b–d). These results show that ON bipolar cells are required for the PLR at light intensities at which rods are required for the PLR, indicating that rods use an ON bipolar cell to mediate the PLR.

While the most likely candidate ON bipolar cell is the rod bipolar cell, rod signals can also avoid rod bipolar cells by utilizing the secondary rod circuit: utilizing gap junctions between rods and cones and traveling along the cone to cone bipolar cell to RGCs. We find this possibility unlikely because rod-cone gap junctions vary in a diurnal manner are closed during the day¹³¹ and all our experiments were performed during the day. Additionally, we previously found that a mouse line that lacks cone cell bodies by genetic ablation (*Cone-DTA*)²²⁵ and therefore has no ability for rod signals to pass through cones had a PLR identical to wildtype (Fig. 3.7b).

The only remaining conventional rod ON circuit is the primary rod circuit. Connexin36-containing gap junctions are required for the primary rod circuit between All amacrine cells and cone bipolar cells (as well in the secondary circuit at rod-cone gap

junctions)²⁴¹. ON RGCs in *Cx36*^{-/-} mice (also known as *Gjd2*^{-/-}) have reduced light sensitivity with a threshold near cone threshold^{242,243}, consistent with a lack of rod input. To test if rods utilize the primary rod circuit to mediate the PLR, we utilized *Cx36*^{-/-} mice, which should have an identical PLR to rod mutant mice and ON bipolar cell mutant mice.

However, when we tested the PLR in *Cx36*^{-/-} mice, we found that they were almost identical to wildtype, albeit with a slight decrease in sensitivity (Fig. 4.3b–d). *Cx36*^{-/-} mice were ~2-log units more sensitive than mice lacking rod function and ON bipolar cell function (Fig. 4.3b–d). These results show that rods are capable of driving the PLR using an ON circuit that does not require the AII amacrine circuit or the rod-cone gap junction circuit, the two conventional means for rod signals to reach RGCs. In total, these results implicate a potential physiological contribution of rod bipolar cell synaptic input to ipRGCs.

Discussion

Here we identified the rod circuits required for the pupillary light reflex. We have provided compelling evidence that rod circuits to ipRGCs are distinct from those for conventional RGCs. While rods require ON bipolar cell function for the PLR, they do not require the connexin36-containing gap junctions that are presumed to be required for all rod ON signal transmission. In combination with our circuit tracing data revealing rod bipolar cells presynaptic to ipRGCs, this suggests that rod bipolar cells synapse directly with ipRGCs.

We are currently unable to determine the specific ipRGC subtype that receives direct rod bipolar cell input. The M1 subtype of ipRGCs is believed to be the predominant contributor to the PLR^{95,105}. Despite M1 cells stratifying in the OFF

sublamina of the inner plexiform layer (IPL), all ipRGCs receive almost exclusively ON pathway input^{101,118,251}. In addition, ON pathway is required for the rod/cone input to the PLR^{252–254}. However, we could not confirm that rod bipolar cell ribbon synapses are localized to M1 ipRGC soma, as has been previously proposed¹²³.

The specific ON pathway components driving ipRGCs in general and the PLR in particular has remained a mystery. The ON bipolar cells driving ipRGCs are both sensitive and sustained^{101,118,237,251,255}. Very few subtypes of cone ON bipolar cells relay sustained input⁴⁸ and there is sparse cone bipolar input to M1 ipRGCs^{120–122}. In combination with the fact that cones are relatively dispensable for the PLR (Fig. 3.4) suggests that cone bipolar cells are not the predominant input to ipRGCs.

In total, we believe the available evidence indicates the most likely input is the rod bipolar cell without the use of their conventional downstream circuits. While rod bipolar cells relay sustained light information, the AII amacrine cells are relatively transient⁴⁰. This transient signaling of AII amacrine cells, coupled with our *Cx36*^{-/-} PLR data showing only a minor deficit in sensitivity, indicate that the primary rod pathway is not required for the PLR, although it may be involved specifically at very dim light intensities²⁵⁵. Rod bipolar cells avoiding the AII circuit to directly synapse on ipRGCs would facilitate their role in sustained ambient light detection. While synaptic input to conventional RGCs relaxes toward baseline within seconds, rod input to ipRGCs produces spiking up to 10 hours²³⁷. This indicates that rods must utilize a remarkably sustained circuit to reach ipRGCs that is distinct from rod circuits to conventional RGCs.

Interestingly, mice lacking both the primary and secondary rod pathways and cone function (*Cx36*^{-/-}; *Gnat2*^{-/-}) still retain rod responses in the dorsal lateral geniculate

nucleus (dLGN)²⁵⁶. The dLGN is known to receive projections from the non-M1 ipRGCs⁹⁹, indicating non-conventional rod circuits may be broadly utilized. We hypothesize that this direct rod bipolar cell to ipRGC circuit would be especially useful for encoding ambient light intensity for many aspects of vision.

Acknowledgments

We would like to thank Alapakkam Sampath for providing the *Cx36*^{-/-} mice and Marquis Walker and Craig Montell for the *Trmp1*^{-/-} mice.

Methods

Animal husbandry

C57Bl/6 x Sv129 hybrid mice were used in all experiments and were housed according to guidelines from the Animal Care and Use Committee of Johns Hopkins University. Male and female mice age 2–8 months were housed in plastic translucent cages with steel-lined lids in an open room. Ambient room temperature and humidity were monitored daily and tightly controlled. Food and water were available *ad libitum*. All mice were maintained in a 12hr:12hr light-dark cycle of ~500 lux for the entirety of their lives.

Molecular cloning and virus production

The AscI site in pAAV-Ef1a-DIO eYFP construct was changed to SpeI restriction site using overlapping PCR and then cut with SpeI and NheI for the vector backbone. The mCherry-IRES-WGA-Flpo was PCR amplified with SpeI and NheI sites and inserted into the mutated AAV-Ef1a-DIO backbone by quick ligase (from NEB). The clones were completely sequence verified. pAAV-Ef1a-fd-YFP has been described previously²⁵⁷. Both constructs were packaged at the UNC Vector Core.

Viral circuit tracing

Mice were anesthetized by intraperitoneal injection of avertin (2, 2, 2-Tribromoethanol) and placed under a stereo microscope. 0.5–1 μ l of both AAV8-Ef1a-DIO-mCherry-IRES-WGA-Flp and AAV5-Ef1a-fd-YFP was mixed on a piece of Parafilm and drawn into a 10- μ l microcapillary tube (Sigma P0674) that had been pulled to a needle (Sutter Instruments, Model P-2000). The loaded needle was then placed in the

holster of a pico-injector (Harvard Apparatus PLI-90). The needle punctured the eye posterior to the ora serrata and air pressure was used to drive the viral solution into the vitreous chamber of the eye to ensure delivery specifically to the retina. Mice recovered from surgery on a heating pad until they woke from anesthesia.

Immunofluorescence

All mice were euthanized by intraperitoneal injection of avertin and cervical dislocation. For viral tracing experiments, mice were euthanized at least 4 weeks following injection. For whole mount images, retinas were fresh dissected in PBS, fixed in 4% paraformaldehyde (PFA), rinsed in PBS, and stained overnight in primary antibody solution. For retina sections, eyes were removed, rinsed in PBS, fixed in 4% PFA, rinsed again, then placed overnight in 30% sucrose at 4 °C. Eyes were then embedded in OCT (Tissue-Tek) on dry ice and stored at -20 °C or -80 °C overnight. Eyes were then sectioned at 10 or 20 µm on a cryostat. After drying onto slides overnight, retina sections were briefly rinsed in PBS and then subjected to the same immunofluorescence protocol as whole mount retinas.

Primary antibodies include chicken anti-GFP (Abcam ab13970), mouse IgG2a anti-PKCa (Sigma P5704), rabbit anti-OPN4 (Advanced Targeting Systems AB-N38), and/or anti-CtBP2 (BD Transduction Laboratories 612044), overnight in 4% goat serum at 4 °C. Retinas were then rinsed in PBS and stained for 2 hours at room temperature in secondary antibody solution containing goat anti-rabbit 405 (Life Technologies A31556), goat anti-chicken 488 (Life Technologies A11039), goat anti-rabbit 488 (Life Technologies A11034), goat anti-mouse IgG2a 546 (Invitrogen A21133), and/or goat

anti-mouse IgG1 647 (Life Technologies A21240) before mounting on a slide with Fluoromount (Sigma) with or without DAPI. All antibodies were used at 1:1000.

Confocal microscopy and image processing

Slides were imaged on either a Zeiss LSM 700 confocal microscope or a Zeiss LSM 510 META confocal microscope with 63× oil or 20× air objectives. *z*-stack images were subjected to a *z*-stack of 0.53 μm spacing at 63× or 1.00 μm at 20× covering the entire ganglion cell layer, inner plexiform layer, and inner nuclear layer. Images were then loaded into FIJI (<http://fiji.sc>) and background subtracted and brightness and contrast was adjusted before preparing figures.

Pupillometry

All mice were dark-adapted for at least 30 minutes prior to any experiments and all PLR experiments were performed between Zeitgeber times (ZT) 2 and 10. Mice were restrained manually under a 10-, 13-, or 23-Watt compact fluorescent light bulb (GE Daylight FLE10HT3/2/D or Sylvania Daylight CF13EL and CF23EL) with a color temperature of 6500 K to simulate natural sunlight. The light intensity was measured using a light meter (EXTECH Foot Candle/Lux Light Meter, 401025) at the surface on which the mouse was held. The light meter was initially calibrated by EXTECH using a Tungsten 2856 K light source; because our experiments used a fluorescent bulb of 6500 K, all measured light intensities reported here may vary by 0.92–1.12 times the actual light intensity. Light intensity was adjusted by a combination of altering the distance of the light bulb(s) from the mouse and/or applying neutral density filters (Roscolux). The light meter is incapable of detecting light intensities below 1 lux, so one neutral density filter cutting the light intensity by 12.5% was applied to the bulb to estimate 1-log unit

decreases in illumination below 1 lux. Light intensities above 500 lux required the use of multiple light bulbs.

Videos of the eye were taken using a Sony Handycam (DCR-HC96) mounted on a tripod a fixed distance from the mouse. Manual focus was maintained on the camera to ensure that only one focal plane existed for each mouse and that therefore variable distance from the camera should not contribute to differences in relative pupil area throughout the video. Pupil size was first recorded under dim red light and the endogenous infrared light source of the camera to capture the dark-adapted pupil size. Following at least 5 seconds of recording in dark, the pupil was continuously recorded for at least 30 seconds of a light step stimulus. All pupil images presented in the paper were cropped to a fixed square area (generally 100 x 100 pixels) surrounding the eye using GNU Image Manipulation Program (GIMP). The images were made grayscale and then brightness and contrast were adjusted to enhance visibility of the pupil and exported as PNG files.

Data analysis

Videos were transferred from the camera to a computer as Audio Video Interleave (AVI) files and individual frames were taken using VLC media player (www.videolan.org/vlc/) and saved in portable network graphics format (PNG). Images were taken in the dark, at 5 seconds, and 30 seconds following stimulus onset. Pupil area was then quantified manually in ImageJ (<http://rsbweb.nih.gov/ij/>) software. First, the image was enlarged to 300% normal size. Then, the image was converted to grayscale and brightness and contrast were adjusted so as to confine the borders of the input channel (black → white) to the edges of the pixel intensity histogram. The pupil area was

measured in pixels using the oval tool in which the 4 cardinal points of the oval were touching their respective edges of the pupil. The relative pupil area was calculated using LibreOffice Calc or Microsoft Excel in which the area during the light stimulus was divided by the area prior to lights onset. The minimum relative pupil size of either 5 seconds or 30 seconds after stimulus was used for all genotypes.

The intensity-response curve was fit using a variable slope sigmoidal dose-response curve in Graphpad Prism 6. The top and bottom of the fit were constrained to 1.0 and between 0 and 0.10, respectively, to ensure the EC_{50} for each genotype was represented by similar curves. The sensitivity for each genotype was calculated using the same process of fitting each individual animal's data points with a sigmoidal dose-response curve to generate EC_{50} .

Statistical analysis

All statistical tests were performed in Graphpad Prism 6. Specific statistical comparisons are listed in the figure captions. Because the EC_{50} data appears to be a normal distribution on a log scale (log-normal distribution), all statistical tests and data analysis involving EC_{50} were performed on the log transformed data set.

Figures

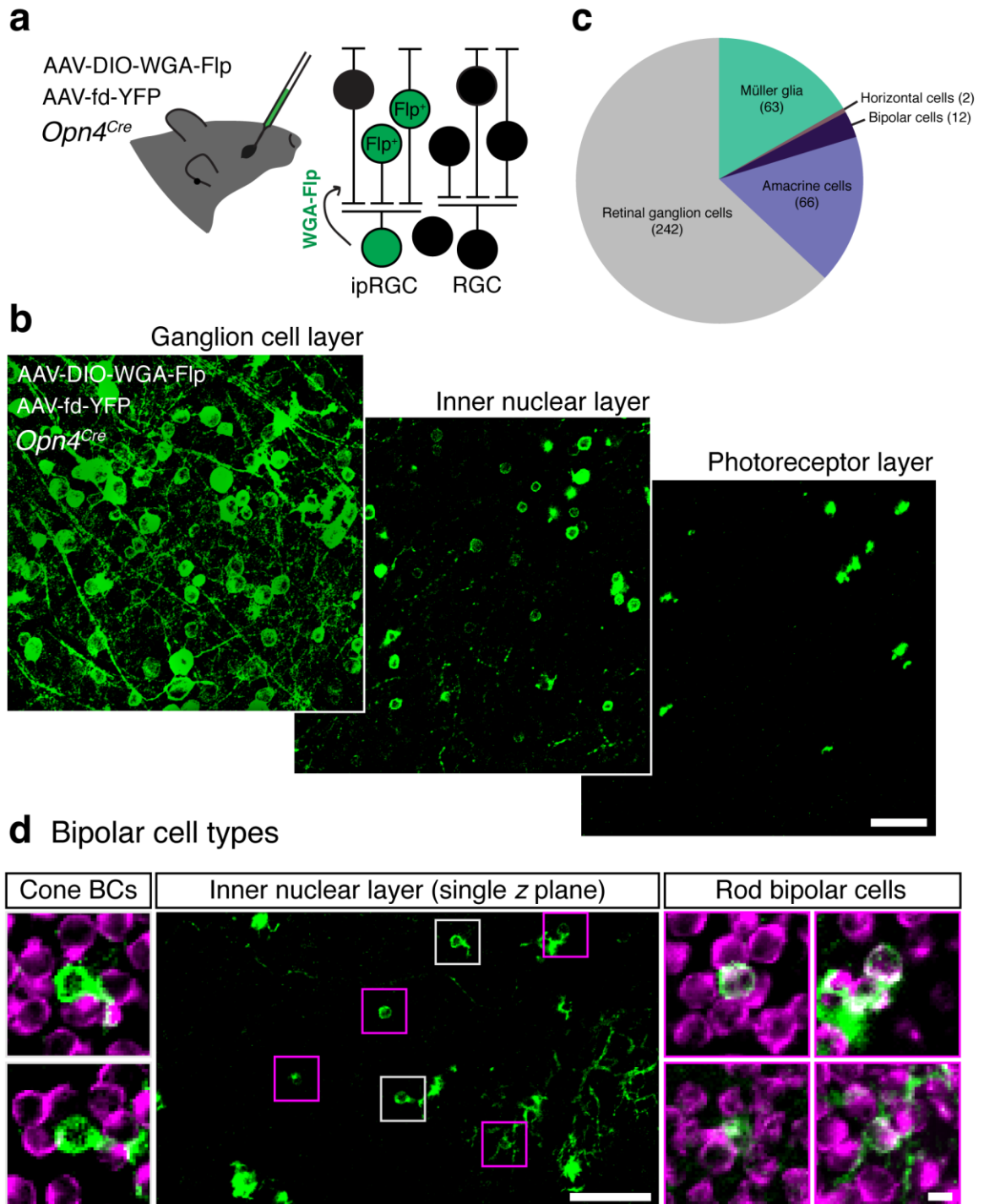


Figure 4.1: Transsynaptic circuit tracing reveals rod bipolar cells upstream of ipRGCs.

(a) We employed an adeno-associated viral (AAV) circuit tracing strategy involving injection of two AAVs into the vitreous of melanopsin-Cre mice (*Opn4^{Cre}*): (1) AAV carrying a Cre-dependent expression of WGA-Flp (AAV-DIO-WGA-Flp) and (2) AAV carrying a Flp-dependent YFP (AAV-fd-YFP). WGA-Flp will only be expressed in ipRGCs and will be carried retrograde to cells upstream, which will be labeled with YFP.

(b) Example images of YFP+ cells stained with anti-GFP antibody to enhance the signal. Most signal is present in the ganglion cell layer, though many cells in the inner nuclear layer are also labeled. We never observed cells in the photoreceptor layer labeled; the green signal in the outer nuclear layer is the processes of Müller glia. Scale bar = 50 μm .

(c) Quantification of the cell types labeled from 8 regions of 3 retinas. (d) Immunofluorescence image of a single *z* plane through the inner nuclear layer for rod bipolar cells (anti-PKCa, magenta) reveals that most YFP+ (green) bipolar cells are rod bipolar cells (magenta boxes, zoomed images to right), with some cone bipolar cells labeled (gray boxes, zoomed images to left). Again, the other YFP signal that is not boxed in is from Müller glia and one horizontal cell. Scale bar on main image = 50 μm , on the zoomed images = 5 μm .

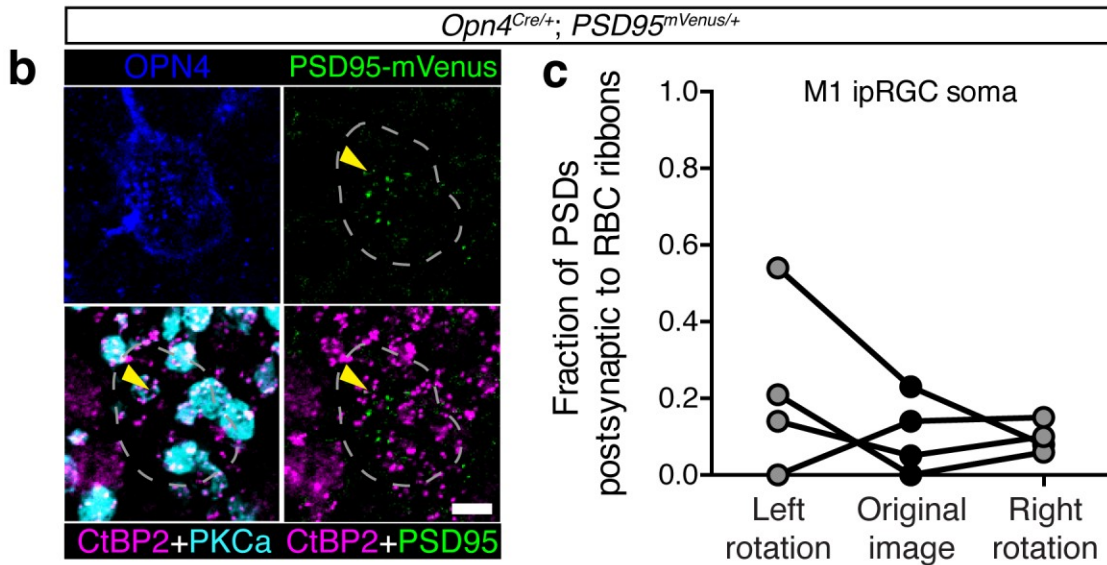
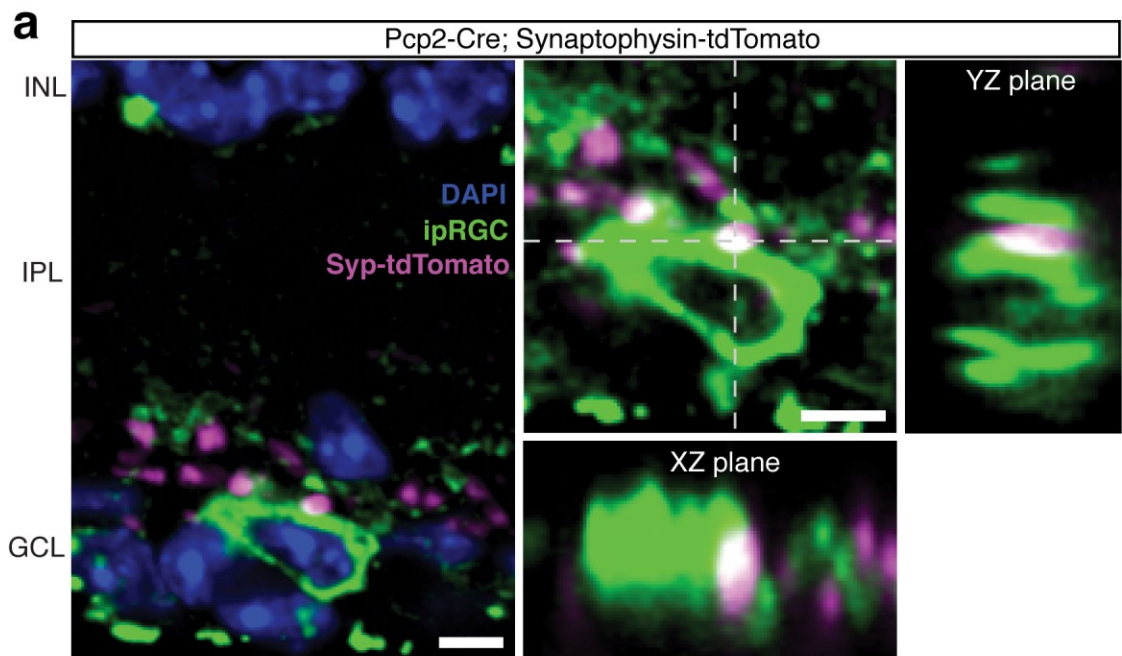


Figure 4.2: Using genetically labeled pre- and postsynapses to identify ipRGC synaptic input locations.

(a) Labeling rod bipolar cell presynapses with Pcp2-Cre; *ROSA^{Synaptophysin-tdTomato/+}* (Syp-tdTomato, magenta) shows that rod bipolar cell release sites are deep in the IPL near RGC soma and proximal dendrites. Immunofluorescence for ipRGCs (anti-OPN4, green)

shows that rod bipolar cell release sites are near ipRGC soma and proximal dendrites. **(b)** Immunofluorescence of an OPN4-PSD95mVenus retina (*Opn4^{Cre/+}; PSD95^{mVenus/+}*), stained for presynaptic bipolar cell ribbon synapses (anti-CtBP2, magenta) and rod bipolar cells (anti-PKC α , cyan), M1 ipRGCs (anti-OPN4, blue), and raw immunofluorescence from PSD95-mVenus (green). Yellow arrow indicates presumptive synaptic contact between a rod bipolar cell ribbon synapse and an ipRGC PSD. **(c)** Quantification of the fraction of postsynaptic densities on M1 ipRGC soma that are apposed to a rod bipolar cell (RBC) presynaptic ribbon synapse. Control experiments rotating the presynaptic channel (PKC α and CtBP2) 90° left or right reveals that rod bipolar cell ribbon inputs to M1 ipRGC soma does not occur above random levels. Scale bars = 5 μ m.

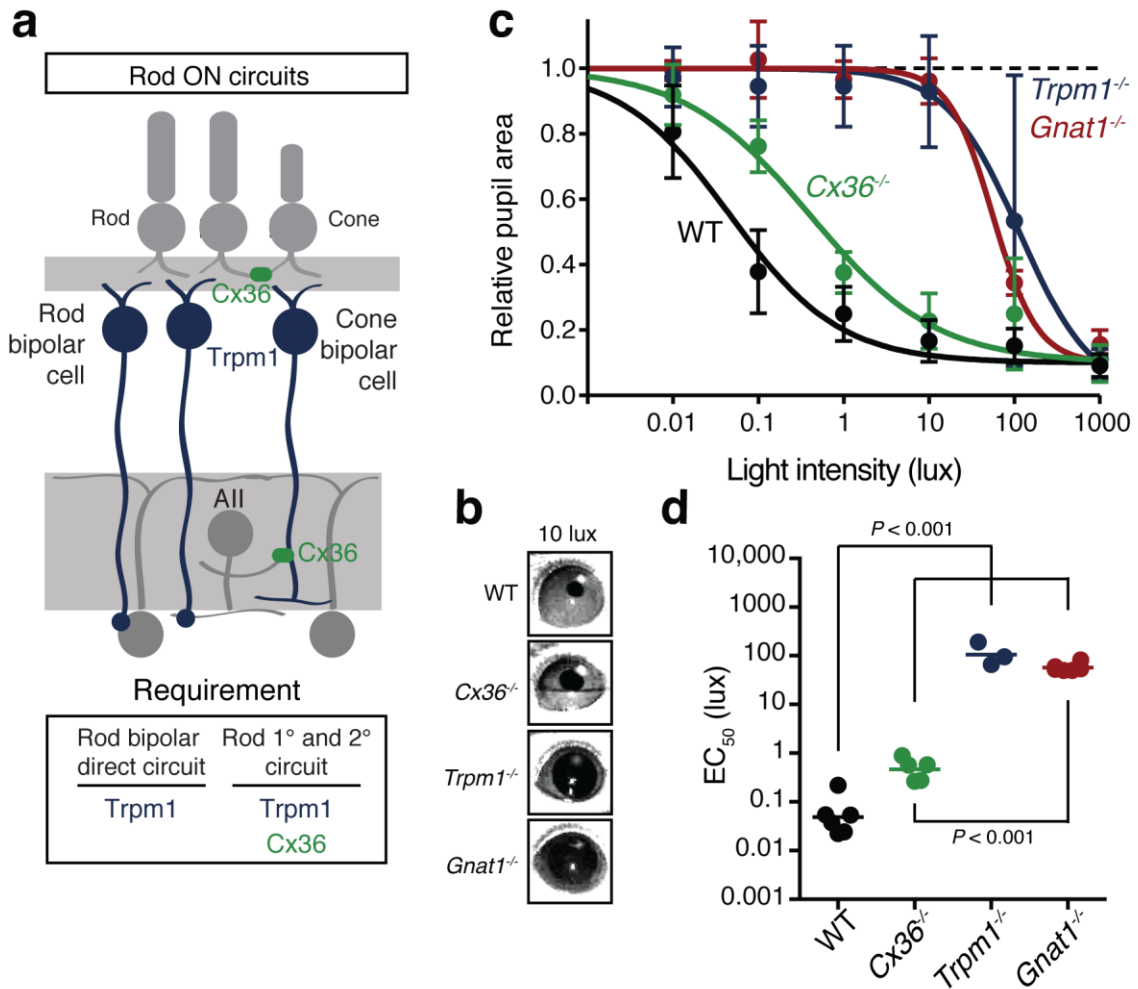


Figure 4.3: A non-conventional rod circuit drives the PLR.

(a) Cartoon depicting the potential rod ON circuits in the retina. The primary (1°) and secondary (2°) rod circuits (right) require Trpm1 function in ON bipolar cells and Cx36 function in rod-cone gap junctions and AII amacrine cell-cone bipolar cell gap junctions. However, a direct rod bipolar cell to RGC circuit would only require Trpm1, but not Cx36. (b) Representative images of WT, *Cx36*^{-/-}, *Trpm1*^{-/-}, and *Gnat1*^{-/-} mice at 10 lux. (c) Intensity-response curve of the PLR for different retinal mutant mouse lines: WT (black, *n* = 6), *Cx36*^{-/-} (green, *n* = 5), *Trpm1*^{-/-} (dark blue, *n* = 3), *Gnat1*^{-/-} (red, *n* = 6, replotted from Fig. 3.4). All data are mean ± 95% CI and fit with a sigmoidal dose-response curve. (d) Sensitivity (*EC*₅₀) of the different lines, with a point for every mouse and a line at the mean. Statistical comparisons are one-way ANOVA followed by Sidak's post-test.

Chapter 5

Distinct ipRGC subtypes mediate acute and circadian regulation of body temperature

This chapter is based on a manuscript currently in preparation:

Rupp AC, Altimus CM, Fernandez DC, and Hattar S. Distinct ipRGC subpopulations mediate light's acute and circadian effects on body temperature.

Abstract

Abnormal light environments negatively impact human alertness, mood, and cognition by acutely disrupting physiological processes and misaligning circadian rhythms. A small population of retinal neurons, intrinsically photosensitive retinal ganglion cells (ipRGCs), has been implicated in both light's acute and circadian regulation of many processes, including mood, cognition, and body temperature. We show here that ipRGCs accomplish this by utilizing distinct genetic subpopulations for either light's acute or circadian regulation of body temperature. Mice with genetic ablation of ipRGCs that express *Brn3b* display normal circadian photoentrainment of body temperature, but no acute body temperature decrease in response to light. Conversely, chemogenetic activation of Brn3b-positive retinal cells alone drives acute body temperature decreases. We also confirm that acute and circadian regulation utilize distinct coding mechanisms; acute regulation requires melanopsin phototransduction but circadian photoentrainment does not. Our results provide a cellular basis for using light to promote cognition and alertness while avoiding circadian disruption.

Introduction

Many essential functions are influenced by light both indirectly through alignment of circadian rhythms (photoentrainment) and acutely by a direct mechanism^{8-10,12,258}. Dysregulation of the circadian system by abnormal lighting conditions has many negative consequences, which has motivated decades of work to identify the mechanisms of circadian photoentrainment²⁵⁹. In contrast, it has only recently become apparent that light exposure can also acutely influence human alertness, cognition, and physiology²⁶⁰. As a result, there is a developing awareness of light quality in everyday life¹⁸⁰. It is therefore essential to human health and society to elucidate the circuitry and coding mechanisms underlying light's acute effects.

Circadian photoentrainment is coordinated by relay of light information from intrinsically photosensitive retinal ganglion cells (ipRGCs) of the retina to the master circadian pacemaker, the suprachiasmatic nucleus (SCN)^{95-97,261}. ipRGC genetic ablation results in normal circadian rhythms that 'free-run' with respect to the light/dark cycle⁹⁵⁻⁹⁷, suggesting the SCN is normal but does not receive light information. Further, ablation of all ipRGCs except those that project to the SCN results in normal circadian photoentrainment¹⁰⁵. ipRGCs seem to use redundant light-detection mechanisms to support photoentrainment, relaying light information from either indirect synaptic input from the rod/cone photoreceptors^{85,86,178,228,262} or from their endogenous melanopsin phototransduction cascade^{73,77,88,89,263}.

In addition to their role in circadian photoentrainment, ipRGCs have been implicated in some aspects of acute light responses. Genetic ablation of ipRGCs or their melanopsin phototransduction cascade blocks or attenuates the acute effects of light on

sleep⁸⁻¹⁰ and mood¹². This dual role of ipRGCs in circadian and acute light responses suggests they may share a common circuit mechanism. However, the circuit basis for ipRGCs in the acute effects of light has yet to be identified. Further, ipRGCs project broadly in the brain beyond the SCN^{83,84,102,264} and are comprised of multiple subpopulations with distinct genetic, morphological, and electrophysiological signatures^{98,99,102}, raising the possibility that distinct subpopulations mediate acute and circadian roles of ipRGCs^{62,105}.

There are multiple potential models for how ipRGCs mediate both the acute and circadian effects of light, including (1) ipRGCs mediate both acute and circadian light responses through their innervation of the SCN, (2) ipRGCs mediate circadian photoentrainment through the SCN, but send collateral projections elsewhere in the brain to mediate acute light responses, or (3) the subpopulation(s) of ipRGCs that project to the SCN for circadian regulation are distinct from the subpopulation(s) that projects elsewhere to mediate acute light responses. To date, a role for the SCN in both acute and circadian responses has predominated^{265,266}. However, it has been controversial due to complications associated with SCN lesions²⁶⁷ and alternative models proposing a role for direct ipRGC input to other central targets^{9,10,265,267,268} (with no reference to whether those are collateral projections from SCN-projecting ipRGCs). Here, we sought to address the question of how environmental light information—through ipRGCs—mediates both the circadian and acute regulation of behavior and physiology. To do so, we investigated the ipRGC subpopulations and coding mechanisms that mediate acute body temperature and activity regulation by light.

Results

To identify mechanisms of acute physiological regulation by light, we maintained mice on a 12-hr/12-hr light/dark cycle and then presented a 3-hr light pulse two hours into the night (Zeitgeber time 14, ZT14) while measuring core body temperature and general activity simultaneously (Fig. 5.1a). The nocturnal light pulse paradigm is well-established for studying acute regulation of sleep and wheel-running activity^{8,9,258,269}. We focused on body temperature because of its critical role in cognition and alertness^{270,271}, sleep induction and quality²⁷², metabolic control²⁷³, and circadian resetting⁹⁴.

Body temperature photoentrains to the light/dark cycle with peaks during the night and troughs during the day (Fig. 5.1b,d). Both rodents and humans utilize ocular light detection to acutely adjust body temperature in response to a nocturnal light pulse^{274,275}, though how this body temperature change is initiated by the retina and relayed to the brain is unknown. When we presented wildtype mice with a nocturnal light pulse, we observed a decrease in both body temperature and general activity compared to the previous night. Further, the decrease in body temperature and activity was sustained for the entire 3-hr stimulus, with moderate rundown (Fig. 5.1c,e). Interestingly, we found a positive correlation between the magnitude of body temperature and activity reductions (Fig. 5.1f), suggesting they may share at least some common mechanisms.

We observed that acute body temperature regulation only occurred at relatively bright light intensities (>500 lux) (Fig. 5.2). This, in combination with previous reports that body temperature regulation is most sensitive to short-wavelength light²⁷⁵, suggest it may be mediated by melanopsin phototransduction in ipRGCs because melanopsin is most sensitive to blue light and ipRGC phototransduction is relatively insensitive

compared to rods and cones^{79,244,276}. To test this, we measured body temperature and activity in mice lacking either functional rods and cones (melanopsin-only: *Gnat1*^{-/-}; *Gnat2*^{-/-}) or lacking melanopsin (melanopsin KO: *Opn4*^{-/-}). Both genotypes photoentrained their body temperature (Fig. 5.3a,b), with an amplitude indistinguishable from wildtype (Fig. 5.3c). However, we found that acute body temperature decrease to a nocturnal light pulse was present in melanopsin-only mice (*Gnat1*^{-/-}; *Gnat2*^{-/-}) (Fig. 5.3d,e), but absent from melanopsin knockout mice (*Opn4*^{-/-}) (Fig. 5.3f,g). This indicates that melanopsin is critical for light's ability to drive acute body temperature decreases, as it is for acute sleep induction⁸⁻¹⁰.

Importantly, this impaired thermoregulation in melanopsin knockout mice is not a consequence of altered general activity, because simultaneous general activity measurements revealed that melanopsin knockout mice reduce their activity in response to light (Fig. 5.4). Light's acute effects on wheel-running activity appears to involve conscious visual perception²⁷⁷, while ipRGCs are largely regulate non-spatial vision, suggesting that rod/cone light information through other RGC types can regulate activity. In summary, these results indicate that ipRGCs, using their melanopsin phototransduction cascade, are the only retinal cells that are necessary and sufficient for light's acute effects on body temperature.

ipRGCs comprise multiple subtypes with distinct gene expression profiles, light responses, and central projections⁹⁸, prompting us to ask which subtypes mediate acute thermoregulation. Brn3b(+) ipRGCs project to many structures including the olivary pretectal nucleus (OPN) and dorsal lateral geniculate nucleus (dLGN), but largely avoid the SCN¹⁰⁵. In contrast, Brn3b(-) ipRGCs project extensively to the SCN and

intergeniculate leaflet (IGL), while avoiding the OPN and dLGN¹⁰⁵ (**Fig**). Ablation of Brn3b(+) ipRGCs using melanopsin-Cre and a Cre-dependent diphtheria toxin knocked into the *Brn3b* locus (Brn3b-DTA: *Opn4*^{Cre/+}; *Brn3b*^{DTA/+}) removes virtually all ipRGC input to brain areas aside from the SCN and IGL, and these mice retain circadian photoentrainment of wheel-running activity¹⁰⁵.

When we measured body temperature in Brn3b-DTA mice, we found that their body temperature was photoentrained with a similar amplitude to controls (Fig. 5.5a–c). However, despite the presence of melanopsin in Brn3b-DTA mice, they did not acutely decrease body temperature in response to a nocturnal light pulse (Fig. 5.5f,g). Importantly, melanopsin heterozygous control mice (*Opn4*^{Cre/+}) displayed a normal body temperature decrease in response to a nocturnal light pulse (Fig. 5.5d,e). Furthermore, Brn3b-DTA mice retained acute activity suppression by light, though the magnitude was reduced compared to controls (Fig. 5.6). This finding supports our previous results in melanopsin knockout mice that non-ipRGC cells are capable of contributing to light's effects on general activity. These results demonstrate that Brn3b-positive ipRGCs are required for acute body temperature regulation by light, revealing that light information to the SCN is sufficient for circadian photoentrainment of body temperature, but not its acute regulation.

This suggests that there are two functionally distinct populations of ipRGCs that regulate the same physiological function: (1) Brn3b-negative ipRGCs that project to the SCN to mediate circadian photoentrainment of body temperature and (2) Brn3b-positive ipRGCs that project elsewhere in the brain to mediate acute thermoregulation. To test if Brn3b-positive ipRGCs are sufficient for acute thermoregulation, we expressed a

chemogenetic activator in Brn3b(+) RGCs (Fig. 5.7a, *Brn3b*^{Cre/+} with intravitreal AAV2-hSyn-DIO-hM3D(G_q)-mCherry, we refer to these mice as Brn3b-hM3D(G_q). This technique allows us to acutely activate the Brn3b(+) RGCs with the DREADD agonist clozapine N-oxide (CNO). We found that after intravitreal viral delivery, many RGCs were infected, including melanopsin-expressing ipRGCs (Fig. 5.7a).

Importantly, all Brn3b-hM3D(G_q) mice photoentrained to a normal light/dark cycle (Fig. 5.7b). Following CNO administration at ZT14 to depolarize the Brn3b-positive RGCs, we observed a robust decrease in body temperature (Fig. 5.7d) compared to PBS injection the previous night (Fig. 5.7c,e) that lasted at least 6 hours. Importantly, nocturnal CNO administration had no significant effect on wildtype body temperature (Fig. 5.8). Together, these results demonstrate that Brn3b-positive ipRGCs mediate the acute effects of light on body temperature and activity through extra-SCN projection(s), while Brn3b-negative ipRGCs mediate circadian photoentrainment by projections to the SCN and/or IGL.

Discussion

We show here that for the same physiological outcome, the acute effects of light are relayed through distinct circuitry from that of circadian photoentrainment, despite both processes using the same class of retinal neurons. Our results indicate that ipRGCs can be genetically and functionally segregated into Brn3b(+) ‘acute’ cells, and Brn3b(-) ‘circadian’ cells. Because Brn3b(+) cells largely avoid the SCN, and Brn3b(-) cells preferentially target the SCN, our results discount a critical role for the SCN in acute light responses, and instead implicate direct ipRGC projections to other brain areas⁸⁴.

The areas that mediate the acute effects of light on physiology are essentially completely unknown. There are many candidate areas that both receive direct ipRGC innervation and have been documented to be involved in light's acute effects on physiology, including the preoptic area^{278,265}, the ventral subparaventricular zone²⁷⁹, and the pretectum/superior colliculus²⁸⁰. Aside from the SCN, ipRGC projections to the median (MPO) and ventrolateral preoptic (VLPO) areas have been the most widely supported. The preoptic areas are involved in sleep and body temperature regulation^{278,281} and are activated by an acute light pulse¹⁰. However, ipRGC projections to these areas are sparse^{84,264}, suggesting their activation by light may be indirect. In contrast, the superior colliculus and pretectum receive robust innervation from ipRGCs^{83,84,99,264} and lesions in these areas block light's acute effects on sleep²⁸⁰. However, these lesions were rather large and could have indirect consequences on sleep regulation. It is also possible (and perhaps probable), that multiple direct ipRGC target regions are involved, with distinct areas mediating distinct physiological responses. Future studies silencing each retinorecipient target while activating Brn3b(+) ipRGCs will be necessary to tease apart the downstream circuits mediating light's acute effects on physiology.

An alternative hypothesis is that direct ipRGC projections to a single area that controls body temperature is the primary and critical step for all acute responses to light that are mediated by ipRGCs. In support of this, changes in body temperature and heat loss can directly influence sleep induction²⁷². This change in sleep is presumably causative of many of the documented effects of light on general locomotor activity²⁵⁸. Further, core body temperature can acutely regulate cognition and alertness^{270,271}. It is

therefore possible that ipRGCs can have widespread influence on an animal's basic physiology and cognitive function simply by regulating body temperature.

Despite their criticality for body temperature regulation by light, neither melanopsin nor Brn3b(+) ipRGCs were absolutely required for general activity suppression. This is consistent with previous findings that melanopsin is only partially required for wheel-running suppression²⁶⁹. This indicates that rods and cones can drive activity suppression through either conventional RGCs or Brn3b(-) ipRGCs. Because wheel-running activity suppression by light involves visual cortex²⁷⁷ and ipRGCs largely regulate subcortical processes⁶⁹, it is most likely that activity regulation by light involves a combination of input from both ipRGCs and conventional RGCs.

Together, our identification of the photopigment and the retinal circuits mediating acute body temperature and general activity regulation will facilitate better methods to promote or avoid human alertness and cognition at appropriate times of day²⁶⁰. Our results support many recent efforts to capitalize on the specific light-detection properties of melanopsin¹⁸⁰, such as its insensitivity and short-wavelength preference, to promote or avoid its activation at different times of day. However, this approach has been problematic because acute activation of melanopsin to promote attention has the unintended effect of shifting the circadian clock, thereby making subsequent sleep difficult²⁶³. Our identification that the Brn3b-positive ipRGCs specifically mediate light's acute effects on body temperature provides a cellular basis for developing targeted methods for promoting acute alertness, while minimizing circadian misalignment.

Methods

Animal husbandry

C57Bl/6 x Sv129 hybrid mice were used in all experiments and were housed according to guidelines from the Animal Care and Use Committee of Johns Hopkins University. Male and female mice age 2–8 months were housed in plastic translucent cages with steel-lined lids in an open room. Ambient room temperature and humidity were monitored daily and tightly controlled. Food and water were available *ad libitum*. All mice were maintained in a 12hr:12hr light-dark cycle for the entirety of their lives with a light intensity around 500 lux during the day.

Telemetry

Each mouse was housed individually and implanted with a telemetric probe in the peritoneal cavity to monitor core body temperature and activity remotely in continuous 1- or 2-min bins (Respironics/STARR Life Sciences G2 E-Mitter and ER-4000 energizer/receiver). Data was collected using VitalView data acquisition system. All experiments were conducted at least 10 days after surgery. Brn3b-DTA general activity recordings utilized infrared beam detectors and data was collected in 10-min bins.

Statistical analysis

All statistical tests were performed in Graphpad Prism 6. Specific statistical comparisons are listed in the figure legends.

Viral infection

Mice were anesthetized by intraperitoneal injection of avertin (2, 2, 2-Tribromoethanol) and placed under a stereo microscope. 1 μ l AAV-DIO-hM3DG_q-

mCherry (4.6×10^{12} viral particles/ml, Roth lab, UNC Vector Core) was placed on a piece of Parafilm and drawn into a 10- μ l microcapillary tube (Sigma P0674) that had been pulled to a needle (Sutter Instruments, Model P-2000). The loaded needle was then placed in the holster of a pico-injector (Harvard Apparatus PLI-90). The needle punctured the eye posterior to the ora serrata and air pressure was used to drive the viral solution into the vitreous chamber of the eye to ensure delivery specifically to the retina. Mice recovered from surgery on a heating pad until they woke from anesthesia. All experiments and confocal imaging were done at least 3 weeks following viral injection. CNO was delivered intraperitoneally at a concentration of 1 mg/kg, dissolved in PBS.

Confocal microscopy

Mice that had been infected with the AAV were anesthetized with avertin and then euthanized using cervical dislocation. The eyes were removed and the retinas were dissected in PBS and then fixed in 4% paraformaldehyde for 1–2 hours on ice. The retinas were then washed in PBS at least three times before either mounting on a microscope slide (Fisher) in Fluoromount (Sigma) with DAPI (2-(4-amidinophenyl)-1H-indole-6-carboxamide) or preparing for immunofluorescence. Immunofluorescence was performed in 4% goat serum with antibody concentrations as follows: rabbit anti-melanopsin 1:1000 (Advanced Targeting Systems) and goat anti-rabbit 488 1:1000. Images were taken on a Zeiss LSM 710 confocal microscope using a 20X objective. After imaging, images were background subtracted, and brightness and contrast were adjusted in FIJI (<http://fiji.sc>) for the image presented in the chapter.

Figures

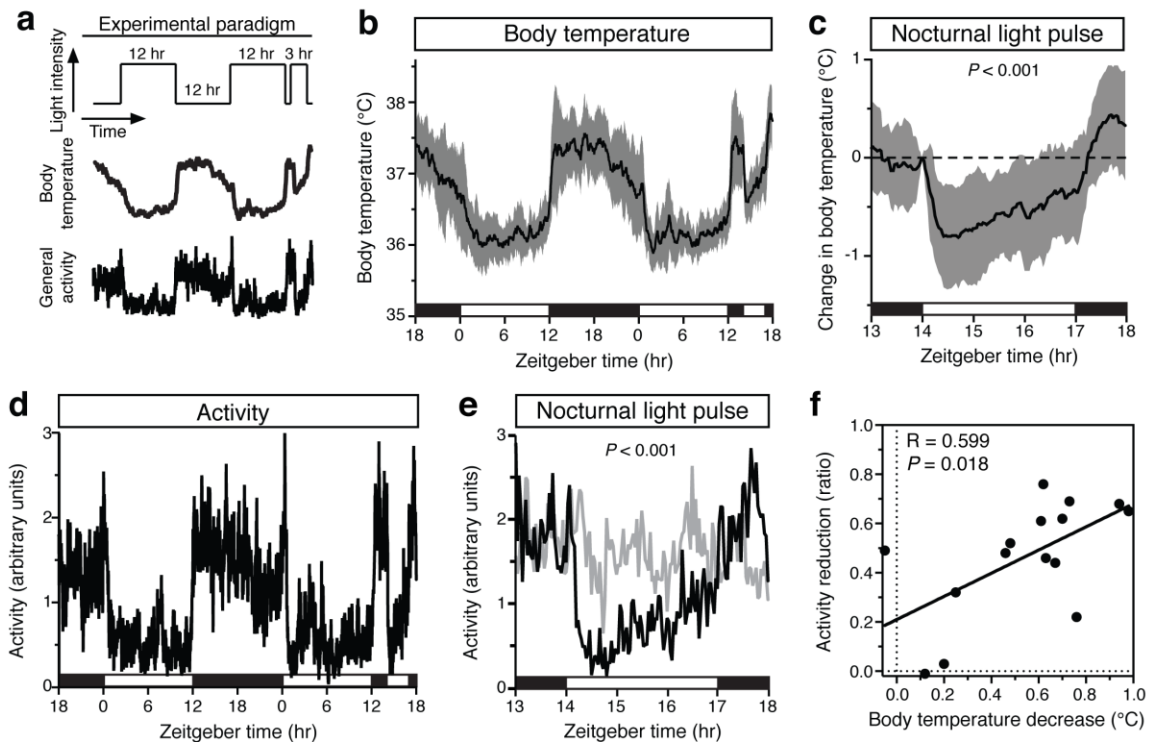


Figure 5.1: Mice use light information to both photoentrain and acutely regulate body temperature.

(a) Experimental paradigm depicting a 3-hr light pulse two hours into the subjective night (Zeitgeber time 14, ZT14) while simultaneously measuring core body temperature and general activity (ambulations). For all experiments using a nocturnal light pulse, light intensity is 500 lux. All data in this figure is $n = 15$ animals. (b) Mice photoentrain body temperature to a 12-hr/12-hr light dark cycle and acutely decrease body temperature in response to light at night. (c) A magnified view of the nocturnal light pulse relative to the body temperature at time of light pulse to show the rapid and sustained decrease in body temperature. Body temperature is significantly lower than previous night control ($P < 0.001$) by repeated measures two-way ANOVA followed by Sidak's post-test. For b and c, line is mean and shading represents standard deviation. (d) Simultaneous general activity measurements display robust photoentrainment of activity and acute regulation of activity in response to nocturnal light. (e) A magnified view of the nocturnal light pulse to show the rapid and sustained decrease in activity (black) compared to previous control

night (gray). Activity is significantly lower than previous night control ($P < 0.001$) by repeated measures two-way ANOVA followed by Sidak's post-test. For **d** and **e**, line is mean. **(f)** A significant correlation between body temperature reduction and activity suppression was observed across animals. Pearson's correlation coefficient $R = 0.599$ ($P = 0.018$).

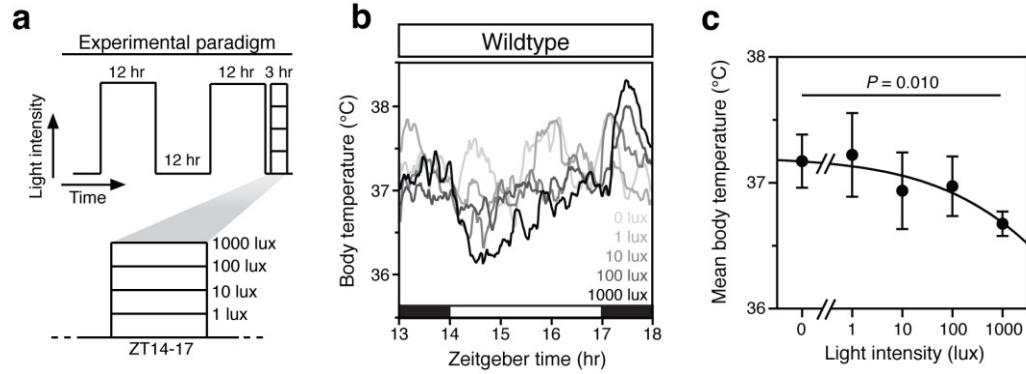


Figure 5.2: Light intensity-dependence of acute body temperature decrease.

(a) The same experimental paradigm as in Fig. 5.1, except animals were subjected to different light pulse intensities at night, while being maintained on constant bright light during the day. (b) Multiple nocturnal light pulse intensities (1, 10, 100, 1000 lux) in wildtype mice ($n = 4$, mean) results in a light intensity-dependent decrease in body temperature. (c) Quantification of the mean body temperature during the 3-hr light pulse from b shows an intensity-dependent decrease in body temperature by the main effect of light intensity in a two-way repeated measures ANOVA ($P = 0.010$). Data is mean and standard deviation and fit with sigmoidal dose-response curve.

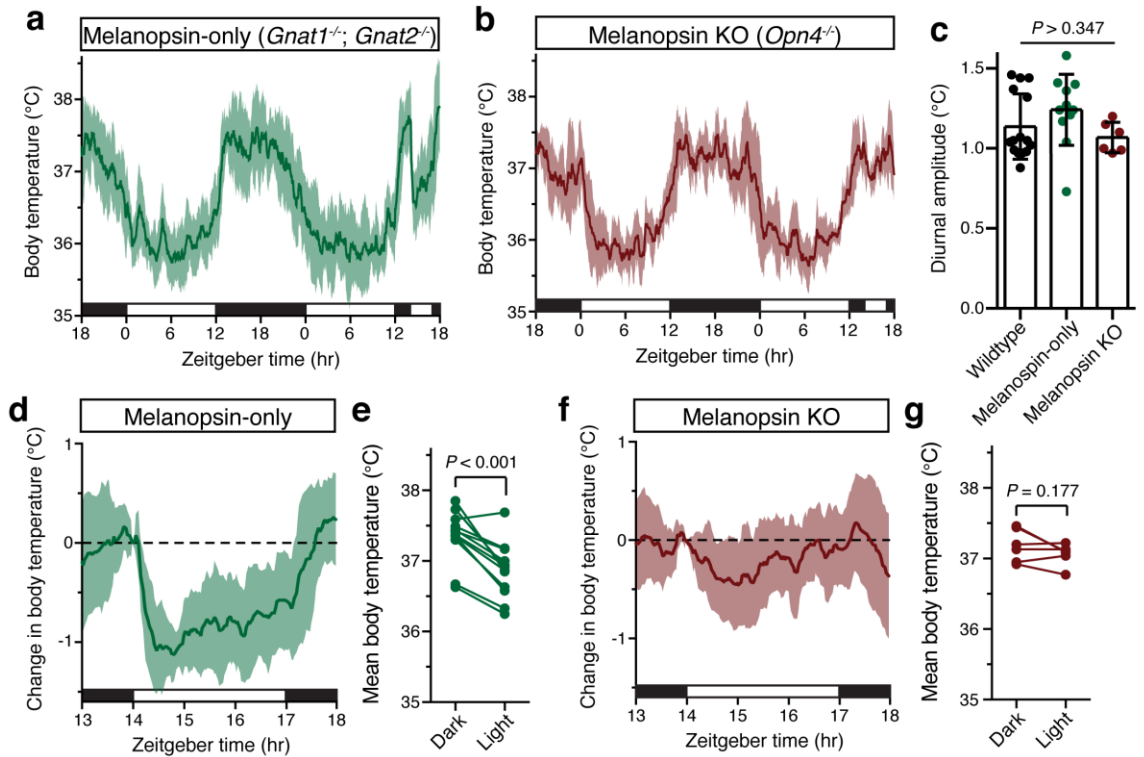


Figure 5.3: Melanopsin is both necessary and sufficient for acute thermoregulation by light.

(a,b) Body temperature was monitored continuously in melanopsin-only (*Gnat1*^{-/-};*Gnat2*^{-/-}, *n* = 12) and melanopsin knockout (*Opn4*^{-/-}, *n* = 6) mice and a single light pulse was applied at ZT14. Both lines photoentrain with (c) a similar diurnal amplitude of body temperature. (d) Acute body temperature decrease in melanopsin-only mice relative to body temperature at start of light pulse. (e) Mean body temperature during 3-hr light pulse compared to previous night control at same Zeitgeber time. (f) Acute body temperature decrease in melanopsin knockout mice relative to body temperature at start of light pulse. (g) Mean body temperature during 3-hr light pulse compared to previous night control at same Zeitgeber time.

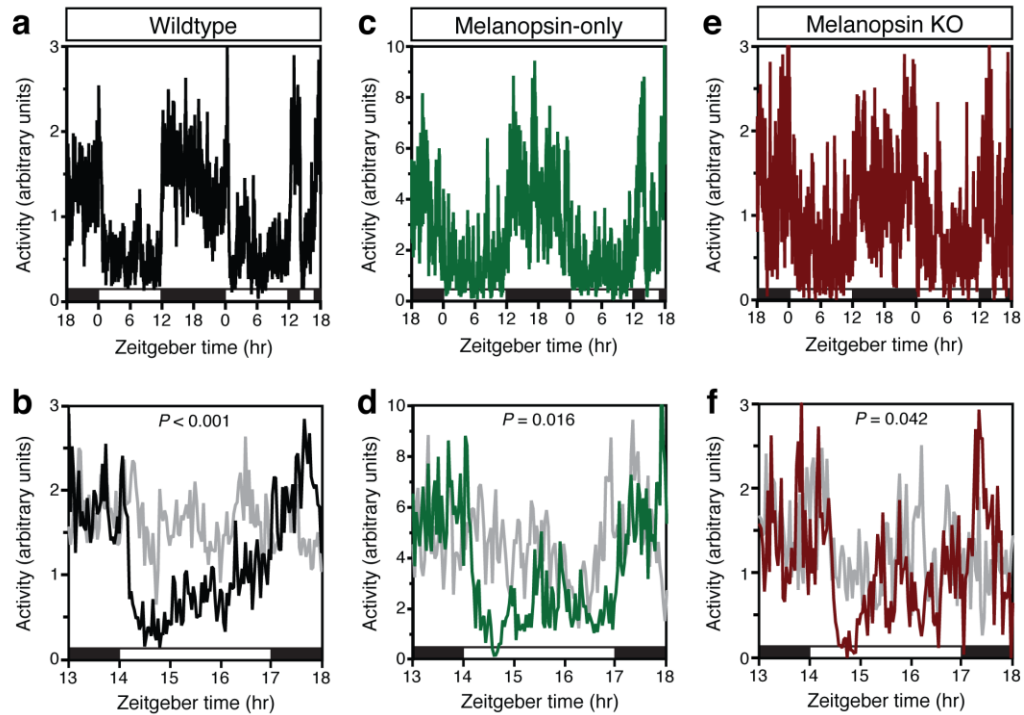


Figure 5.4: Acute activity regulation is intact in melanopsin knockout mice.

(a–f) All genotypes tested show robust photoentrainment of general activity (a,c,e) and acute reduction in activity (b,d,f: colored lines) compared to a previous night’s control (gray line). Data is presented as mean, wildtype $n = 15$, melanopsin-only $n = 12$, melanopsin knockout $n = 6$. Statistics are repeated-measures two-way ANOVA, P value indicates a significant effect of light on activity compared to the previous night.

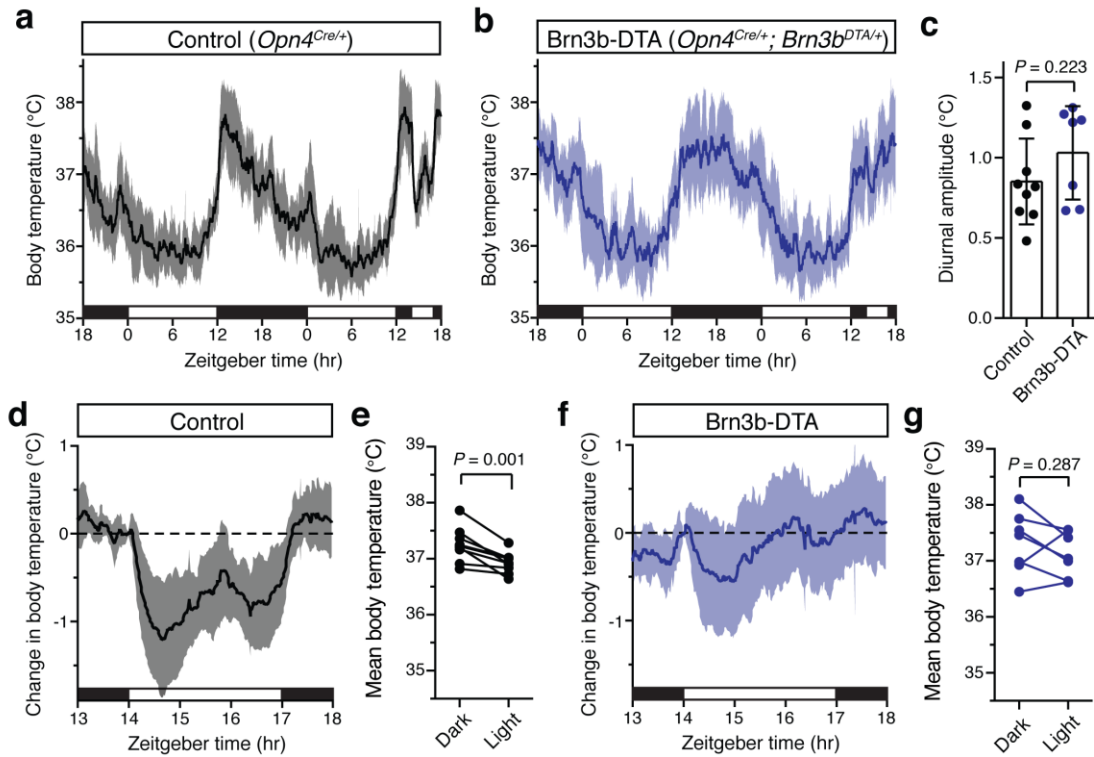


Figure 5.5: Brn3b-positive ipRGCs are required for acute body temperature decrease by light.

(a,b) Continuous measurement of body temperature in control mice (*Opn4^{Cre/+}*, $n = 8$) and Brn3b-DTA mice (*Opn4^{Cre/+}; Brn3b^{DTA/+}*, $n = 7$) across 48 hr of a light/dark cycle. (c) Diurnal amplitude (difference in mean body temperature during night and day) in both control and Brn3b-DTA mice. (d–g) Change in body temperature in (d,e) control and (f,g) Brn3b-DTA mice during the nocturnal light pulse relative to the body temperature at the beginning of the light. In e,g, mean body temperature across the 3-hr light pulse is reported. All data is mean and standard deviation. Statistical test in c is unpaired two-tailed *t*-test; statistical tests in e,g are paired two-tailed *t*-tests.

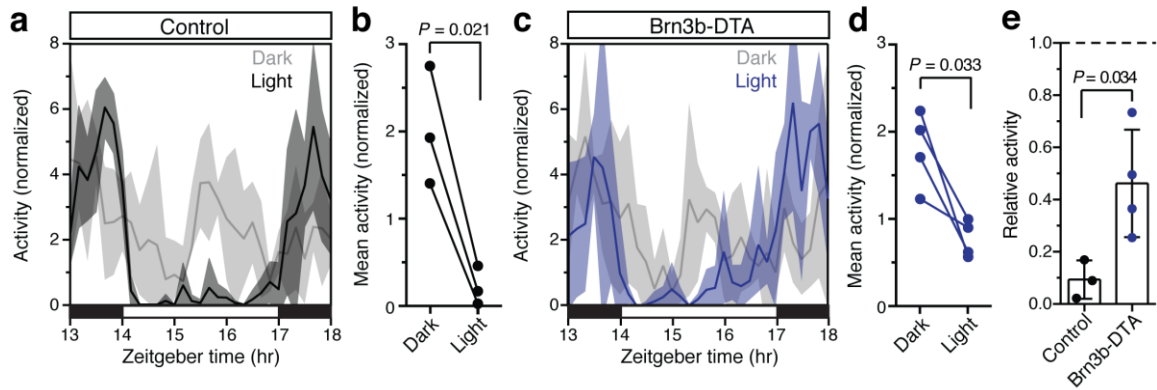


Figure 5.6: Acute activity suppression in Brn3b-DTA mice.

(a,b) Control mice (*Opn4^{Cre/+}*, $n = 3$) display acute activity suppression in response to a light pulse at night. (c,d) Brn3b-DTA mice (*Opn4^{Cre/+};Brn3b^{DTA/+}*, $n = 4$) also display a decrease in activity in response to a nocturnal light pulse. (e) The activity suppression amplitude is decreased in Brn3b-DTA mice compared to controls. All data is mean and error is standard deviation. Statistical tests in b,d are paired two-tailed *t*-tests, statistical test in e is unpaired two-tailed *t*-test.

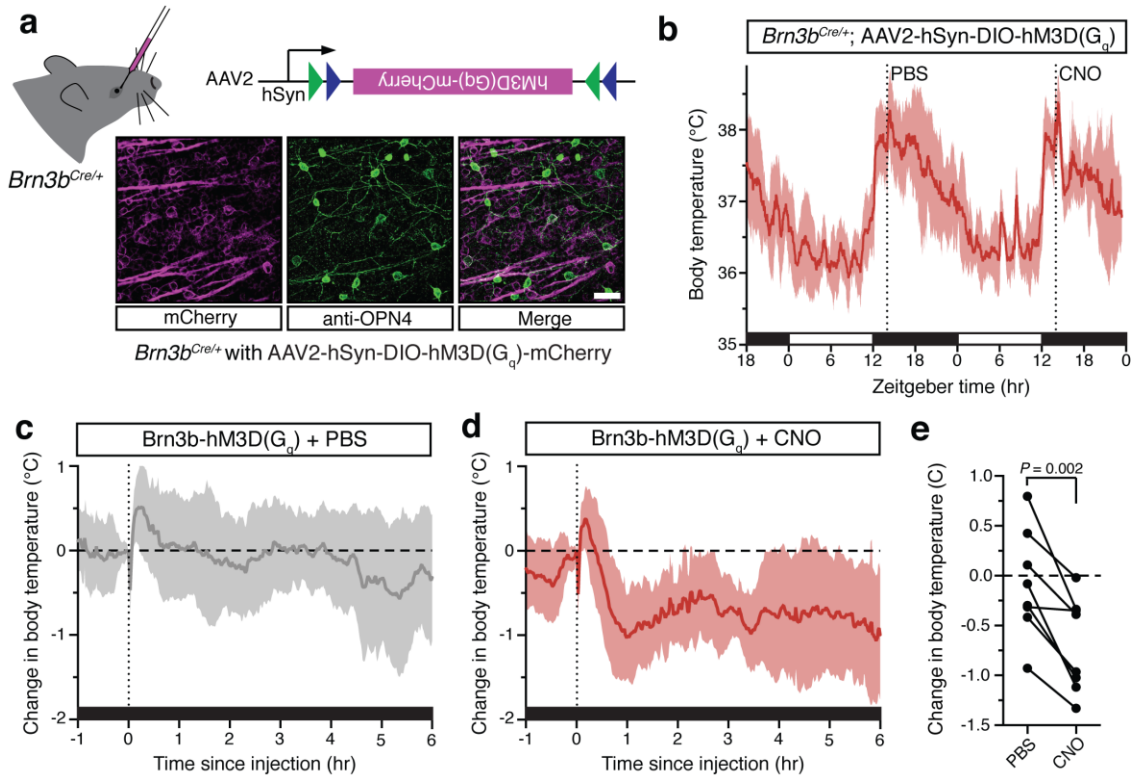


Figure 5.7: Chemogenetic activation of *Brn3b*(+) RGCs is sufficient for sustained body temperature decrease.

(a) Intravitreal delivery of AAV2-hSyn-DIO-hM3D(G_q)-mCherry into *Brn3b*^{Cre/+} mice and subsequent infection and expression in ipRGCs labeled by melanopsin immunofluorescence. (b) Continuous monitoring of body temperature during a light/dark cycle, with injections of PBS or CNO on subsequent nights, depicted with dotted lines ($n = 8$). (c,d) Close-up view of relative change in body temperature following (c) PBS (gray) or (d) CNO (red) injection. Data is represented as mean and error as standard deviation. (e) CNO elicits a significant reduction in body temperature over 6 hr compared to PBS injection. Statistical test is paired two-tailed t -test.

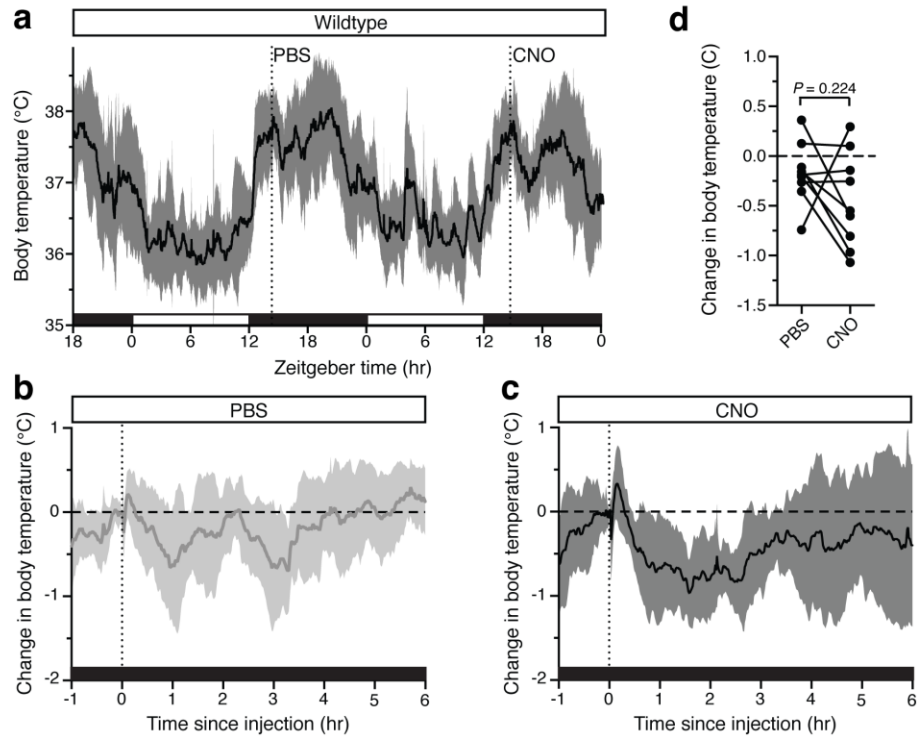


Figure 5.8: CNO has no measurable effect on wildtype body temperature.

(a) Wildtype ($n = 9$) body temperature during a light/dark cycle, with PBS injection and CNO injection at ZT14 on subsequent nights. (b) Change in body temperature after PBS injection relative to body temperature at injection time. (c) Change in body temperature after CNO injection relative to body temperature at injection time. Data in a–c is mean and error is standard deviation. (d) Change in body temperature after either PBS injection or CNO injection. Statistical test is paired two-tailed *t*-test.

Chapter 6

Concluding remarks

In this thesis, I have provided evidence that the mammalian pupillary light reflex (PLR) is driven rapidly by activation of rod photoreceptors, with minimal contribution from the intrinsic iris muscle, cone photoreceptors, or melanopsin phototransduction until bright light intensities. I also provide evidence that rods can utilize a non-conventional circuit in the retina to relay signals to ipRGCs for the PLR. While these studies provide a picture of how the rapid PLR occurs under dark-adapted conditions, I do not mean to imply that PLR is solved and there will be no more studies. On the contrary, I hope this thesis will open the door to more detailed and broader studies of the PLR.

The questions remaining in the PLR

By all accounts we are in a new era of neuroscience research. At a steady pace, new tools and technologies are becoming available to specifically silence, activate, or modulate any cell type of interest in a behaving animal. In this thesis, I had the fortune of access to dozens of mouse lines and tools to control rod, cone, or melanopsin-cell function. No longer do we need to design stimuli that will selectively modulate one neuron or rely on imprecise ablations or non-specific drugs. Therefore, I hope that similar approaches can be useful in future studies of the PLR where many open questions remain.

Perhaps the most important question remaining is the precise central circuitry of the PLR. In Chapter 2, I identified that the Brn3b-positive ipRGCs drive the PLR using an asymmetric brain circuit. However, I have no data implicating the anatomical basis for this asymmetry. In fact, relatively little is known about the precise PLR circuits in the brain in general. The majority of studies of the PLR circuit occurred at a time in which only rudimentary circuit tracing and cell activating/silencing technologies existed. These studies were invaluable in providing a general map of the PLR circuit, but we still lack a

precise understanding of the relative importance of each brain region and whether there are functional subdomains within these brain regions. Especially lacking is how signals converge and diverge along the circuit and how the other areas of the highly interconnected visual system modulate them. The application of genetic tools to gain access to the cells specific to the PLR circuit will refine our currently rough knowledge.

Also in Chapter 2, I showed that despite intrinsic photosensitivity in the mouse iris muscle, it does not contribute to the PLR. The non-mammalian vertebrate iris muscle has been most widely studied for the intrinsic PLR by removing it from the eye and placing it in a dish. Because its *in vitro* response is so robust, most studies have widely assumed that the neural mechanisms of the PLR in these species are of negligible importance. In support of weak neuronal input, studies of the consensual PLR in non-mammalian vertebrates have shown that it is incredibly weak and insensitive. However, the results in this thesis that *in vitro* functionality is not a precise predictor of *in vivo* function and the bilateral asymmetry in the neuronal circuit will force a reexamination of the contributions of the intrinsic and neural mechanisms of the PLR in non-mammalian vertebrates.

In Chapter 3, I showed that rods are the predominant mediators of the PLR. However, I should note that I have only studied the rapid PLR under dark-adapted conditions. This was primarily because dark adaptation simplifies the situation by putting each photoreceptor in its resting state and allows me to compare my data to previous studies that have overwhelmingly used dark-adapted conditions. However, there are numerous studies that indicate that the PLR in light-adapted conditions is distinct from that under dark adaptation. Rapid changes in pupil size when there is a bright background

appear to be driven instead by cones¹⁶⁸. In fact, even the static pupil size appears to use distinct photoreceptive mechanisms than the rapid changes in pupil size¹⁶⁵. Recent evidence from Bill Keenan in our lab suggests that melanopsin phototransduction, while dispensable for the rapid PLR, is critical for the static PLR. Identifying the diversity of situations in the environment in which rods, cones, or melanopsin predominate is critical to understand how the PLR occurs across the day.

Lastly, in Chapter 4, while I have provided evidence that a non-conventional retinal circuit is *sufficient* to relay rod signals for the PLR, there is still substantial uncertainty about what retinal circuits predominate for the PLR under normal conditions. This is because we have no clear picture of (1) the full catalog of retinal circuits that reach ipRGCs and (2) a way to specifically activate or silence them. Even among ipRGCs, it is not clear which subtypes are required for the PLR. It is clear that the Brn3b-positive ipRGCs are required, but this encompasses every subtype from M1–M5. At least M1 and M2 ipRGCs project to the OPN^{84,102,282}, and the complete projections of M3, M4, and M5 are unknown and may include the OPN as well. Given that these different subtypes each likely receive very different input from the inner retina^{99,101}, it is likely that many retinal circuits all independently drive the PLR under normal conditions. Emerging cell type-specific circuit-tracing technologies such as G-deleted rabies²⁸³ will be invaluable in determining the specific ipRGC subtypes that project to the OPN and their upstream circuits.

The pupillary light reflex as a model visual behavior

A complete knowledge of the function of the nervous system requires reliable functional outputs. Arguably the most ideal situation is an awake and behaving subject

that reports its own sensations and perceptions following some experimental perturbation. However, for both technical and ethical reasons, this is generally not practicable. Instead, the gold standard of laboratory research is a reliable behavioral assay in a model organism.

However, to date, most behavioral assays are far from ideal. For instance, many assays are subjective such as those that require an experimenter to score a behavior, are indirect measures of functional outputs such as assays of complex emotions or cognitive functions, are impractical due to requiring extensive animal training, or are only quasi-quantifiable. Until these difficulties are overcome, *in vivo* investigation of the nervous system of model organisms will face debates and uncertainties.

On the other hand, the PLR requires no animal training, is a direct physiological readout of the system you intend to study, is rapid, inexpensive, can be monitored in real time, and is highly quantitative. With this in mind, I propose that the PLR be used as a model behavior for detailed studies of the nervous system. The effects of altering specific circuits can be tested almost immediately and most importantly can be clearly quantified compared to other circuit alterations.

Additionally, the PLR encompasses many different levels of nervous system function, including sensory detection and adaptation, brain circuits, cortical modulation, circadian modulation, peripheral nervous system function including para- versus sympathetic activation, and even smooth muscle function. Therefore, many questions can likely be addressed within a subsystem in the PLR.

One counterpoint that I anticipate is that to study say, depression, one has to study the circuits involved in depression, not the PLR. And because the PLR is less socially and

clinically important than depression, we should not be wasting our limited time and resources understanding a relatively dispensable function. Therefore, imperfect behavioral assays are simply the reality of studying complex neural functions and should not be discarded for studying a less important easy question. First, I do not suggest we stop studying depression. But most importantly, I believe the PLR can act as a model behavior in that it can provide general insights of nervous system function.

The vast majority of our basic understandings of the nervous system have come from studying relatively obscure functions. Just think of the *Aplysia* gill withdrawal reflex, *C. elegans* chemotaxis, or innervation of the *Drosophila* neuromuscular junction. Here, the PLR offers the opportunity to study a mammalian behavior with practical simplicity but functional and anatomical complexity that can yield insights reaching far beyond its study.

References

1. Nagel, G. *et al.* Channelrhodopsin-1: A light-gated proton channel in green algae. *Science (80-.)*. **296**, 2395–2398 (2002).
2. Duboué, E. R., Keene, A. C. & Borowsky, R. L. Evolutionary convergence on sleep loss in cavefish populations. *Curr. Biol.* **21**, 671–6 (2011).
3. Kim, E. B. *et al.* Genome sequencing reveals insights into physiology and longevity of the naked mole rat. *Nature* **479**, 223–7 (2011).
4. Rieke, F. & Rudd, M. E. The challenges natural images pose for visual adaptation. *Neuron* **64**, 605–16 (2009).
5. Aschoff, J. Circadian rhythms in man. *Science (80-.)*. **148**, 1427–32 (1965).
6. Aschoff, J. *et al.* Human circadian rhythms in continuous darkness: Entrainment by social cues. *Science (80-.)*. **171**, 213–5 (1971).
7. DeCoursey, P. J. Daily light sensitivity in a rodent. *Science (80-.)*. **131**, 33–5 (1960).
8. Altimus, C. M. *et al.* Rods-cones and melanopsin detect light and dark to modulate sleep independent of image formation. *Proc. Natl. Acad. Sci. USA* **105**, 19998–20003 (2008).
9. Lupi, D., Oster, H., Thompson, S. & Foster, R. G. The acute light-induction of sleep is mediated by OPN4-based photoreception. *Nat. Neurosci.* **11**, 1068–1073 (2008).
10. Tsai, J. W. *et al.* Melanopsin as a sleep modulator: circadian gating of the direct effects of light on sleep and altered sleep homeostasis in *Opn4*^{-/-} mice. *PLoS Biol.* **7**, e1000125 (2009).
11. Nosedá, R. *et al.* A neural mechanism for exacerbation of headache by light. *Nat. Neurosci.* **13**, 239–45 (2010).
12. Legates, T. A. *et al.* Aberrant light directly impairs mood and learning through

- melanopsin-expression neurons. *Nature* **491**, 594–598 (2012).
13. Masland, R. H. The neuronal organization of the retina. *Neuron* **76**, 266–80 (2012).
 14. Nathans, J., Thomas, D. & Hogness, D. S. Molecular genetics of human color vision: the genes encoding blue, green, and red pigments. *Science (80-.)*. **232**, 193–202 (1986).
 15. Nathans, J. & Hogness, D. S. Isolation, sequence analysis, and intron-exon arrangement of the gene encoding bovine rhodopsin. *Cell* **34**, 807–814 (1983).
 16. Nathans, J. & Hogness, D. S. Isolation and nucleotide sequence of the gene encoding human rhodopsin. *Proc. Natl. Acad. Sci. USA* **81**, 4851–4855 (1984).
 17. Wald, G., Durell, J. & St. George, R. C. C. The light reaction in the bleaching of rhodopsin. *Science (80-.)*. **111**, 179–181 (1950).
 18. Dowling, J. E. & Wald, G. The biological function of vitamin A acid. *Proc. Natl. Acad. Sci. USA* **46**, 587–608 (1960).
 19. Dowling, J. E. & Wald, G. Vitamin A deficiency and night blindness. *Proc. Natl. Acad. Sci. USA* **44**, 648–661 (1958).
 20. Wald, G. The chemistry of rod vision. *Science (80-.)*. **113**, 287–291 (1951).
 21. Wald, G. Carotenoids and the visual cycle. *J. Gen. Physiol.* 351–71 (1935).
 22. Calvert, P. D. *et al.* Phototransduction in transgenic mice after targeted deletion of the rod transducin α -subunit. *Proc. Natl. Acad. Sci. USA* **97**, 13913–8 (2000).
 23. Chang, B. *et al.* Cone photoreceptor function loss-3, a novel mouse model of achromatopsia due to a mutation in *Gnat2*. *Invest. Ophthalmol. Vis. Sci.* **47**, 5017–21 (2006).
 24. Lerea, C. L., Bunt-Milam, A. H. & Hurley, J. B. Alpha transducin is present in blue-, green-, and red-sensitive cone photoreceptors in the human retina. *Neuron* **3**, 367–376 (1989).
 25. Lochrie, M. A., Hurley, J. B. & Simon, M. I. Sequence of the alpha subunit of photoreceptor G protein: Homologies between transducin, ras, and elongation factors. *Science (80-.)*. **228**, 96–99 (1985).

26. Tanabe, T. *et al.* Primary structure of the α -subunit of transducin and its relationship to ras proteins. *Nature* **315**, 242–5 (1985).
27. Medynski, D. C. *et al.* Amino acid sequence of the α subunit of transducin deduced from the cDNA sequence. *Proc. Natl. Acad. Sci. USA* **82**, 4311–4315 (1985).
28. Yatsunami, K. & Khorana, H. G. GTPase of bovine rod outer segments: the amino acid sequence of the α subunit as derived from the cDNA sequence. *Proc. Natl. Acad. Sci. USA* **82**, 4316–4320 (1985).
29. Morgans, C. W. *et al.* TRPM1 is required for the depolarizing light response in retinal ON-bipolar cells. *Proc. Natl. Acad. Sci. USA* **106**, 19174–8 (2009).
30. Shen, Y. *et al.* A transient receptor potential-like channel mediates synaptic transmission in rod bipolar cells. *J. Neurosci.* **29**, 6088–93 (2009).
31. Masu, M. *et al.* Specific deficit of the ON response in visual transmission by targeted disruption of the mGluR6 gene. *Cell* **80**, 757–65 (1995).
32. DeVries, S. H. Bipolar cells use kainate and AMPA receptors to filter visual information into separate channels. *Neuron* **28**, 847–56 (2000).
33. DeVries, S. H., Li, W. & Saszik, S. Parallel processing in two transmitter microenvironments at the cone photoreceptor synapse. *Neuron* **50**, 735–48 (2006).
34. Dreosti, E., Esposti, F., Baden, T. & Lagnado, L. In vivo evidence that retinal bipolar cells generate spikes modulated by light. *Nat. Neurosci.* **14**, 951–952 (2011).
35. Baden, T., Esposti, F., Nikolaev, A. & Lagnado, L. Spikes in retinal bipolar cells phase-lock to visual stimuli with millisecond precision. *Curr. Biol.* 1859–1869 (2011). doi:10.1016/j.cub.2011.09.042
36. Baden, T., Berens, P., Bethge, M. & Euler, T. Spikes in mammalian bipolar cells support temporal layering of the inner retina. *Curr. Biol.* **23**, 48–52 (2013).
37. Koch, S. M. *et al.* Pathway-specific genetic attenuation of glutamate release alters select features of competition-based visual circuit refinement. *Neuron* **71**, 235–42 (2011).

38. Nirenberg, S. & Meister, M. The light response of retinal ganglion cells is truncated by a displaced amacrine circuit. *Neuron* **18**, 637–650 (1997).
39. Yoshida, K. *et al.* A key role of starburst amacrine cells in originating retinal directional selectivity and optokinetic eye movement. *Neuron* **30**, 771–780 (2001).
40. Nelson, R. AII amacrine cells quicken time course of rod signals in the cat retina. *J. Neurophysiol.* **47**, 928–947 (1982).
41. Chen, S. & Li, W. A color-coding amacrine cell may provide a blue-Off signal in a mammalian retina. *Nat. Neurosci.* **15**, 954–6 (2012).
42. Wei, W., Hamby, A. M., Zhou, K. & Feller, M. B. Development of asymmetric inhibition underlying direction selectivity in the retina. *Nature* **469**, 402–6 (2011).
43. Crook, J. D., Manookin, M. B., Packer, O. S. & Dacey, D. M. Horizontal cell feedback without cone type-selective inhibition mediates ‘red-green’ color opponency in midget ganglion cells of the primate retina. *J. Neurosci.* **31**, 1762–1772 (2011).
44. Qian, H. & Dowling, J. E. Novel GABA responses from rod-driven retinal horizontal cells. *Nature* **361**, 162–4 (1993).
45. Jeon, C., Strettoi, E. & Masland, R. H. The major cell populations of the mouse retina. *J. Neurosci.* **18**, 8936–46 (1998).
46. Masland, R. H. The fundamental plan of the retina. *Nat. Neurosci.* **4**, 877–86 (2001).
47. Helmstaedter, M. *et al.* Connectomic reconstruction of the inner plexiform layer in the mouse retina. *Nature* **500**, 168–174 (2013).
48. Euler, T., Haverkamp, S., Schubert, T. & Baden, T. Retinal bipolar cells: Elementary building blocks of vision. *Nat. Rev. Neurosci.* **15**, 507–519 (2014).
49. Puller, C., Ondreka, K. & Haverkamp, S. Bipolar cells of the ground squirrel retina. *J. Comp. Neurol.* **519**, 759–74 (2010).
50. Ghosh, K. K., Bujan, S., Haverkamp, S., Feigenspan, A. & Wässle, H. Types of bipolar cells in the mouse retina. *J. Comp. Neurol.* **469**, 70–82 (2004).

51. Pang, J.-J. *et al.* Direct rod input to cone BCs and direct cone input to rod BCs challenge the traditional view of mammalian BC circuitry. *Proc. Natl. Acad. Sci. USA* **107**, 395–400 (2010).
52. Breuninger, T., Puller, C., Haverkamp, S. & Euler, T. Chromatic bipolar cell pathways in the mouse retina. *J. Neurosci.* **31**, 6504–17 (2011).
53. Chang, L., Breuninger, T. & Euler, T. Chromatic coding from cone-type unselective circuits in the mouse retina. *Neuron* **77**, 559–571 (2013).
54. Sanes, J. R. & Masland, R. H. The types of retinal ganglion cells: Current status and implications for neuronal classification. *Annu. Rev. Neurosci.* **38**, 221–46 (2015).
55. Sümbül, U. *et al.* A genetic and computational approach to structurally classify neuronal types. *Nat. Commun.* **5**, 3512 (2014).
56. Barlow, H. B. & Levick, W. R. The mechanism of directionally selective units in rabbit's retina. *J. Physiol.* **178**, 477–504 (1965).
57. Wei, W. & Feller, M. B. Organization and development of direction-selective circuits in the retina. *Trends Neurosci.* **34**, 638–45 (2011).
58. Rivlin-Etzion, M. *et al.* Transgenic mice reveal unexpected diversity of On-Off direction-selective retinal ganglion cell subtypes and brain structures involved in motion processing. *J. Neurosci.* **31**, 8760–9 (2011).
59. Vaney, D. I., Sivyer, B. & Taylor, W. R. Direction selectivity in the retina: Symmetry and asymmetry in structure and function. *Nat. Rev. Neurosci.* **13**, (2012).
60. Dhande, O. S. *et al.* Genetic dissection of retinal inputs to brainstem nuclei controlling image stabilization. *J. Neurosci.* **33**, 17797–813 (2013).
61. Huberman, A. D. *et al.* Genetic identification of an On-Off direction-selective retinal ganglion cell subtype reveals a layer-specific subcortical map of posterior motion. *Neuron* **62**, 327–34 (2009).
62. Schmidt, T. M. *et al.* A role for melanopsin in alpha retinal ganglion cells and contrast detection. *Neuron* **82**, 781–788 (2014).

63. Freed, M. A. & Sterling, P. The ON-alpha ganglion cell of the cat retina and its presynaptic cell types. *J. Neurosci.* **8**, 2303–20 (1988).
64. Huberman, A. D. *et al.* Architecture and activity-mediated refinement of axonal projections from a mosaic of genetically identified retinal ganglion cells. *Neuron* **59**, 425–38 (2008).
65. Bleckert, A., Schwartz, G. W., Turner, M. H., Rieke, F. & Wong, R. O. L. Visual space is represented by nonmatching topographies of distinct mouse retinal ganglion cell types. *Curr. Biol.* **24**, 310–5 (2014).
66. Weick, M. & Demb, J. B. Delayed-rectifier K channels contribute to contrast adaptation in mammalian retinal ganglion cells. *Neuron* **71**, 166–79 (2011).
67. Kim, I., Zhang, Y., Yamagata, M., Meister, M. & Sanes, J. R. Molecular identification of a retinal cell type that responds to upward motion. *Nature* **452**, 478–482 (2008).
68. Güler, A. D., Altimus, C. M., Ecker, J. L. & Hattar, S. Multiple photoreceptors contribute to nonimage-forming visual functions predominantly through melanopsin-containing retinal ganglion cells. *Cold Spring Harb. Symp. Quant. Biol.* **72**, 509–515 (2007).
69. Berson, D. M. Strange vision: ganglion cells as circadian photoreceptors. *Trends Neurosci.* **26**, 314–320 (2003).
70. Berson, D. M., Dunn, F. A. & Takao, M. Phototransduction by retinal ganglion cells that set the circadian clock. *Science (80-.)*. **295**, 1070–3 (2002).
71. Ebihara, S. & Tsuji, K. Entrainment of the circadian activity rhythm to the light cycle: effective light intensity for a Zeitgeber in the retinal degenerate C3H mouse and the normal C57BL mouse. *Physiol. Behav.* **24**, 523–7 (1980).
72. Yoshimura, T., Nishio, M., Goto, M. & Ebihara, S. Differences in circadian photosensitivity between retinally degenerate CBA/J mice (rd/rd) and normal CBA/N mice (+/+). *J. Biol. Rhythm.* **9**, 51–60 (1994).
73. Foster, R. G. *et al.* Circadian photoreception in the retinally degenerate mouse (rd/rd). *J. Comp. Physiol. A. Neuroethol. Sens. Neural. Behav. Physiol.* **169**, 39–50

- (1991).
74. Keeler, C. E. Iris movements in blind mice. *Am. J. Physiol.* **81**, 107–112 (1927).
 75. Provencio, I. & Foster, R. G. Circadian rhythms in mice can be regulated by photoreceptors with cone-like characteristics. *Brain Res.* **694**, 183–190 (1995).
 76. Czeisler, C. A. *et al.* Suppression of melatonin secretion in some blind patients by exposure to bright light. *N. Eng. J. Med.* **332**, 6–11 (1995).
 77. Freedman, M. S. *et al.* Regulation of mammalian circadian behavior by non-rod, non-cone, ocular photoreceptors. *Science (80-.)*. **284**, 502–4 (1999).
 78. Lucas, R. J., Freedman, M. S., Munoz, M., Garcia-Fernandez, J. M. & Foster, R. G. Regulation of the mammalian pineal by non-rod, non-cone ocular photoreceptors. *Science (80-.)*. **284**, 505–7 (1999).
 79. Lucas, R. J., Douglas, R. H. & Foster, R. G. Characterization of an ocular photopigment capable of driving pupillary constriction in mice. *Nat. Neurosci.* **4**, 621–6 (2001).
 80. Mrosovsky, N., Lucas, R. J. & Foster, R. G. Persistence of masking responses to light in mice lacking rods and cones. *J. Biol. Rhythm.* **16**, 585–587 (2001).
 81. Provencio, I., Jiang, G., De Grip, W. J., Hayes, W. P. & Rollag, M. D. Melanopsin: An opsin in melanophores, brain, and eye. *Proc. Natl. Acad. Sci. USA* **95**, 340–5 (1998).
 82. Provencio, I. *et al.* A novel human opsin in the inner retina. *J. Neurosci.* **20**, 600–605 (2000).
 83. Hattar, S., Liao, H., Takao, M., Berson, D. M. & Yau, K. Melanopsin-containing retinal ganglion cells: architecture, projections, and intrinsic photosensitivity. *Science (80-.)*. **295**, 1065–70 (2002).
 84. Hattar, S. *et al.* Central projections of melanopsin- expressing retinal ganglion cells in the mouse. *J. Comp. Neurol.* **349**, 326–349 (2006).
 85. Ruby, N. F. *et al.* Role of melanopsin in circadian responses to light. *Science (80-.)*. **298**, 2211–3 (2002).

86. Panda, S. *et al.* Melanopsin (Opn4) requirement for normal light-induced circadian phase shifting. *Science (80-.)*. **298**, 2213–6 (2002).
87. Lucas, R. J. *et al.* Diminished pupillary light reflex at high irradiances in melanopsin-knockout mice. *Science (80-.)*. **299**, 245–7 (2003).
88. Hattar, S. *et al.* Melanopsin and rod–cone photoreceptive systems account for all major accessory visual functions in mice. *Nature* **424**, 76–81 (2003).
89. Panda, S. *et al.* Melanopsin is required for non-image-forming photic responses in blind mice. *Science (80-.)*. **301**, 525–7 (2003).
90. Thresher, R. J. *et al.* Role of mouse cryptochrome blue-light photoreceptor in circadian photoresponses. *Science (80-.)*. **282**, 1490–1494 (1998).
91. Van Gelder, R. N., Wee, R., Lee, J. A. & Tu, D. C. Reduced pupillary light responses in mice lacking cryptochromes. *Science (80-.)*. **299**, 222 (2003).
92. Selby, C. P., Thompson, C., Schmitz, T. M., Van Gelder, R. N. & Sancar, A. Functional redundancy of cryptochromes and classical photoreceptors for nonvisual ocular photoreception in mice. *Proc. Natl. Acad. Sci. USA* **97**, 14697–702 (2000).
93. Miyamoto, Y. & Sancar, A. Vitamin B2-based blue-light photoreceptors in the retinohypothalamic tract as the photoactive pigments for setting the circadian clock in mammals. *Proc. Natl. Acad. Sci. USA* **95**, 6097–102 (1998).
94. Buhr, E. D. & Van Gelder, R. N. Local photic entrainment of the retinal circadian oscillator in the absence of rods, cones, and melanopsin. *Proc. Natl. Acad. Sci. USA* **111**, 8625–30 (2014).
95. Güler, A. D. *et al.* Melanopsin cells are the principal conduits for rod–cone input to non-image-forming vision. *Nature* **453**, 102–5 (2008).
96. Göz, D. *et al.* Targeted destruction of photosensitive retinal ganglion cells with a saporin conjugate alters the effects of light on mouse circadian rhythms. *PLoS One* **3**, e3153 (2008).
97. Hatori, M. *et al.* Inducible ablation of melanopsin-expressing retinal ganglion cells

- reveals their central role in non-image forming visual responses. *PLoS One* **3**, e2451 (2008).
98. Schmidt, T. M., Chen, S.-K. & Hattar, S. Intrinsically photosensitive retinal ganglion cells: many subtypes, diverse functions. *Trends Neurosci.* **34**, 572–80 (2011).
 99. Ecker, J. L. *et al.* Melanopsin-expressing retinal ganglion-cell photoreceptors: cellular diversity and role in pattern vision. *Neuron* **67**, 49–60 (2010).
 100. Schmidt, T. M. & Kofuji, P. Functional and morphological differences among intrinsically photosensitive retinal ganglion cells. *J. Neurosci.* **29**, 476–82 (2009).
 101. Schmidt, T. M. & Kofuji, P. Differential cone pathway influence on intrinsically photosensitive retinal ganglion cell subtypes. *J. Neurosci.* **30**, 16262–71 (2010).
 102. Baver, S. B., Pickard, G. E., Sollars, P. J. & Pickard, G. E. Two types of melanopsin retinal ganglion cell differentially innervate the hypothalamic suprachiasmatic nucleus and the olivary pretectal nucleus. *Eur. J. Neurosci.* **27**, 1763–70 (2008).
 103. Schmidt, T. M. & Kofuji, P. Structure and function of bistratified intrinsically, photosensitive retinal ganglion cells in the mouse. *J. Comp. Neurol.* **1504**, 1492–1504 (2010).
 104. Estevez, M. E. *et al.* Form and function of the M4 cell, an intrinsically photosensitive retinal ganglion cell type contributing to geniculocortical vision. *J. Neurosci.* **32**, 13608–20 (2012).
 105. Chen, S.-K., Badea, T. C. & Hattar, S. Photoentrainment and pupillary light reflex are mediated by distinct populations of ipRGCs. *Nature* **476**, 92–95 (2011).
 106. Sweeney, N. T., Tierney, H. & Feldheim, D. a. Tbr2 is required to generate a neural circuit mediating the pupillary light reflex. *J. Neurosci.* **34**, 5447–5453 (2014).
 107. Mao, C.-A. *et al.* T-box transcription regulator Tbr2 is essential for the formation and maintenance of Opn4/melanopsin-expressing intrinsically photosensitive retinal ganglion cells. *J. Neurosci.* **34**, 13083–95 (2014).

108. Brown, T. M. *et al.* Melanopsin-based brightness discrimination in mice and humans. *Curr. Biol.* **22**, 1134–41 (2012).
109. Brown, T. M. *et al.* Melanopsin contributions to irradiance coding in the thalamo-cortical visual system. *PLoS Biol.* **8**, e1000558 (2010).
110. Allen, A. E. *et al.* Melanopsin-driven light adaptation in mouse vision. *Curr. Biol.* **24**, 2481–2490 (2014).
111. Zaidi, F. H. *et al.* Short-wavelength light sensitivity of circadian, pupillary, and visual awareness in humans lacking an outer retina. *Curr. Biol.* **17**, 2122–8 (2007).
112. Badea, T. C., Cahill, H., Ecker, J. L., Hattar, S. & Nathans, J. Distinct roles of transcription factors Brn3a and Brn3b in controlling the development, morphology, and function of retinal ganglion cells. *Neuron* **61**, 852–864 (2009).
113. Kim, I., Zhang, Y., Meister, M. & Sanes, J. R. Laminal restriction of retinal ganglion cell dendrites and axons: subtype-specific developmental patterns revealed with transgenic markers. *J. Neurosci.* **30**, 1452–62 (2010).
114. Yamagata, M. & Sanes, J. R. Dscam and Sidekick proteins direct lamina-specific synaptic connections in vertebrate retina. *Nature* **451**, 465–469 (2008).
115. Yamagata, M. & Sanes, J. R. Expanding the Ig superfamily code for laminal specificity in retina: Expression and role of contactins. *J. Neurosci.* **32**, 14402–14 (2012).
116. Yamagata, M., Weiner, J. a. & Sanes, J. R. Sidekicks: Synaptic adhesion molecules that promote lamina-specific connectivity in the retina. *Cell* **110**, 649–660 (2002).
117. Duan, X., Krishnaswamy, A., De la Huerta, I. & Sanes, J. R. Type II cadherins guide assembly of a direction-selective retinal circuit. *Cell* **158**, 793–807 (2014).
118. Wong, K. Y., Dunn, F. A., Graham, D. M. & Berson, D. M. Synaptic influences on rat ganglion-cell photoreceptors. *J. Physiol.* **582**, 279–96 (2007).
119. Grünert, U., Jusuf, P. R., Lee, S. C. S. & Nguyen, D. T. Bipolar input to melanopsin containing ganglion cells in primate retina. *Vis. Neurosci.* **28**, 39–50

- (2011).
120. Dumitrescu, O. N., Pucci, F. G., Wong, K. Y. & Berson, D. M. Ectopic retinal ON bipolar cell synapses in the OFF inner plexiform layer: Contacts with dopaminergic amacrine cells and melanopsin ganglion cells. *J. Comp. Neurol.* **517**, 226–244 (2009).
 121. Hoshi, H., Liu, W.-L., Massey, S. C. & Mills, S. L. ON inputs to the OFF layer: Bipolar cells that break the stratification rules of the retina. *J. Neurosci.* **29**, 8875–83 (2009).
 122. Belenky, M. A., Smeraski, C. A., Provencio, I., Sollars, P. J. & Pickard, G. E. Melanopsin retinal ganglion cells receive bipolar and amacrine cell synapses. *J. Comp. Neurol.* **460**, 380–93 (2003).
 123. Østergaard, J., Hannibal, J. & Fahrenkrug, J. Synaptic contact between melanopsin-containing retinal ganglion cells and rod bipolar cells. *Invest. Ophthalmol. Vis. Sci.* **48**, 3812–20 (2007).
 124. Dowling, J. E. & Ehinger, B. The interplexiform cell system I. Synapses of the dopaminergic neurons of the goldfish retina. *Proc. R. Soc. Lond. B* **201**, 7–26 (1978).
 125. Kolb, H., Cuenca, N., Wang, H.-H. & Dekorver, L. The synaptic organization of the dopaminergic amacrine cell in the cat retina. *J. Neurocytol.* **366**, 343–366 (1990).
 126. Dacey, D. M. The dopaminergic amacrine cell. *J. Comp. Neurol.* **489**, 461–489 (1990).
 127. Viney, T. J. *et al.* Local retinal circuits of melanopsin-containing ganglion cells identified by transsynaptic viral tracing. *Curr. Biol.* **17**, 981–8 (2007).
 128. Vugler, A. A. *et al.* Dopamine neurones form a discrete plexus with melanopsin cells in normal and degenerating retina. *Exp. Neurol.* **205**, 26–35 (2007).
 129. Matsuoka, R. L. *et al.* Transmembrane semaphorin signalling controls laminar stratification in the mammalian retina. *Nature* **470**, 259–63 (2011).

130. Jackson, C. R. *et al.* Retinal dopamine mediates multiple dimensions of light-adapted vision. *J. Neurosci.* **32**, 9359–9368 (2012).
131. Ribelayga, C., Cao, Y. & Mangel, S. C. The circadian clock in the retina controls rod-cone coupling. *Neuron* **59**, 790–801 (2008).
132. Blasic, J. R., Brown, R. L. & Robinson, P. R. Phosphorylation of mouse melanopsin by protein kinase A. *PLoS One* **7**, e45387 (2012).
133. Van Hook, M. J., Wong, K. Y. & Berson, D. M. Dopaminergic modulation of ganglion-cell photoreceptors in rat. *Eur. J. Neurosci.* **35**, 507–18 (2012).
134. Sakamoto, K. *et al.* Dopamine regulates melanopsin mRNA expression in intrinsically photosensitive retinal ganglion cells. *Eur. J. Neurosci.* **22**, 3129–36 (2005).
135. Weng, S., Wong, K. Y. & Berson, D. M. Circadian modulation of melanopsin-driven light response in rat ganglion-cell photoreceptors. *J. Biol. Rhythm.* **24**, 391–402 (2009).
136. Boycott, B. B. & Wässle, H. The morphological types of ganglion cells of the domestic cat's retina. *J. Physiol.* **240**, 397–419 (1974).
137. Enroth-Cugell, C. & Robson, J. G. The contrast sensitivity of retinal ganglion cells of the cat. *J. Physiol.* **187**, 517–552 (1966).
138. Shapley, R. M. & Victor, J. D. The effect of contrast on the transfer properties of cat retinal ganglion cells. *J. Physiol.* **285**, 275–298 (1978).
139. Okawa, H., Della Santina, L., Schwartz, G. W., Rieke, F. & Wong, R. O. L. Interplay of cell-autonomous and nonautonomous mechanisms tailors synaptic connectivity of converging axons in vivo. *Neuron* **82**, 125–137 (2014).
140. Montell, C. Drosophila visual transduction. *Trends Neurosci.* **35**, 356–363 (2012).
141. Scott, K., Becker, A., Sun, Y., Hardy, R. & Zuker, C. S. Gq α protein function in vivo: genetic dissection of its role in photoreceptor cell physiology. *Neuron* **15**, 919–927 (1995).
142. Bloomquist, B. T. *et al.* Isolation of a putative phospholipase C gene of Drosophila,

- norpA, and its role in phototransduction. *Cell* **54**, 723–733 (1988).
143. Huang, J. *et al.* Activation of TRP channels by protons and phosphoinositide depletion in *Drosophila* photoreceptors. *Curr. Biol.* **20**, 189–97 (2010).
 144. Hardie, R. C. & Minke, B. The *trp* gene is essential for a light-activated Ca²⁺ channel in *Drosophila* photoreceptors. *Neuron* **8**, 643–651 (1992).
 145. Phillips, A. M., Bull, A. & Kelly, L. E. Identification of a *Drosophila* gene encoding a calmodulin-binding protein with homology to the *trp* phototransduction gene. *Neuron* **8**, 631–642 (1992).
 146. Hardie, R. C. & Franze, K. Photomechanical responses in *Drosophila* photoreceptors. *Science* (80-.). **338**, 260–263 (2012).
 147. Xue, T. *et al.* Melanopsin signalling in mammalian iris and retina. *Nature* **479**, 67–73 (2011).
 148. Graham, D. M. *et al.* Melanopsin ganglion cells use a membrane-associated rhabdomic phototransduction cascade. *J. Neurophysiol.* **99**, 2522–32 (2008).
 149. Chew, K. S., Schmidt, T. M., Rupp, A. C., Kofuji, P. & Trimarchi, J. M. Loss of Gq/11 genes does not abolish melanopsin phototransduction. *PLoS One* **9**, e98356 (2014).
 150. Siegart, S. *et al.* Transcriptional code and disease map for adult retinal cell types. *Nat. Neurosci.* **15**, (2012).
 151. Hughes, S. *et al.* Using siRNA to define functional interactions between melanopsin and multiple G protein partners. *Cell. Mol. Life Sci.* (2014). doi:10.1007/s00018-014-1664-6
 152. Hartwick, A. T. E. *et al.* Light-evoked calcium responses of isolated melanopsin-expressing retinal ganglion cells. *J. Neurosci.* **27**, 13468–80 (2007).
 153. Sekaran, S. *et al.* 2-aminoethoxydiphenylborane is an acute inhibitor of directly photosensitive retinal ganglion cell activity in vitro and in vivo. *J. Neurosci.* **27**, 3981–6 (2007).
 154. Perez-Leighton, C. E., Schmidt, T. M., Abramowitz, J., Birnbaumer, L. & Kofuji,

- P. Intrinsic phototransduction persists in melanopsin-expressing ganglion cells lacking diacylglycerol-sensitive TRPC subunits. *Eur. J. Neurosci.* **7**, 1–12 (2011).
155. Panda, S. *et al.* Illumination of the melanopsin signaling pathway. *Science (80-.)*. **307**, 600–4 (2005).
156. Bailes, H. J. & Lucas, R. J. Human melanopsin forms a pigment maximally sensitive to blue light ($L_{max} = 479$ nm) supporting activation of Gq/11 and Gi/o signalling cascades. *Proc. R. Soc. Lond. B* **280**, 20122987 (2013).
157. Schmidt, T. M., Taniguchi, K. & Kofuji, P. Intrinsic and extrinsic light responses in melanopsin-expressing ganglion cells during mouse development. *J. Neurophysiol.* **100**, 371–84 (2008).
158. Tu, D. C. *et al.* Physiologic diversity and development of intrinsically photosensitive retinal ganglion cells. *Neuron* **48**, 987–99 (2005).
159. Butler, M. P. & Silver, R. Divergent photic thresholds in the non-image-forming visual system: Entrainment, masking and pupillary light reflex. *Proc. R. Soc. Lond. B* **278**, 745–50 (2011).
160. Campbell, F. W. & Gregory, A. H. Effect of size of pupil on visual acuity. *Nature* **187**, 1121–3 (1960).
161. Binda, P., Pereverzeva, M. & Murray, S. O. Attention to bright surfaces enhances the pupillary light reflex. *J. Neurosci.* **33**, 2199–204 (2013).
162. Kahneman, D. & Beatty, J. Pupil diameter and load on memory. *Science (80-.)*. **154**, 1583–1585 (1966).
163. Hess, E. H. & Polt, J. M. Pupil size as related to interest value of visual stimuli. *Science (80-.)*. **132**, 349–350 (1960).
164. Levy, D. E. *et al.* Predicting outcome from hypoxic-ischemic coma. *JAMA* **253**, 1420–6 (1985).
165. Bouma, H. H. Size of the static pupil as a function of wave-length and luminosity of the light incident on the human eye. *Nature* **193**, 690–1 (1962).
166. Pennesi, M. E., Lyubarsky, A. L. & Pugh Jr., E. N. Extreme responsiveness of the

- pupil of the dark-adapted mouse to steady retinal illumination. *Invest. Ophthalmol. Vis. Sci.* **39**, 2148–56 (1998).
167. ten Doesschate, J. & Alpern, M. Response of the pupil to steady-state retinal illumination: Contribution by cones. *Science (80-.)*. **149**, 989–991 (1965).
 168. Alpern, M. & Campbell, F. W. The spectral sensitivity of the consensual light reflex. *J. Physiol.* **164**, 478–507 (1962).
 169. Barrionuevo, P. A. *et al.* Assessing rod, cone, and melanopsin contributions to human pupil flicker responses. *Invest. Ophthalmol. Vis. Sci.* **55**, 719–27 (2014).
 170. Kimura, E. & Young, R. S. L. Sustained pupillary constrictions mediated by an L- and M-cone opponent process. *Vis. Res.* **50**, 489–96 (2010).
 171. Kimura, E. & Young, R. S. L. Nature of the pupillary responses evoked by chromatic flashes on a white background. *Vis. Res.* **35**, 897–906 (1995).
 172. Kimura, E. & Young, R. S. L. S-cone contribution to pupillary responses evoked by chromatic flash offset. *Vis. Res.* **39**, 1189–1197 (1999).
 173. Young, R. S. L. & Kimura, E. Pupillary correlates of light-evoked melanopsin activity in humans. *Vis. Res.* **48**, 862–71 (2008).
 174. Tsujimura, S., Ukai, K., Ohama, D., Nuruki, A. & Yunokuchi, K. Contribution of human melanopsin retinal ganglion cells to steady-state pupil responses. *Proc. Biol. Sci.* **277**, 2485–92 (2010).
 175. McDougal, D. H. & Gamlin, P. D. R. The influence of intrinsically-photosensitive retinal ganglion cells on the spectral sensitivity and response dynamics of the human pupillary light reflex. *Vis. Res.* **50**, 72–87 (2010).
 176. Gamlin, P. D. R. *et al.* Human and macaque pupil responses driven by melanopsin-containing retinal ganglion cells. *Vis. Res.* **47**, 946–54 (2007).
 177. Gooley, J. J. *et al.* Melanopsin and rod-cone photoreceptors play different roles in mediating pupillary light responses during exposure to continuous light in humans. *J. Neurosci.* **32**, 14242–14253 (2012).
 178. Lall, G. S. *et al.* Distinct contributions of rod, cone, and melanopsin

- photoreceptors to encoding irradiance. *Neuron* **66**, 417–28 (2010).
179. Allen, A. E., Brown, T. M. & Lucas, R. J. A distinct contribution of short-wavelength-sensitive cones to light-evoked activity in the mouse pretectal olivary nucleus. *J. Neurosci.* **31**, 16833–16843 (2011).
 180. Lucas, R. J. *et al.* Measuring and using light in the melanopsin age. *Trends Neurosci.* **37**, 1–9 (2014).
 181. Laurens, H. Studies on the relative physiological value of spectral lights. III. The pupillomotor effects of wave-lengths of equal energy content. *Am. J. Physiol.* **64**, 97–119 (1922).
 182. Mure, L. S. *et al.* Melanopsin bistability: A fly's eye technology in the human retina. *PLoS One* **4**, e5991 (2009).
 183. Brown-Séquard, C.-É. Note complémentaire d'un Mémoire sur l'action de la lumière et d'un changement de température sur l'iris. *C. R. Acad. Sci.* 508–10 (1847).
 184. Brown-Séquard, C.-É. Recherches expérimentales sur l'action de la lumière et sur celle d'un changement de température sur l'iris, dans les cinq classes d'animaux vertébrés. *C. R. Acad. Sci.* 482–3 (1847).
 185. Steinach, E. Untersuchungen zur vergleichenden Physiologie der Iris. *Pflügers Arch. Gesamte Physiol. Menschen Tiere* **47**, 495–525 (1892).
 186. Barr, L. & Alpern, M. Photosensitivity of the frog iris. *J. Gen. Physiol.* **46**, 1249–1265 (1963).
 187. Seliger, H. H. Direct action of light in naturally pigmented muscle fibers. I. Action spectrum for contraction in eel iris sphincter. *J. Gen. Physiol.* **46**, 333–42 (1962).
 188. Tu, D. C., Batten, M. L., Palczewski, K. & Van Gelder, R. N. Nonvisual photoreception in the chick iris. *Science (80-.)*. **306**, 129–31 (2004).
 189. Armstrong, P. B. & Bell, A. L. Pupillary responses in the toad as related to innervation of the iris. *Am. J. Physiol.* **214**, 566–573 (1968).
 190. Pilar, G., Nuñez, R., McLennan, I. S. & Meriney, S. D. Muscarinic and nicotinic

- synaptic activation of the developing chicken iris. *J. Neurosci.* **7**, 3813–3826 (1987).
191. Nilsson, S. Sympathetic nervous control of the iris sphincter of the atlantic cod, *Gadus morhua*. *J. Comp. Physiol. A. Neuroethol. Sens. Neural. Behav. Physiol.* **138**, 149–155 (1980).
 192. Bitó, L. & Turansky, D. G. Photoactivation of pupillary constriction in the isolated in vitro iris of a mammal (*Mesocricetus auratus*). *Comp. Biochem. Physiol. Comp. Physiol.* **50**, 407–413 (1975).
 193. Lau, K. C., So, K.-F., Campbell, G. & Lieberman, A. R. Pupillary constriction in response to light in rodents, which does not depend on central neural pathways. *J. Neurol. Sci.* **113**, 70–79 (1992).
 194. Semo, M., Gias, C., Ahmado, A. & Vugler, A. A. A role for the ciliary marginal zone in the melanopsin-dependent intrinsic pupillary light reflex. *Exp. Eye Res.* **119**, 8–18 (2014).
 195. Vugler, A. A. *et al.* A role for the outer retina in development of the intrinsic pupillary light reflex in mice. *Neuroscience* **286C**, 60–78 (2014).
 196. ten Doesschate, J. & Alpern, M. Effect of photoexcitation of the two retinas on pupil size. *J. Neurophysiol.* **30**, 562–76 (1967).
 197. Davies, W. L., Hankins, M. W. & Foster, R. G. Vertebrate ancient opsin and melanopsin: divergent irradiance detectors. *Photochem. Photobiol. Sci.* **9**, 1444–14457 (2010).
 198. Murakami, M. & Kouyama, T. Crystal structure of squid rhodopsin. *Nature* **453**, 363–367 (2008).
 199. Engbretson, G. a & Lent, C. M. Parietal eye of the lizard: neuronal photoresponses and feedback from the pineal gland. *Proc. Natl. Acad. Sci. USA* **73**, 654–657 (1976).
 200. Deguchi, T. Rhodopsin-like photosensitivity of isolated chicken pineal gland. *Nature* **290**, 706–7 (1981).

201. Solessio, E. & Engbretson, G. a. Antagonistic chromatic mechanisms in photoreceptors of the parietal eye of lizards. *Nature* **364**, 442–445 (1993).
202. Finn, J. T., Solessio, E. C. & Yau, K. A cGMP-gated cation channel in depolarizing photoreceptors of the lizard parietal eye. *Nature* **385**, 815–9 (1997).
203. Su, C. *et al.* Parietal-eye phototransduction components and their potential evolutionary implications. *Science (80-.)*. **311**, 1617–21 (2006).
204. Jackson, P. C. Innervation of the iris by individual parasympathetic axons in the adult mouse. *J. Physiol.* **378**, 485–495 (1986).
205. Moore, R. Y., Heller, A., Wurtman, R. J. & Axelrod, J. Visual pathway mediating pineal response to environmental light. *Science (80-.)*. **155**, 220–3 (1967).
206. Campbell, S. S. & Murphy, P. J. Extraocular circadian phototransduction in humans. *Science (80-.)*. **279**, 396–399 (1998).
207. Wright, K. P. J. & Czeisler, C. A. Absence of circadian phase resetting in response to bright light behind the knees. *Science (80-.)*. **297**, 571 (2002).
208. Weale, R. A. Observations on the direct effect of light on the irides of *Rana temporaria* and *Xenopus laevis*. *J. Physiol.* **132**, 257–266 (1956).
209. Matsui, M. *et al.* Mice lacking M2 and M3 muscarinic acetylcholine receptors are devoid of cholinergic smooth muscle contracts but still viable. *J. Neurosci.* **22**, 10627–10632 (2002).
210. Armbruster, B. N., Li, X., Pausch, M. H., Herlitze, S. & Roth, B. L. Evolving the lock to fit the key to create a family of G protein-coupled receptors potently activated by an inert ligand. *Proc. Natl. Acad. Sci. USA* **104**, 5163–5168 (2007).
211. Rupp, A. C. *et al.* ipRGCs mediate ipsilateral pupil constriction. *Invest. Ophthalmol. Vis. Sci.* **54**, 310 (2013).
212. Schmidt, T. M. *et al.* A retinal projection to the iris mediates pupil constriction. *Invest. Ophthalmol. Vis. Sci.* **55**, 1231 (2014).
213. Pérez de Sevilla Müller, L., Sargoy, A., Rodriguez, A. R. & Brecha, N. C. Melanopsin ganglion cells are the most resistant retinal ganglion cell type to

- axonal injury in the rat retina. *PLoS One* **9**, e93274 (2014).
214. Valiente-Soriano, F. J. *et al.* Distribution of melanopsin positive neurons in pigmented and albino mice: Evidence for melanopsin interneurons in the mouse retina. *Front. Neuroanat.* **8**, 1–17 (2014).
 215. Loewenfeld, I. E. & Lowenstein, O. *The pupil: Anatomy, physiology, and clinical applications.* (Wayne State University Press, 1993).
 216. Grozdanic, S. D., Kecova, H. & Lazic, T. Rapid diagnosis of retina and optic nerve abnormalities in canine patients with and without cataracts using chromatic pupil light reflex testing. *Vet. Ophthalmol.* 1–12 (2012). doi:10.1111/vop.12003
 217. Kuchnow, K. P. The elasmobranch pupillary response. *Vis. Res.* **11**, 1395–1406 (1971).
 218. Ye, H., Baba, M. D., Peng, R. & Fussenegger, M. A synthetic optogenetic transcription device enhances blood-glucose homeostasis in mice. *Science (80-.)*. **332**, 1565–8 (2011).
 219. Alpern, M. & Ohba, N. The effect of bleaching and backgrounds on pupil size. *Vis. Res.* **12**, 943–51 (1972).
 220. Ho Mien, I. *et al.* Effects of exposure to intermittent versus continuous red light on human circadian rhythms, melatonin suppression, and pupillary constriction. *PLoS One* **9**, e96532 (2014).
 221. Park, J. C. & McAnany, J. J. Effect of stimulus size and luminance on the rod-, cone-, and melanopsin-mediated pupillary light reflex. *J. Vis.* **15**, 1–13 (2015).
 222. Kardon, R. *et al.* Chromatic pupil responses: Preferential activation of the melanopsin-mediated versus outer photoreceptor-mediated pupil light reflex. *Ophthalmology* **116**, 1564–73 (2009).
 223. Biel, M. *et al.* Selective loss of cone function in mice lacking the cyclic nucleotide-gated channel CNG3. *Proc. Natl. Acad. Sci. USA* **96**, 7553–7 (1999).
 224. McCall, M. A. *et al.* Morphological and physiological consequences of the selective elimination of rod photoreceptors in transgenic mice. *Exp. Eye Res.* **63**,

- 35–50 (1996).
225. Soucy, E. R., Wang, Y., Nirenberg, S., Nathans, J. & Meister, M. A novel signaling pathway from rod photoreceptors to ganglion cells in mammalian retina. *Neuron* **21**, 481–93 (1998).
 226. Nathan, J. *et al.* Scotopic and photopic visual thresholds and spatial and temporal discrimination evaluated by behavior of mice in a water maze. *Photochem. Photobiol.* **82**, 1489–94 (2006).
 227. Naarendorp, F. *et al.* Dark light, rod saturation, and the absolute and incremental sensitivity of mouse cone vision. *J. Neurosci.* **30**, 12495–507 (2010).
 228. Altimus, C. M. *et al.* Rod photoreceptors drive circadian photoentrainment across a wide range of light intensities. *Nat. Neurosci.* **13**, 1107–12 (2010).
 229. Alam, N. M., Altimus, C. M., Douglas, R. M., Hattar, S. & Prusky, G. T. Photoreceptor regulation of spatial visual behavior. *Invest. Ophthalmol. Vis. Sci.* **56**, 1842–9 (2015).
 230. Cahill, H. & Nathans, J. The optokinetic reflex as a tool for quantitative analyses of nervous system function in mice: application to genetic and drug-induced variation. *PLoS One* **3**, e2055 (2008).
 231. Zhao, X., Stafford, B. K., Godin, A. L., King, W. M. & Wong, K. Y. Photoresponse diversity among the five types of intrinsically photosensitive retinal ganglion cells. *J. Physiol.* **592**, 1619–36 (2014).
 232. Smallwood, P. M. *et al.* Genetically engineered mice with an additional class of cone photoreceptors: Implications for the evolution of color vision. *Proc. Natl. Acad. Sci. USA* **100**, 11706–11 (2003).
 233. van Oosterhout, F. *et al.* Ultraviolet light provides a major input to non-image-forming light detection in mice. *Curr. Biol.* **22**, 1–6 (2012).
 234. Spitschan, M., Jain, S., Brainard, D. H. & Aguirre, G. K. Opponent melanopsin and S-cone signals in the human pupillary light response. *Proc. Natl. Acad. Sci. USA* **111**, 15568–72 (2014).

235. Arshavsky, V. Y. & Burns, M. E. Photoreceptor signaling: supporting vision across a wide range of light intensities. *J. Biol. Chem.* **287**, 1620–6 (2012).
236. Zele, A. J. & Cao, D. Vision under mesopic and scotopic illumination. *Front. Psychol.* **5**, 1–15 (2015).
237. Wong, K. Y. A retinal ganglion cell that can signal irradiance continuously for 10 hours. *J. Neurosci.* **32**, 11478–11485 (2012).
238. Dacheux, R. F. & Raviola, E. The rod pathway in the rabbit retina: A depolarizing bipolar and amacrine cell. *J. Neurosci.* **6**, 331–345 (1986).
239. Kolb, H. & Famiglietti Jr., E. V. Rod and cone pathways in the inner plexiform layer of cat retina. *Science (80-)*. **186**, 47–49 (1974).
240. Kolb, H. The inner plexiform layer in the retina of the cat: electron microscopic observations. *J. Neurocytol.* **8**, 295–329 (1979).
241. Mills, S. L., O'Brien, J. J., Li, W., O'Brien, J. & Massey, S. C. Rod pathways in the mammalian retina use connexin 36. *J. Comp. Neurol.* **436**, 336–50 (2001).
242. Deans, M. R., Volgyi, B., Goodenough, D. A., Bloomfield, S. A. & Paul, D. L. Connexin36 is essential for transmission of rod-mediated visual signals in the mammalian retina. *Neuron* **36**, 703–12 (2002).
243. Volgyi, B., Deans, M. R., Paul, D. L. & Bloomfield, S. A. Convergence and segregation of the multiple rod pathways in mammalian retina. *J. Neurosci.* **24**, 11182–92 (2004).
244. Do, M. T. H. *et al.* Photon capture and signalling by melanopsin retinal ganglion cells. *Nature* **457**, 281–7 (2009).
245. Braz, J. M., Rico, B. & Basbaum, A. I. Transneuronal tracing of diverse CNS circuits by Cre-mediated induction of wheat germ agglutinin in transgenic mice. *Proc. Natl. Acad. Sci. USA* **99**, 15148–15153 (2002).
246. Zhang, D.-Q. *et al.* Intraretinal signaling by ganglion cell photoreceptors to dopaminergic amacrine neurons. *Proc. Natl. Acad. Sci. USA* **105**, 14181–6 (2008).
247. Joo, H. R., Peterson, B. B., Dacey, D. M., Hattar, S. & Chen, S.-K. Recurrent axon

- collaterals of intrinsically photosensitive retinal ganglion cells. *Vis. Neurosci.* **30**, 175–82 (2013).
248. Bloomfield, S. A. & Völgyi, B. The diverse functional roles and regulation of neuronal gap junctions in the retina. *Nat. Rev. Neurosci.* **10**, 495–506 (2009).
249. Fortin, D. A. *et al.* Live imaging of endogenous PSD-95 using ENABLED: A conditional strategy to fluorescently label endogenous proteins. *J. Neurosci.* **34**, 16698–16712 (2014).
250. Dowling, J. E. & Boycott, B. B. Organization of the primate retina: Electron microscopy. *Proc. R. Soc. Lond. B* **166**, 80–111 (1966).
251. Dacey, D. M. *et al.* Melanopsin-expressing ganglion cells in primate retina signal colour and irradiance and project to the LGN. *Nature* **433**, 749–754 (2005).
252. Iwakabe, H., Katsuura, G., Ishibashi, C. & Nakanishi, S. Impairment of pupillary responses and optokinetic nystagmus in the mGluR6-deficient mouse. *Neuropharmacology* **36**, 135–43 (1997).
253. Thompson, S. *et al.* Different inner retinal pathways mediate rod-cone input in irradiance detection for the pupillary light reflex and regulation of behavioral state in mice. *Invest. Ophthalmol. Vis. Sci.* **52**, 618–23 (2011).
254. Hughes, S. *et al.* Profound defects in pupillary responses to light in TRPM-channel null mice: a role for TRPM channels in non-image-forming photoreception. *Eur. J. Neurosci.* **35**, 34–43 (2012).
255. Weng, S., Estevez, M. E. & Berson, D. M. Mouse ganglion-cell photoreceptors are driven by the most sensitive rod pathway and by both types of cones. *PLoS One* **8**, e66480 (2013).
256. Brown, T. M. *et al.* Visual responses in the lateral geniculate evoked by Cx36-independent rod pathways. *Vis. Res.* **51**, 280–287 (2011).
257. Fenno, L. E. *et al.* Targeting cells with single vectors using multiple-feature Boolean logic. *Nat. Methods* (2014). doi:10.1038/nmeth.2996
258. Mrosovsky, N., Foster, R. G. & Salmon, P. A. Thresholds for masking responses

- to light in three strains of retinally degenerate mice. *J. Comp. Physiol. A. Neuroethol. Sens. Neural. Behav. Physiol.* **184**, 423–8 (1999).
259. Golombek, D. A. & Rosenstein, R. E. Physiology of circadian entrainment. *Physiol. Rev.* **90**, 1063–102 (2010).
260. Chellappa, S. L. *et al.* Non-visual effects of light on melatonin, alertness and cognitive performance: Can blue-enriched light keep us alert? *PLoS One* **6**, e16429 (2011).
261. Jones, J. R., Tackenberg, M. C. & McMahon, D. G. Manipulating circadian clock neuron firing rate resets molecular circadian rhythms and behavior. *Nat. Neurosci.* **18**, 373–5 (2015).
262. Dkhissi-Benyahya, O., Gronfier, C., Vanssay, W. De, Flamant, F. & Cooper, H. M. Modeling the role of mid-wavelength cones in circadian responses to light. *Neuron* **53**, 677–87 (2007).
263. Provencio, I., Wong, S., Lederman, A. B., Argamaso, S. M. & Foster, R. G. Visual and circadian responses to light in aged retinally degenerate mice. *Vis. Res.* **34**, 1799–1806 (1994).
264. Gooley, J. J., Lu, J., Fischer, D. & Saper, C. B. A broad role for melanopsin in nonvisual photoreception. *J. Neurosci.* **23**, 7093–7106 (2003).
265. Muindi, F., Zeitzer, J. M. & Heller, H. C. Retino-hypothalamic regulation of light-induced murine sleep. *Front. Syst. Neurosci.* **8**, 1–9 (2014).
266. Morin, L. P. A path to sleep is through the eye. *eNeuro* **2**, (2015).
267. Redlin, U. & Mrosovsky, N. Masking by light in hamsters with SCN lesions. *J Comp Physiol A* **184**, 439–48 (1999).
268. Hubbard, J., Ruppert, E., Gropp, C.-M. & Bourgin, P. Non-circadian direct effects of light on sleep and alertness: Lessons from transgenic mouse models. *Sleep Med. Rev.* **17**, 445–452 (2013).
269. Mrosovsky, N. & Hattar, S. Impaired masking responses to light in melanopsin-knockout mice. *Chronobiol. Int.* **20**, 989–99 (2003).

270. Darwent, D. *et al.* Contribution of core body temperature, prior wake time, and sleep stages to cognitive throughput performance during forced desynchrony. *Chronobiol. Int.* **27**, 898–910 (2010).
271. Wright, K. P. J., Hull, J. T. & Czeisler, C. A. Relationship between alertness, performance, and body temperature in humans. *Am. J. Physiol. Regul. Integr. Comp. Physiol.* **283**, R1370–R1377 (2002).
272. Kräuchi, K., Cajochen, C., Werth, E. & Wirz-justice, A. Warm feet promote the rapid onset of sleep. *Nature* **401**, 36–37 (1999).
273. Kooijman, S., van den Heuvel, J. K. & Rensen, P. C. N. Neuronal control of brown fat activity. *Trends Endocrinol. Metab.* **xx**, 1–12 (2015).
274. Dijk, D. J., Cajochen, C. & Borbély, A. A. Effect of a single 3-hour exposure to bright light on core body temperature and sleep in humans. *Neurosci. Lett.* **121**, 59–62 (1991).
275. Cajochen, C. *et al.* High sensitivity of human melatonin, alertness, thermoregulation, and heart rate to short wavelength light. *J. Clin. Endocrinol. Metab.* **90**, 1311–1316 (2005).
276. Takahashi, J. S., DeCoursey, P. J., Bauman, L. & Menaker, M. Spectral sensitivity of a novel photoreceptive system mediating entrainment of mammalian circadian rhythms. *Nature* **308**, 186–8 (1984).
277. Redlin, U., Cooper, H. M. & Mrosovsky, N. Increased masking response to light after ablation of the visual cortex in mice. *Brain Res.* **965**, 1–8 (2003).
278. Nakamura, K. Central circuitries for body temperature regulation and fever. *Am. J. Physiol. Regul. Integr. Comp. Physiol.* **305**, 1207–1228 (2011).
279. Kramer, A. *et al.* Regulation of daily locomotor activity and sleep by hypothalamic EGF receptor signaling. *Science (80-.)*. **294**, 2511–5 (2001).
280. Miller, A. M., Obermeyer, W. H., Behan, M. & Benca, R. M. The superior colliculus–pretectum mediates the direct effects of light on sleep. *Proc. Natl. Acad. Sci. USA* **95**, 8957–8962 (1998).

281. Szymusiak, R. & McGinty, D. Hypothalamic regulation of sleep and arousal. *Ann. N. Y. Acad. Sci.* **1129**, 275–286 (2008).
282. Osterhout, J. A. *et al.* Cadherin-6 mediates axon-target matching in a non-image-forming visual circuit. *Neuron* **71**, 632–9 (2011).
283. Wall, N. R., Wickersham, I. R., Cetin, A., De La Parra, M. & Callaway, E. M. Monosynaptic circuit tracing in vivo through Cre-dependent targeting and complementation of modified rabies virus. *Proc. Natl. Acad. Sci. USA* **107**, 21848–53 (2010).

Alan C. Rupp

Curriculum Vitae

January 2016

ADDRESS

Johns Hopkins University

Department of Biology

3400 N. Charles Street, Baltimore, MD 21211, USA

410-516-7641

arupp2@jhu.edu

EDUCATION

- 2016 Ph.D. in Cellular, molecular, developmental biology, and biophysics
 Johns Hopkins University, Baltimore, Maryland
 Thesis title: “The photoreceptors and neural circuits driving the pupillary
 light reflex.”
 Advisor: Samer Hattar, Ph.D.
- 2008 B.S. in Bioengineering with honors and minor in Physics, *Cum laude*
 University of Toledo, Toledo, Ohio
 Senior Design Project/Honors Thesis: “Design and implementation of a
 catheter flow sensor.”
 Advisor: Ronald L. Fournier, Ph.D.

EMPLOYMENT AND TEACHING EXPERIENCE

- 2008–09 Research assistant
 University of Toledo Medical Center, Department of Immunology
 Laboratory of Akira Takashima, M.D., Ph.D.
- 2007–08 Undergraduate independent research
 University of Toledo, Department of Physics
 Advisor: Scott Lee, Ph.D.

2007 Summer undergraduate research
Indiana University, School of Optometry
Advisors: S.P. Srinivas, Ph.D. and Larry N. Thibos, Ph.D.

Teaching assistanceships

Johns Hopkins University

Evolution (2013, 2014, 2015)

Introduction to the Human Brain (2013, 2014, 2015)

Introduction to Human Genetics (2012)

Cell Biology (2011)

Genetics (2010)

Guest lecturer

Johns Hopkins University

Optogenetics lecture in Emerging Strategies in Biomedical Research (2013, 2015)

HONORS AND AWARDS

2014 FASEB travel award

2014 Ramon Dacheux II Memorial Travel Grant

2013 J. Brien Key Fund travel award

2012 Poster award, Department of Biology annual retreat

2010 DuPont Teaching Award, Genetics

2008 Graduated *cum laude* with honors

PROFESSIONAL MEMBERSHIPS

Association for Research in Vision and Ophthalmology

Society for Research in Biological Rhythms

Society for Neuroscience

INVITED PEER REVIEW

J. Neurosci. Methods

PUBLICATIONS

Research articles

*Indicates equal contribution

Active manuscripts:

Rupp AC, Schmidt TM, Bray ER, Somasundaram P, Hiriyanna S, Yungher BJ, Tufford A, Cui Y, Simon MI, Wu Z, Badea TC, Robinson PR, Cayouette M, Wess J, Birnbaumer L, Park KK, Hattar S. Melanopsin-expressing cells of the retina, not iris, mediate the pupillary light reflex. In revision.

Keenan WT*, **Rupp AC***, Somasundaram P, Hiriyanna S, Wu Z, Badea TC, Robinson PR, Hattar S. A visual circuit uses discrete mechanisms to support transient and sustained pupil constriction. In submission.

2015 Walker MT, **Rupp A**, Elsaesser R, Güler AD, Shen W, Weng S, Berson DM, Hattar S, Montell C. RdgB2 is required for dim-light input into intrinsically photosensitive retinal ganglion cells, *Mol. Biol. Cell* **26**, 3671-3678 (2015).

Riazifar H, Sun G, Wang X, **Rupp A**, Vemaraju S, Ross-Cisneros FN, Lang RA, Sadun AA, Hattar S, Guan M-X, Huang T. Phenotypic and functional characterization of *Bst*^{+/-} mouse retina. *Dis. Model. Mech.* **8**, 969-976 (2015).

Xue Y, Shen SQ, Jui J, **Rupp AC**, Byrne LC, Hattar S, Flannery JG, Corbo JC, Kefalov VJ. CRALBP is required for the function of the mammalian retina visual cycle and normal cone vision. *J. Clin. Invest.* **125**, 727-38 (2015).

2014 Chew KS, Schmidt TM, **Rupp AC**, Kofuji P, Trimarchi JM. Loss of G_{q/11} genes does not abolish melanopsin phototransduction. *PLoS ONE* **9**, e98356 (2014).

Bedont JL, LeGates TA, Slat EA, Byerly MS, Wang H, Hu J, **Rupp AC**, Qian J, Wong GW, Herzog ED, Hattar S, Blackshaw S. Lhx1 controls terminal differentiation and circadian function of the suprachiasmatic nucleus. *Cell Rep.* **7**, 609–22 (2014).

Book chapters

Rupp AC, Hattar S. “The functional properties of the G protein-coupled receptor melanopsin in intrinsically photosensitive retinal ganglion cells.” In: Martemyanov KA, Sampath AP, editors. *G Protein Signaling Mechanisms in the Retina*, Springer (2014).

PRESENTATIONS

Public talks

Rupp AC, Ramakrishnan C, Deisseroth K, Hattar S. Genetic dissection of retinal circuits underlying the pupillary light reflex (2014). FASEB Retinal Neurobiology and Visual Processing Data Blitz, Saxtons River, Vermont.

Rupp AC, Hattar S. Genetic dissection of retinal circuits underlying the pupillary light reflex (2014). Association for Research in Vision and Ophthalmology annual meeting, Orlando, Florida.

Rupp AC, Altimus CM, Hattar S. Cone-dependent regulation of ipRGC sensitivity (2011). Johns Hopkins Medical Institute, Department of Neuroscience, Baltimore, Maryland. Part of a Hattar Lab colloquium.

Poster presentations

Rupp AC, Ramakrishnan C, Deisseroth K, Hattar S (2014). Rods drive the pupillary light reflex using non-conventional circuitry. Baltimore chapter of the Society for Neuroscience annual meeting, Baltimore, Maryland.

Rupp AC, Ramakrishnan C, Deisseroth K, Hattar S (2014). Genetic dissection of retinal circuits underlying the pupillary light reflex. FASEB Retinal Neurobiology and Visual Processing biannual meeting, Saxtons River, Vermont.

Schmidt TM*, **Rupp AC***, Chew KS, Yungher B, Cui Y, Wess J, Park KK, Hattar S (2014). A retinal projection to the iris mediates pupil constriction. Association for Research in Vision and Ophthalmology annual meeting, Orlando, Florida.

Rupp AC, Hattar S (2013). Rods drive the pupillary light reflex using non-conventional circuitry. Genes, Circuits, and Behavior *Cell* symposium, Toronto, Ontario.

Rupp AC*, Schmidt TM*, Chew KS, Yungher B, Park KK, Hattar S (2013). ipRGCs mediate ipsilateral pupil constriction. Association for Research in Vision and Ophthalmology annual meeting, Seattle, Washington

Rupp AC, Altimus CM, Hattar S (2012). Photoreceptor regulation and retinal pathways of masking. Society for Research on Biological Rhythms biennial meeting, Sandestin, Florida.

Rupp AC, Hattar S (2011). Rod input to ipRGCs may require connexin36 gap junctions. Society for Neuroscience annual meeting, Washington, DC.

Rupp AC, Altimus CM, Hattar S (2011). Melanopsin drives acute light-dependent changes in body temperature against cone-mediated inhibition. Association for Research in Vision and Ophthalmology annual meeting, Fort Lauderdale, Florida.

Altimus CM, **Rupp AC**, Hattar S (2010). Determining retinal photoreceptor contribution in light-dependent acute changes in body temperature. Society for Research on Biological Rhythms biennial meeting, Sandestin, Florida.

REFERENCES

Samer Hattar, Ph.D.

Marnie Halpern, Ph.D.

Haiqing Zhao, Ph.D.